Construction of 3-D Velocity Structure Model of the Kathmandu Basin, Nepal, based on Geological Information and Earthquake Ground Motion Records

地質情報および地震観測記録に基づくネパール・カトマンズ盆地の3次元速度構造モデルの構築

by

Subeg M BIJUKCHHEN

In partial fulfilment of the requirements for the degree of

Doctor of Engineering

Supervisor

Associate Professor Nobuo TAKAI

Department of Architecture and Structural Design

Graduate School of Engineering

Hokkaido University

September 2018

ABSTRACT

The Himalayan region experiences many seismic activities due to the collision of two continental tectonic plates. With a number of small earthquakes and occasional large earthquakes occurring at certain intervals, this region is one of the most seismically vulnerable regions of the world. Nepal, covering about 900 km of the Himalayan arc (known as the Nepal Himalaya), has suffered a number of interplate and intraplate earthquakes in the past. There are accounts of more than 20 damaging earthquakes occurring in or near the Nepal Himalaya since the thirteenth century that have left trails of damage.

The study area is Kathmandu Basin, locally referred to as the Kathmandu Valley in central Nepal. It is a tectonic basin filled with lake and river sediments and surrounded by high mountains. The deposits are estimated to be more than 600 m thick. A location in a seismically active region and the possible amplification of seismic waves due to thick sediments have made the Kathmandu Basin seismically vulnerable. It has suffered devastation due to earthquakes several times in the past resulting in huge loss of life and property as it is the largest and the most densely populated settlement of Nepal. The earthquake vulnerability of the Kathmandu Basin was apparent during the Gorkha Earthquake (M_w 7.8) on April 25, 2015, when the main shock and ensuing aftershocks claimed more than 1,700 lives and nearly 13% of buildings inside the valley were completely damaged. Preparing safe and up-to-date building codes to reduce seismic risk requires a thorough study of ground motion amplification. An earthquake that seems to have no effect over hard ground can be felt as a strong tremor and might cause severe damage in areas over soft and unconsolidated sediments due to amplification of seismic waves. Past earthquakes in the Kathmandu Basin have shown significant amplification of long period waves in the sediment sites. To study the ground motion amplification of any area, a proper understanding of underground structure is very important. The present study is the construction of a 3-D underground model of the Kathmandu Basin based on geological data and earthquake records and ground motion simulation on the constructed model.

To accomplish this goal, the study fulfils the following tasks: a) to describe the geology and collect available geological and underground data of the Kathmandu Basin, b) to study the strong-motion characteristics of the Kathmandu Basin based on earthquake data, c) to construct 1-D velocity models of sediments beneath the seismic stations d) to construct a 3-D underground structure, and e) to simulate ground motion on the constructed 3-D basin structure.

The structure of the dissertation comprises of six chapters. Chapter I is the introductory chapter. This deals with the background of the study, the introduction of the study area, statement of purpose, and objectives of the study.

Chapter II deals with the tectonics and geology of the Kathmandu Basin. The Kathmandu Basin has coarser proto-Bagmati sediment at the bottom overlain by finer sediments of lake origin in the upper and central part. The widely distributed lake sediments give way to recent river sediments deposited after the drying up of the lake indicating a change in depositional environment. There is a lack of data regarding the underground structure of Kathmandu. The available borehole logs, which were made during the underground water prospecting don't clearly describe the physical properties of layers in detail. In addition to that, there are no publicly available P-S logging data below 30 m. By going through few available geological cross-sections, microtremor study results, and gravity survey data, one can understand that the basement topography of the basin is not smooth but highly undulated.

Chapter III is about the seismicity and strong-motion characteristic of the Kathmandu Basin. The response of basin sediments is described based on the past earthquakes and available earthquake records. The earthquake records from an array of strong-motion accelerometers installed by Hokkaido University and Tribhuvan University were studied. The data from four continuous recording permanent stations KTP, TVU, PTN, and THM, as well as other four temporary stations BKT, RNB, PPR, and KPN, were used for the study. The nonlinear characteristics of the Kathmandu

Basin sediments and high amplification of seismic waves in sediment sites are described through earthquake records and damage assessment of buildings in Kathmandu during the 2015 Gorkha Earthquake.

Chapter IV is the estimation of 1-D velocity models of station sites. Available borehole data, geological maps, and geological cross-sections were consulted to prepare initial 1-D velocity models of sediments beneath the stations. These initial models were then tuned by forward modelling of low-frequency S-waves. Filtered records (0.1-0.5 Hz) of a moderate-sized (mb4.9) earthquake and three moderate-sized (M_w 5.1, M_w 5.1, and M_w 5.5) aftershocks of the 2015 Gorkha Earthquake from one of the accelerometers installed at a rock site, were used as input motion for modelling of low-frequency S-waves. These final 1-D models show that the basin has an undulating topography and the sediment sites have deposits of varying thicknesses, from 155-440 m. These models also show high velocity contrast at the bedrock depth which results in significant wave amplification.

Chapter V focuses on the construction of a 3-D underground velocity model of the Kathmandu Basin based on the 1-D models, geological maps, and geological cross-sections. Several points in the cross-sections and geological maps were considered to construct five layers of sediments and a weathered rock layer which were then interpolated into individual surface layers of 100 m x 100 m grid by kriging method. The 3-D underground model shows the depth of sediment to be more than 600 m at the centre of the basin. The chapter also deals with the ground motion simulation of M_w 7.3 earthquake by finite difference method on the 3-D model to study the basin effect. The M_w 7.3 earthquake was chosen as the mainshock of Gorkha earthquake was affected by nonlinearity in the Kathmandu Basin. The study of the simulated waveform and its comparison with observed waveform indicate high amplification in the sedimentary sites due to thick sediments and presence of strong basin effect. The basin effects in simulated waveform were a good fit with those in the observed records but basin effects in all sites could not be replicated accurately.

Chapter VI is the conclusion and discussion part. The 3-D basement model of the Kathmandu Basin has not been prepared in detail before. This study shows that even with a lack of proper data on subsurface geology, velocity logs, and soil profiles, the construction of a 3-D velocity structure of a basin can be undertaken based on geological data and earthquake records which can further be used for earthquake disaster management studies.

Contents

CHAPTER I

INTRODUCTION

CHAPTER I. INTRODUCTION

1.1 BACKGROUND

The ongoing subduction of the Indian plate under the Eurasian plate in the Himalaya arc (Figure 1.1) at a rate of 36-50 mm [1,2] is not intermittent but interrupted by asperities resulting in accumulation of a large amount of stress. This accumulated stress releases periodically in form of small and large tremors. The stress may be released suddenly as mega earthquake or by slow earthquakes and creep. This latter process is termed aseismic slip [3]. The Nepal Himalaya regularly experiences small seismic events (Figure 1.2) with larger events occurring in certain time intervals [4]. Though being one of the seismically active regions of the world, the occurrence of large earthquakes in Nepal Himalaya is comparatively lesser than in other active regions around the world. Nevertheless, the region has seen several interplate and intraplate earthquakes in the past.

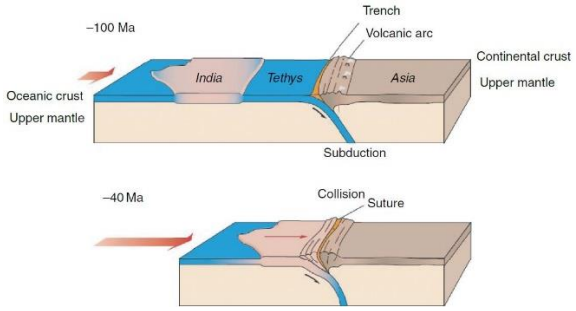

Figure 1. 1 Collision and subduction of the Indian and the Eurasian tectonic plates [5].

There are accounts of more than 20 damaging earthquakes occurring after the thirteenth century [6] including 1833, 1934 Nepal-Bihar, 1980 Bajura, 1988 Udaypur, and 2015 Gorkha earthquake. The latest one, Gorkha earthquake left trail of damage in central and eastern Nepal. It claimed life of over 8,000 people. About 12% of buildings inside the capital Kathmandu were reported damaged [7] as a result of the main shock and the subsequent aftershocks.

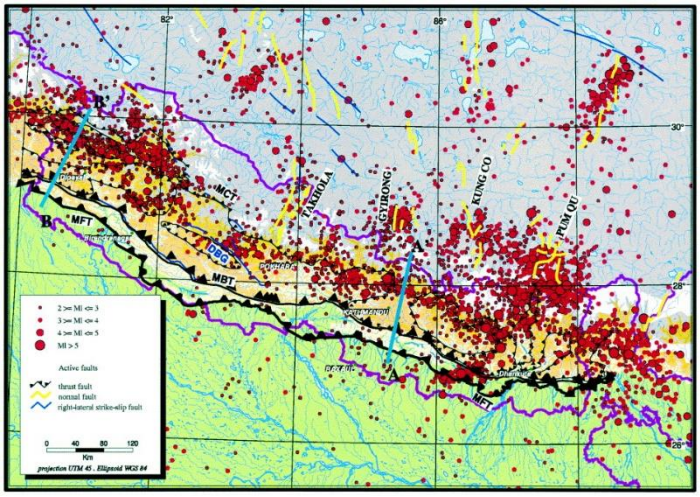

Figure 1. 2 Epicentre of microseismic activities in and around Nepal from 1994-1998 [8].

Though a number or researchers from all over the world have given their expertise and knowledge in the study of the tectonics and seismology of the Himalayan region, detailed study of the Nepal Himalaya is still lacking. But interest in study of tectonics and earthquake pattern in the region has significantly increased following the 2015 Gorkha earthquake.

1.2 STUDY AREA

The present study focuses on the tectonic basin of Kathmandu in central Nepal (Figure 1.3), locally known as the 'Kathmandu Valley'. This bowl shaped basin (665 km^2), referred as 'Kathmandu Basin' hereafter, was formed as a result of the uplift of Himalayan range and was a lake in the past. The eventual draining of the lake has caused the basin to be filled with fluvio-lacustrine sediments which reaches to a depth of ~600 m at the centre. The past earthquakes in Nepal Himalaya have affected Kathmandu causing loss of life and property. Kathmandu suffered badly in the 1934 Nepal-Bihar earthquake and in the latest 2015 Gorkha earthquake as the basin sediments amplified the seismic waves.

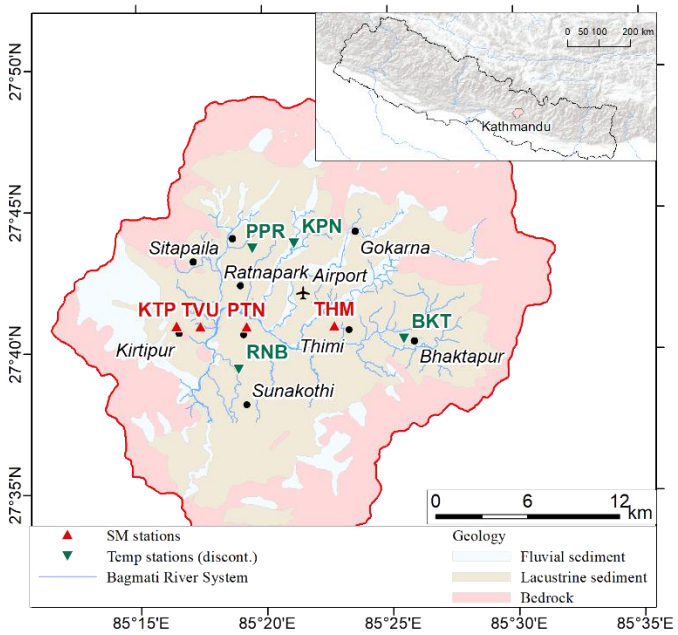

Figure 1. 3 The Kathmandu Basin along with the location of strong-motion seismometers used in the present study. The general geology is based on Shrestha, et al. [9].

The basin was created when the uplift of the mountain range lying to the south dammed the river and created a lake in course of time. After the lake breached the hills, it dried up leaving a sediment filled basin. The lower part of the basin is old river deposit overlain by lake deposit and finally the recent river deposit. The basin is surrounded by mountains of basement rocks on all sides and the sediments have been brought by the rivers from these very mountains.

1.3 STATEMENT OF PURPOSE

The manifestation of an earthquake effect is a combination of source, path, and site characteristics (Figure 1.4). The seismic waves passing through thick layers of soft sediments get amplified on reaching the surface thereby causing more damage than in regions lying above hard ground. The seismic response of the Kathmandu Basin sediments are also similar. The thick sediments amplify the waves and increase the affect. But the sediment deposit of Kathmandu is not evenly distributed and thickness of sediments vary a lot from place to place resulting in varying response in different parts of the basin.

The study of earthquake response in Kathmandu is important because not only is it political, economic, and cultural capital of the country, but it is also the largest urban agglomerate with more than 2.5 million residents [10]. The town and settlements inside Kathmandu boast a vibrant traditional culture and a number of historical monuments including many that are listed in the UNESCO World Heritage sites. These heritage sites are some of the main attraction for tourism industry which is the backbone of the

economy. Earthquake disaster in Kathmandu will not only cause large number of casualties but can also bring the country to a halt due to damages to important infrastructures. This could be worse by the fact that the Kathmandu Basin have seen a recent surge of unmanaged urbanization and haphazard constructions which will hinder the rescue and increase time required to return to normalcy after a disaster. Hence, clear understanding of seismic response in the Kathmandu Basin is important so that seismic vulnerability of Kathmandu can be properly addressed.

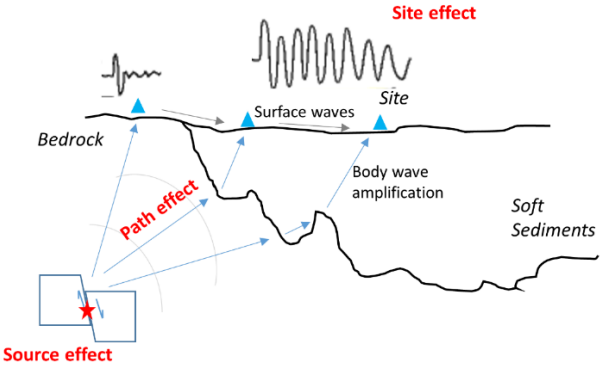

Figure 1. 4 The effect of an earthquake is the combined effect of source, path, and site.

The tectonic origin of the Kathmandu Basin have resulted in an undulated basement topography. The surface as well as the basement of the basin is quite undulated as shown by previous studies [11,12] (Figure 1.5). There are bedrock exposures protruding through the thick sediments at several places indicating an uneven basin floor. This results in complex basin response making the generalisation of seismic characteristics difficult. Hence a detailed 3-D structure of the basin is necessary so that the seismic response of different areas can be correctly ascertained. A proper understanding of underground structure and seismic characteristics of the basin are necessary to further engineering study in the Kathmandu Basin.

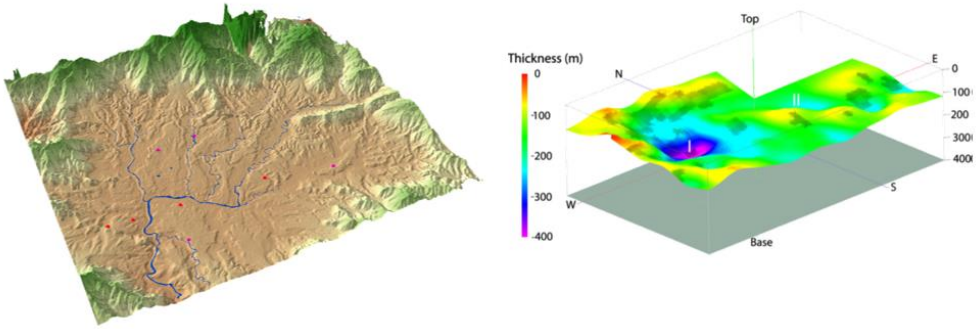

Figure 1. 5 Surface and basement topography[12] of the Kathmandu Basin.

This is necessary because, researchers have pointed out that the western part of the Himalaya has not seen a large earthquake in more than 300 years. The 300 years' worth of accumulated stress increases the probability of a large earthquake in the future. In 2005 it was indicated that an earthquake worth of 7.4 magnitude was pending [13] in the exact region where the 2015 Gorkha earthquake occurred. It is being pointed out that the region west of Gorkha is a 'seismic gap' and a mega earthquake is pending due to the large accumulated stress.

As an earthquake cannot be predicted, the country should brace for the future quakes and take good measures in construction of resilient infrastructures to minimise the damage and number of casualties.

1.4 OBJECTIVES

The present study try to properly ascertain the underground structure and seismic characteristics of the Kathmandu Basin so that the information can be used for further works to mitigate the earthquake damage. To understand the strong-motion characteristics of the basin, Hokkaido University with collaboration of Tribhuvan University, Nepal installed four strong-motion seismometers, KTP, TVU, PTN, and THM in Kathmandu. Four more temporary stations, BKT, RNB, PPR, and KPN were added after the Gorkha earthquake for three months (Figure 1.3). The present study is a part of the ongoing research.

The objectives of the present study can be outlined as follows:

- To understand the basic geological and tectonic setting of Kathmandu
- To analyse strong motion records and understand the seismic characteristics of the Kathmandu Basin sediments
- To estimate 1-D velocity models of sediments under the seismic stations using geological and borehole data
- To tune the 1-D velocity structures by forward modelling of earthquake records
- To prepare a 3-D underground velocity model of the basin using available geological, geophysical, and borehole data.
- To simulate ground motion in the basin by finite difference method using the 3-D velocity model and compare synthetic waves with the observed records to check the accuracy of the model.

1.5 DATA SOURCE

The strong motion data required for the study are records from the eight strong-motion seismometers in the basin. The initial 1-D and 3-D models are based on the available geological map, cross-sections, shallow borehole logs and gravity anomaly data. The data regarding earthquake parameters are obtained from websites of USGS[14] and GCMT[15]. Most of the figures presented here are prepared using the Generic Mapping Tool (GMT)[16].

1.6 STRUCTURE OF THE THESIS

This thesis consists of six chapters. Chapter I is the Introduction with description of the background, study area and objective of the study. The next chapter (Chapter II) deals with geo-tectonics of Nepal Himalaya and geological setting of the Kathmandu Basin. The chapter will generally describe the geological information which were used for the preparation of the underground structure. Chapter III is the study of earthquakes occurred near Kathmandu to comprehend the seismic characteristics of the basin. It also deals with the damage the 2015 earthquake caused around the seismic stations. Chapter IV is the estimation of 1-D velocity models under the seismic stations by forward modelling of the observed seismic waves. Two different methods are employed to tune the 1-D velocity models using earthquake records. Chapter V mainly focusses on the preparation of 3-D underground velocity structure using the geological data and the ground motion simulation using the structure. It presents and validates the model by comparison of synthetic waveform with the observed waveform. Finally, Chapter VI concludes the theme of the thesis and discusses the results of the present study.

References

[1] Feldl, N. & Bilham, R. Great Himalayan earthquakes and the Tibetan plateau. *Nature* **444**, 165-170, doi:10.1038/nature05199 (2006).

[2] Patriat, P. & Achache, J. India-Eurasia collision chronology has implications for crustal shortening and driving mechanism of plates. *Nature* **311**, 615-621 (1984).

[3] Bilham, R. Location and magnitude of the 1833 Nepal Earthquake and its relation to the rupture zones of contiguous great Himalayan earthquakes. *Current Science* **69**, 101-128 (1995).

[4] Sapkota, S. N. *et al.* Primary surface ruptures of the great Himalayan earthquakes in 1934 and 1255. *Nature Geoscience* **6**, 71-76 (2013).

[5] Avouac, J. P. in *Treatise on Geophysics* (ed Gerald Schubert) 377-439 (Elsevier, 2007).

[6] Dixit, A. M., Yatabe, R., Dahal, R. K. & Bhandary, N. P. Initiatives for earthquake disaster risk management in the Kathmandu Valley. *Natural Hazards* **69**, 631-654, doi:10.1007/s11069-013-0732-9 (2013).

[7] Government of Nepal. *Nepal Disaster Risk Reduction Portal*, <http://drrportal.gov.np/> (2015).

[8] Pandey, M. R. in *12th World Conference on Earthquake Engineering* (Auckland, New Zealand, 2000).

[9] Shrestha, O. M. *et al.* (Department of Mines and Geology, Kathmandu, 1998).

[10] Central Bureau of Statistics. National population and housing census 2011. (Kathmandu, 2012).

[11] Moribayashi, S. & Maruo, Y. Basement topography of the Kathmandu valley, Nepal- An application of gravitational method of the survey of a tectonic basin in the Himalayas *Journal of Japan Society of Engineering Geology* **21**, 30-37 (1980).

[12] Paudyal, Y. R., Yatabe, R., Bhandary, N. P. & Dahal, R. K. Basement topography of the Kathmandu Basin using microtremor observation. *Journal of Asian Earth Sciences* **62**, 627-637, doi:10.1016/j.jseaes.2012.11.011 (2013).

[13] Bilham, R. & Wallace, K. Future Mw >8 earthquakes in the Himalaya: implications form the 26th Dec 2004 Mw = 9.0 earthquake on India's eastern plate margin. *Geological Survey of India Special Publication* **85**, 1-14 (2005).

[14] USGS. *Earthquake Hazards Program*, <http://earthquake.usgs.gov/> (2015).

[15] GCMT. *Global CMT Catalog Search*, <http://www.globalcmt.org/> (2015).

[16] Wessel, P., Smith, W. H. F., Scharroo, R., Luis, J. & Wobbe, F. Generic Mapping Tools: Improved version released. *EOS, Transactions American Geophysical Union* **94**, 409-410, doi:10.1002/2013EO450001 (2013).

CHAPTER II
TECTONICS AND GEOLOGY OF THE KATHMANDU BASIN

CHAPTER II. TECTONICS AND GEOLOGY OF THE KATHMANDU BASIN

2.1 TECTONICS OF THE NEPAL HIMALAYA

The Nepal Himalaya is a region of active orogeny with crustal shortening and thickening [1] and rapid erosion process owing to long monsoon climate. The collision of the Eurasian and the Indian tectonic plates, considered to have started around 65-45 million years ago [2-4] resulted in formation of the Himalaya and unceasing seismic activities (Figure 2.1) in the region.

Patriat and Achache [2] mentions that the overall movement of the Indian plate in the Himalaya is 50 mm/yr. Feldl and Bilham [3] on the other hand, mentions the rate as 36-40 mm/yr. where half the movement (18-20 mm/yr.) is constrained in the Himalaya, one third in Tibet, and rest between Mongolia and Tibet. The GPS records in the Nepal Himalaya section also show an annual crustal shortening of about 20 mm [1]. This subduction at the active plate boundary is not continuous, but is interrupted by asperities causing a large amount of stress to accumulate. This accumulated stress is released periodically in form of small and large earthquakes. Another method of stress release is by 'aseismic slip' [4] where the stress is released by slow earthquakes and creep rather than as mega earthquakes.

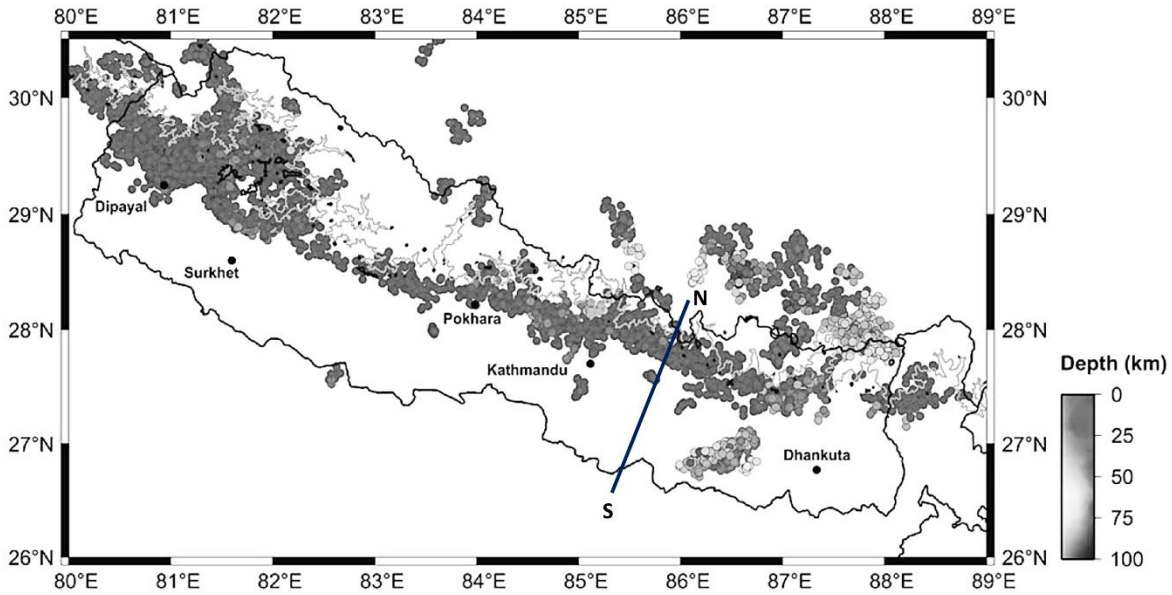

Figure 2. 1 Seismic activity in the Nepal Himalaya shown by epicentres of earthquake exceeding local magnitude of 1 from 1995-2003. The line N-S is the line of cross-section for Fig 2.2. (Modified from Dhital [5] and [6]).

The crustal shortening as a result of collision gave rise to a series of E-W trending regional thrusts running along the length of the entire Himalaya (Figure 2.2). These E-W trending regional thrusts are Main Central Thrust (MCT), Main Boundary Thrust (MBT), and Main Frontal Thrust (MFT) respectively from north to south. The formation of these faults were also in the same order. The MCT, the first thrust to break the Indian crust might have been active from around 23 to 12 million years [7]. The MBT, formed after the MCT, is supposed to have been active from 10 ma [8] to around 5 ma [9]. The MFT is the only active thrust (less than 2 ma) at present and it accommodates the movement of the Indian plate. These three regional thrusts continue to the depth to form the gently sloping decollement zone known as the Main Himalayan Thrust (MHT) (Figure 2.2).

The surface rupture of an earthquake, given the earthquake is strong enough to produce one, should be visible along the MFT, or the northern extreme of the foreland basin. The surface rupture of the great 1934 Nepal-Bihar Earthquake was discovered along the MFT in south-Nepal [10,11].

In addition to these thrust, there is a normal fault beyond the Himalaya termed as South Tibetan Detachment (STD) or North Himalayan Normal Fault which separates the Himalayan rocks from the Tethys sediments (Figure 2.2). Tethys is the sea that once existed between the Indian and Eurasian plate before the collision. The Tethys Sea deposits are found along the margin of the plates around the Indus-Tsangpo suture zone (ITSZ) [12]. Numerous N-S trending faults have also formed apart from these regional thrusts as a result of ongoing collision.

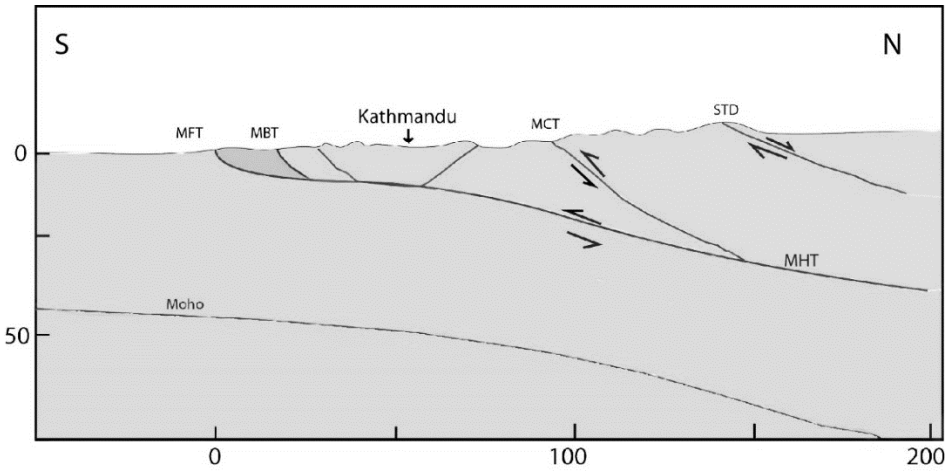

Figure 2. 2 Simplified cross-section of the Nepal Himalaya along N-S in Figure 2.1 showing the major tectonic lineaments. Redrawn from Avouac [1].

Seeber and Armbruster [13] proposed a blind fault on the south of the MFT due to huge damage that occurred in the area during 1934 earthquake. Avouac [1], on the other hand refutes the claim indicating that the extensive damage was due to the local site effect rather than a movement along blind fault.

2.2 GENERAL GEOLOGY OF THE KATHMANDU BASIN

The Nepal Himalaya is fundamentally divided into four east-west extending geological regions along with a foreland basin of Indo-Gangetic plain (Terai) in the south. The geological regions including the foreland basin, from south to north, are Terai, Siwaliks (Churia), Lesser Himalaya, Higher Himalaya, and the Tethys Himalaya [5].

The regional Himalayan faults are important part of this geo-tectonic classification. The MFT marks boundary between the Terai plain and the Siwalik. The Terai plain is the foreland basin consisting of recent fluvial deposit brought by rivers originating and passing through the Himalayas. The sedimentary rocks of the Siwalik are separated from the Lesser Himalayan weakly metamorphosed rocks by the MBT. The Siwalik was the foreland basin in the geological past before the origin of the MFT. The crustal shortening along the MFT resulted in the rapid uplift of the Siwalik region. The northern thrust, MCT divides Lesser Himalayan rocks and the high-grade metamorphic rocks of the Higher Himalaya. Though continuous all along the Himalaya, the MCT branches off at some places giving rise to several complex nappe structures (like Kathmandu) in the region. Nappe is the geological term for a large sheet-like body of rock that has been moved as a result of movement along the thrust faults. The STD in further north, separates the sedimentary rocks of the Tethys Himalaya from that of the Higher Himalaya.

Kathmandu is an intermontane basin filled with fluvio-lacustrine sediment. It is surrounded by mountain ranges of the Lesser Himalaya. and is drained by the Bagmati River with a high valley floor which originates in the Lesser Himalaya unlike other large rivers which have their source in the Higher

Himalaya or the Tibetan Plateau [14]. In the Pleistocene, about 2.5Ma, the rapid uplift of the mountain range south of present-day Kathmandu (Mahabharat Range in Lesser Himalaya) dammed the proto-Bagmati River [15] to form a lake [16]. The tectonic origin of the Kathmandu Basin by crustal shortening rather than by subsidence is the reason behind the undulated basin topography. In due time, the lake breached the hills and eventually dried out about 10ka [17] leaving a basin filled with sediments. These basin sediments have their origin in the basement rocks of the surrounding mountains of the Lesser Himalaya.

The geology of Kathmandu thus can essentially be described as the Basement rocks and the Basin-fill sediments.

2.2.1 Basement rocks

The basement rocks under and around the basin-fill sediments belong to the Lesser Himalaya between the MBT and MCT. These rocks are part of the Mahabharat Synform [5] whose core passes through south of the Kathmandu Basin. Geologically the rocks are classified under the Bhimphedi Group and Phulchauki Group in the Kathmandu Complex [18]. These rocks form the Phulchauki, Chandragiri, and Shivapuri mountain range that surround the Kathmandu Basin.

Bhimphedi Group

The Bhimphedi Group of rocks are attributed to be formed in the Pre-Cambrian. The lithology in this group consists of hard metamorphic rocks like schist, quartzite, and marble. Though there are six formations in the group, only two of them; the Kulikhani Formation and the Markhu Formation, are found in the mountains surrounding the basin in north and east.

Phulchauki Group

The Phulchauki Group of rocks overlie the Bhimphedi Group. It is divided into five formations: Tistung Formation, Sopyang Formation, Chandragiri Formation, Chitlang Formation, and Godavari Limestone. These rocks bound the Kathmandu Basin from south and west (Figure 2.3). The main rock types of this group is meta-sedimentary and weak rocks like limestone, dolomite, slate, and phyllite. The age of these rocks are attributed to be Cambrian to Devonian.

The Shivapuri mountain range lying to the north of the basin however is formed by an intrusive body of gneiss named Sheopuri Injection Complex or Sheopuri Gneiss.

As most of the rock types of Bhimphedi Group lie outside the watershed of the Bagmati River, majority of the sediments in the Kathmandu Basin came from the rocks of the Phulchauki Group and the Sheopuri Gneiss [19].

Though the basin is filled with soft fluvio-lacustrine deposit, the basement topography is highly undulated and there are several rocky hillocks that breach through the sediment to the surface as bedrock exposures [5]. Moreover, the boreholes data collected by JICA [20] show rocks at shallow depth at some sites in the basin.

2.2.2 Basin-fill sediments

The sediment of the Kathmandu Basin is Plio-Plistocene with fluvial, fluvio-lacustrine, and fluvio-deltaic origin [5]. The depth of this sediment can be about 600 m at the thickest part: The gravimetric survey of Moribayashi and Maruo [21] show the central part to be 650 m deep and a borehole by Department of Mines and Geology, Nepal reached a depth of 550 m before encountering bedrock near the centre of the basin [19,20].

Table 2. 1 Correlation of geological classification of the Kathmandu Basin, from Sakai [17]

<table>
<tr><th colspan="3" rowspan="2">Yoshida and Igarashi [22]</th><th rowspan="2">Dongol [23]</th><th rowspan="2">Shrestha, et al. [24]</th><th colspan="2" rowspan="2">Sakai, et al. [25]</th><th colspan="2">Sakai [17]</th></tr>
<tr><th>Southern part</th><th>Central part</th></tr>
<tr><td colspan="3">Patan Fm</td><td rowspan="3">Kalimati Clays</td><td rowspan="5">Gokarna Fm, Tokha Fm, Kalimati Fm and Chapagaon Fm</td><td colspan="2" rowspan="3"></td><td rowspan="5">Itaiti Fm</td><td>Patan Fm</td></tr>
<tr><td colspan="3">Thimi Fm</td><td rowspan="4">Kalimati Fm</td></tr>
<tr><td colspan="3">Gokarna Fm</td></tr>
<tr><td colspan="3">Boregaon Terrace Deposit</td><td rowspan="3">Champi-Itahari Gravel</td><td rowspan="4">Lukundol Formation</td><td rowspan="3">Upper Member</td></tr>
<tr><td colspan="3">Chapagaon Terrace Deposit</td></tr>
<tr><td rowspan="8">Lukundol Fm</td><td rowspan="8">Member</td><td>VII</td></tr>
<tr><td>VI</td></tr>
<tr><td>V</td><td rowspan="4">Nakhu Khola mudstone and Kaseri Nayankhandi Lignite</td><td rowspan="4">Lukundol Fm and Kobagaon Fm</td><td rowspan="4">Middle Member</td><td rowspan="4">Lukundol Fm</td><td rowspan="4">Basal Lignite Member</td></tr>
<tr><td>IV</td></tr>
<tr><td>III</td></tr>
<tr><td>II</td></tr>
<tr><td>I</td><td rowspan="2">Tarebhir Basal Gravel</td><td rowspan="2">Basal Boulder Bed</td><td rowspan="2">Lower Member</td><td rowspan="2">Tarebhir Fm</td><td rowspan="2">Bagmati Fm</td></tr>
<tr><td colspan="2"></td></tr>
</table>

The geological classification of the Kathmandu Basin sediments vary depending on the researchers [17,22-24]. Table 2.1 correlates geological classifications proposed by different authors. The geological map (Figure 2.3) is redrawn from the map published by the Department of Mines and Geology (DMG) based on Shrestha, et al. [24].

Sakai [17] later proposed the new classification based on field work and few boreholes inside the basin. According to him, the lithology of the sediments varies from south to north depending on the origin of sediments and thus should be differentiated as such. Hence, his classification has separate stratigraphic schemes for the southern, central, and northern part of the basin.

Southern Part

The southern part of the basin is divided into 3 formations: Tarebhir Formation, Lukundol Formation, and Itaiti Formation.

The Tarebhir Formation is the oldest basin sediment [17] and lies above the Cambrian rocks of the Tistung Formation. It consists of river deposit of boulder, cobble, and sand lenses of fluvial origin which are derived from the bedrocks in the south. These sediments are from the proto-Bagmati River system and were deposited before the formation of the lake.

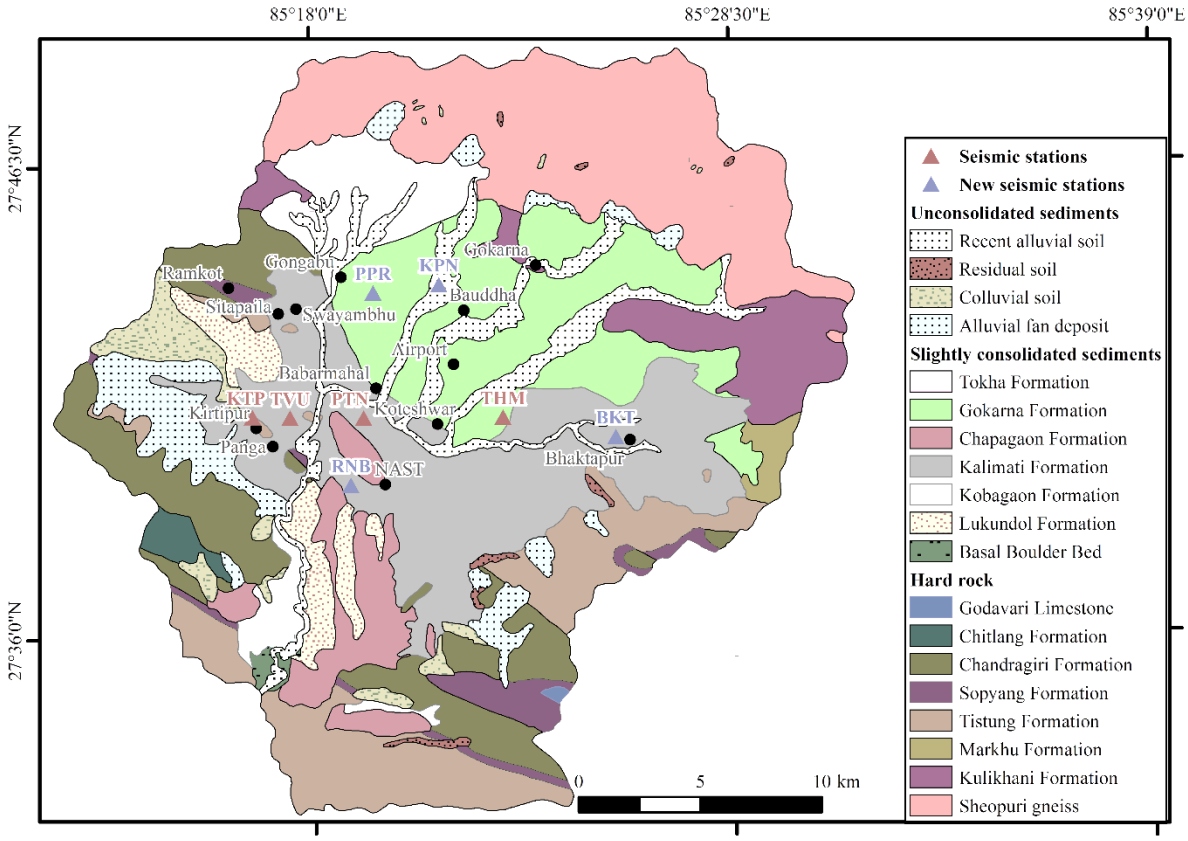

Figure 2. 3 Simplified Geological Map of the Kathmandu Basin (Modified after Shrestha, et al. [24]). Also shown are the locations of strong-motion seismometers used for present study.

Sakai [17] combined both the Nakhu Khola Mudstone and the Kaseri-Nayankhar Lignite of Dongol [23] as well as the Lukundol Formation and the Kobagaon Formation of Shrestha, et al. [24] (Table 2.1) and named it the Lukundol Formation. This formation is comprised of black organic mud and alternating sequence of sand and silt. Occurrence of lignite beds have also been reported in this formation.

Central Part

The Bagmati Formation composed of medium to coarse sand, gravel, and boulder has its provenance in the bedrocks of the northern rim of the basin. These sediments were brought by the drainage system of the proto-Bagmati River [16].

In the central part, the most widely distributed deposit of dark grey carbonaceous clay is termed the Kalimati Formation. The Basal Lignite Member [17] is a thin continuous layer of a lignite bed underlying this formation which is a deposit of shallow water environment. This lignite bed can be considered as the boundary layer between sediments of underlying fluvial and overlying lacustrine facies.

The Thimi Formation [22] is the topmost layer of fluvial sand and mud deposit. The lithology of this sediment shows a fluvial depositional environment after the drying up of the lake [19]. A distinct erosional surface at the bottom of this formation has been reported as well [17].

Northern Part

In the northern part a sand dominant fluvio-lacustrine sediments (the Gokarna Formation) becomes prominent where the clay deposit of the Kalimati Formation pinches out (Figure 2.4). It consists of sand,

silt, clay, and peat layers. The Thimi Formation overrides the Gokarna Formation [17] and contains sand, silt, clay and gravel with gravels exclusively made of gneiss and granite clasts from intrusive rocks of Sheopuri Injection Complex [5].

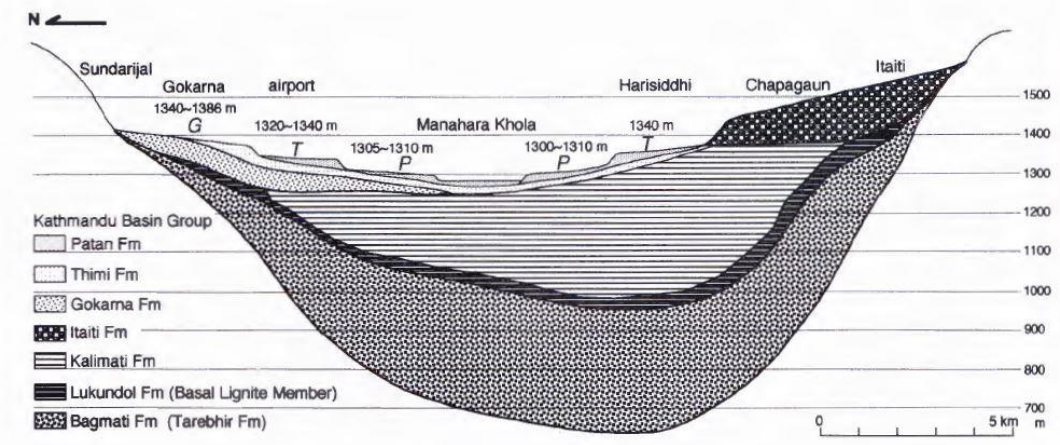

Figure 2. 4 Simplified geological cross section of the Kathmandu Basin, after Sakai [17]

The recent (Holocene) alluvial deposit of 5-15 m are found in the river channels, flood plains, and alluvial fan of the Bagmati River system [22]. These coarse grained sand and silt sediments with high mica content also undoubtedly have their origin in the bedrocks surrounding the basin [19].

2.2.3 Geological structures

The core of the Mahabharat Synform passes south of the Kathmandu Basin and the rocks of Phulchauki Group show extensive faulting and folding at many places. Sakai [17] has mentioned two active faults viz. Chandragiri Fault and Chobhar Fault trending NW-SE in the south of the basin and Nakata, et al. [26] has mentioned nearly E-W trending Kalpu Fault in the north. Sakai [17] surmises that the entire sedimentation of the Kathmandu sediments were controlled by the rough terrain of the basin bottom as well as these active faults.

2.2.4 Basin topography of Kathmandu

There has been but few studies about the basin topography of Kathmandu. Moribayashi and Maruo [21] carried out the Bouguer anomaly study for subsurface mapping of the basin. JICA [20] prepared a database of available borehole data in order to carry out the earthquake disaster mitigation study. Piya [19] used the available borehole data for study of liquefaction hazard in Kathmandu and prepared a number of cross-sections of the basin. Paudyal, et al. [27] performed microtremor observation across the basin to map the basement topography. Sugimura [28] prepared an atlas of geological cross-sections of the Kathmandu Basin based on the geological maps and borehole logs for groundwater study. These study show the undulated basin topography. The observation of bedrock exposures at different places of the Kathmandu Basin like Kirtipur, Pashupati, Gokarna, and Swayambhu also indicate the unevenness of the basement rock topography. The simplified geological cross-section (Figure 2.4) cannot explain this uneven topography, so the complex basement shape will be discussed in more detail in Chapter V.

Though almost all the previous study indicate an uneven basin topography, their result cannot directly be used for the strong motion and seismic response simulation of the basin sediment. As a result, it becomes necessary to construct a 3-D velocity structure of the basin based on the geological information so that ground-motion studies can be carried out.

2.2.5 Geology of the strong- motion stations

One of the strong-motion accelerometers used in this study is installed on a rock site and others over basin sediment. The station KTP is installed near a bedrock exposure. The other three permanent stations TVU, PTN, and THM lie over thick basin deposits.

The station at KTP is on a hill of Kirtipur, a town in western Kathmandu. Bedrock exposures at shallow depth are visible at many places of this town. The locals have observed that the effect of earthquake on this town is less than in other parts of Kathmandu as it lies over bedrock. The rocks are meta-sandstone and phyllite of the Tistung Formation [24]. The surface-wave analysis carried near the station showed a shear-wave velocity of ~720 m/s [29]. Though detailed structure around this place is not well known due to lack of borehole data, a borehole log near Kirtipur shows bedrock encounter at a depth of 1 m.

The TVU and PTN stations, installed in campus premises in two different locations, also lack deep borehole data near them. The available data [19,20] on both these stations are about a kilometre away and they show sediment depths to more than 150 m. A 315m deep borehole [20] about 50 m north of THM shows dominance of sand and clay sediments but it doesn't reach the bedrocks. The shear-wave velocity measurement reveals Vs~ 200 m/s for TVU, PTN, and THM sites indicating that they lie over soft sediments. The surface geological map (Figure 2.3) shows TVU and PTN on the Kalimati Formation and THM on the Gokarna Formation.

The other four temporary stations BKT, RNB, PPR, and KPN also were installed above the basin sediments. Geologically, BKT, RNB, and PPR lie over the Kalimati Formation whereas KPN lies above the Gokarna Formation. There are no available borehole logs near the first three stations, but a borehole log near KPN show sandy top layer with bedrock at a depth of around 100 m.

References

[1] Avouac, J. P. Mountain building, erosion, and the seismic cycle in the Nepal Himalaya. *Advances in Geophysics* **46**, 1-80, doi:10.1016/S0065-2687(03)46001-9 (2003).

[2] Patriat, P. & Achache, J. India-Eurasia collision chronology has implications for crustal shortening and driving mechanism of plates. *Nature* **311**, 615-621 (1984).

[3] Feldl, N. & Bilham, R. Great Himalayan earthquakes and the Tibetan plateau. *Nature* **444**, 165-170, doi:10.1038/nature05199 (2006).

[4] Bilham, R. Location and magnitude of the 1833 Nepal Earthquake and its relation to the rupture zones of contiguous great Himalayan earthquakes. *Current Science* **69**, 101-128 (1995).

[5] Dhital, M. R. *Geology of the Nepal Himalaya - Regional Perspective of the Classic Collided Orogen*. 498 (Springer International Publishing 2015).

[6] Rajaure, S. *et al.* Double difference relocation of local earthquakes in the Nepal Himalaya. *Journal of Nepal Geological Society* **46**, 133-142 (2013).

[7] Upreti, B. N. An overview of the stratigraphy and tectonics of the Nepal Himalaya. *Journal of Asian Earth Sciences* **17**, 577-606, doi:http://dx.doi.org/10.1016/S1367-9120(99)00047-4 (1999).

[8] Meigs, A. J., Burbank, D. W. & Beck, R. A. Middle-late Miocene (>10 Ma) formation of the Main Boundary thrust in the western Himalaya. *Geology* **23**, 423-426, doi:10.1130/0091-7613(1995)023<0423:mlmmfo>2.3.co;2 (1995).

[9] DeCelles, P. G. *et al.* Neogene foreland basin deposits, erosional unroofing, and the kinematic history of the Himalayan fold-thrust belt, western Nepal. *Geological Society of America Bulletin* **110**, 2-21, doi:10.1130/0016-7606(1998)110<0002:nfbdeu>2.3.co;2 (1998).

[10] Sapkota, S. N. *et al.* Primary surface ruptures of the great Himalayan earthquakes in 1934 and 1255. *Nature Geoscience* **6**, 71-76 (2013).

[11] Bollinger, L. *et al.* Estimating the return times of great Himalayan earthquakes in eastern Nepal: Evidence from the Patu and Bardibas strands of the Main Frontal Thrust. *Journal of Geophysical Research: Solid Earth* **119**, 7123-7163, doi:10.1002/2014jb010970 (2014).

[12] Avouac, J. P. in *Treatise on Geophysics* (ed Gerald Schubert) 377-439 (Elsevier, 2007).
[13] Seeber, L. & Armbruster, J. G. in *Earthquake Prediction* 259-277 (American Geophysical Union, 1981).
[14] Yonechi, F. A preliminary report on the geomorphology of Kathmandu valley, Nepal. 153-161 (Tohoku University, 1973).
[15] Sakai, H., Fujii, R. & Kuwahara, Y. Changes in the depositional system of the Paleo-Kathmandu Lake caused by uplift of the Nepal Lesser Himalayas. *Journal of Asian Earth Sciences* **20**, 267-276, doi:http://dx.doi.org/10.1016/S1367-9120(01)00046-3 (2002).
[16] Hagen, T. Report on the geological survey of Nepal. Vol 1: Preliminary reconnaissance *Denkschiiften der Schweizerischen Naturforschenden Gesellschaft* **Band LXXXVI/1**, 185 (1969).
[17] Sakai, H. Stratigraphic division and sedimentary facies of the Kathmandu Basin Group, central Nepal. *Journal of Nepal Geological Society* **25**, 19-32 (2001).
[18] Stocklin, J. & Bhattarai, K. D. Geology of Kathmandu area and central Mahabharat Range, Nepal Himalaya. 86p (HMG/UNDP Mineral Exploration Project, Kathmandu, 1977).
[19] Piya, B. K. *Generation of a geological database for the liquefaction hazard assessment in Kathmandu valley* M.Sc thesis, International Institute for Geo-Information and Earth Observation (ITC), (2004).
[20] JICA. The study of earthquake disaster mitigation in the Kathmandu valley, Kingdom of Nepal. (Japan International Cooperation Agency and Ministry of Home Affairs Nepal, Kathmandu, 2002).
[21] Moribayashi, S. & Maruo, Y. Basement topography of the Kathmandu valley, Nepal- An application of gravitational method of the survey of a tectonic basin in the Himalayas *Journal of Japan Society of Engineering Geology* **21**, 30-37 (1980).
[22] Yoshida, M. & Igarashi, Y. Neogene to Quaternary lacustrine sediments in the Kathmandu valley, Nepal. *Journal of Nepal Geological Society* **4**, 73-100 (1984).
[23] Dongol, G. M. S. Geology of the Kathmandu fluviatile lacustrine sediments in the light of new vertebrate fossil occurrences. *Journal of Nepal Geological Society* **31**, 43-57 (1985).
[24] Shrestha, O. M. *et al.* (Department of Mines and Geology, Kathmandu, 1998).
[25] Sakai, H., Fujii, R., Kuwahara, Y., Upreti, B. N. & Shrestha, S. D. Core drilling of the basin-fill sediments in the Kathmandu valley for palaeoclimatic study: preliminary results. *Journal of Nepal Geological Society* **25**, 9-18 (2001).
[26] Nakata, T., Iwata, S., Yamanaka, H., Yagi, H. & Maemoku, H. Tectonic landforms of several active faults in the western Nepal Himalayas. *Journal of Nepal Geological Society* **4**, 177-200 (1984).
[27] Paudyal, Y. R., Yatabe, R., Bhandary, N. P. & Dahal, R. K. Basement topography of the Kathmandu Basin using microtremor observation. *Journal of Asian Earth Sciences* **62**, 627-637, doi:10.1016/j.jseaes.2012.11.011 (2013).
[28] Sugimura, Y. (Japan Social Fund, Kathmandu, 2012).
[29] Takai, N. *et al.* Shallow underground structure of strong ground motion observation sites in the Kathmandu valley. *Journal of Nepal Geological Society* **48**, 50 (2015).

CHAPTER III
STRONG-MOTION CHARACTERISTICS AND EFFECT OF 2015 GORKHA EARTHQUAKE IN KATHMANDU

CHAPTER III. STRONG- MOTION CHARACTERISTICS AND EFFECT OF 2015 GORKHA EARTHQUAKE IN KATHMANDU

3.1 SEISMICITY IN NEPAL HIMALAYA

Majority of seismic events, as a result of intermittent stress release in the frontal part of the ramp structure in MHT, are micro-seismic activities concentrated south of the Higher Himalayas around 10-20 km depth [1]. Apart from these small earthquakes, the Nepal Himalaya has seen at least seven earthquakes larger than M7.5 after 1897 [2].

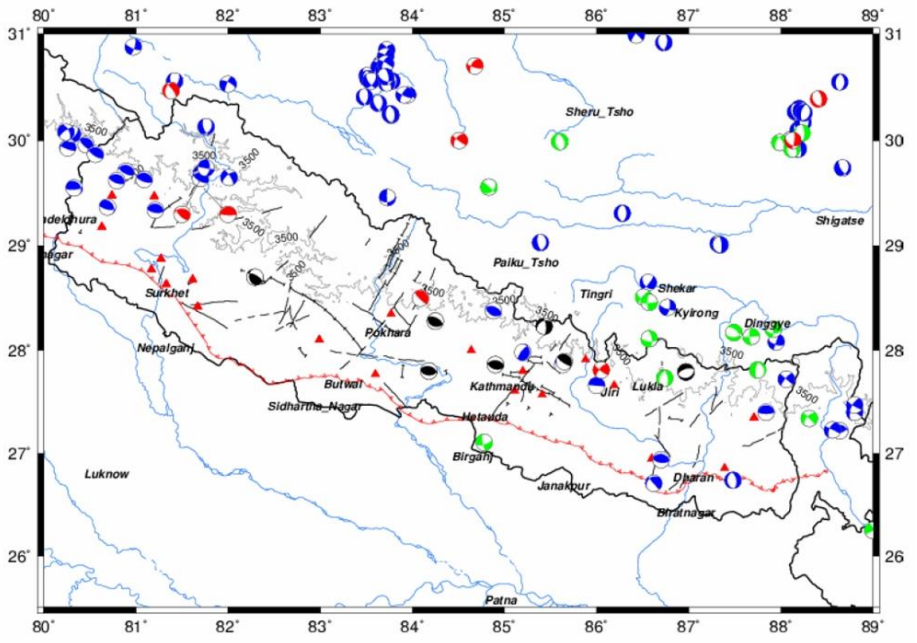

Figure 3. 1 Active faults [3,4] and focal mechanisms [5-7] of earthquakes around Nepal Himalaya. Red line is the surface exposure of the Main Frontal Thrust [8] and grey line is the 3,500 m elevation contour. Modified from Rajaure, et al. [7].

The fault-plane solutions of the past earthquakes indicate E-W trending thrust in the Lesser Himalaya. It has been observed that fault-plane solutions of earthquakes further north are different than that of the southern earthquakes. This is because the maximum compressive stress in the Himalaya is north-south oriented below 3,500 m which leads to thrusting whereas further north, the stress changes to vertical above 3,500 m (Figure 3.1) [9,10].

The very small amount of aseismic creep rate between India and central Nepal in recent years found by GPS measurements [11] led Bilham [12] to point out a possibility of an earthquake with large slip in near future. A study in 2005 indicated stress accumulation in western Nepal that can produce an earthquake of magnitude 7.4 [13]. The 2015 Gorkha Earthquake (M_w 7.8) did occur in the region indicated by the study. The region west of Gorkha lies in the 'seismic gap' where no large earthquakes have occurred after 1505 [14] and this might be where a future large earthquake occurs.

There are not many historical records of earthquake in Nepal before 1833. Nevertheless, one can find mentions of earthquakes in 1255, 1260, 1408, 1681, 1767, 1810, and 1823 in some texts [15]. Even accounts of earthquakes after 1833 are not properly recorded. There are accounts of 1837, 1869, 1897, and 1917 (1918?) earthquakes before the large Nepal-Bihar Earthquake of 1934.

3.2 PAST EARTHQUAKES NEAR THE KATHMANDU BASIN

Based on different studies, following are the short accounts of major earthquakes that occurred near Kathmandu (Figure 3.2) and affected the basin.

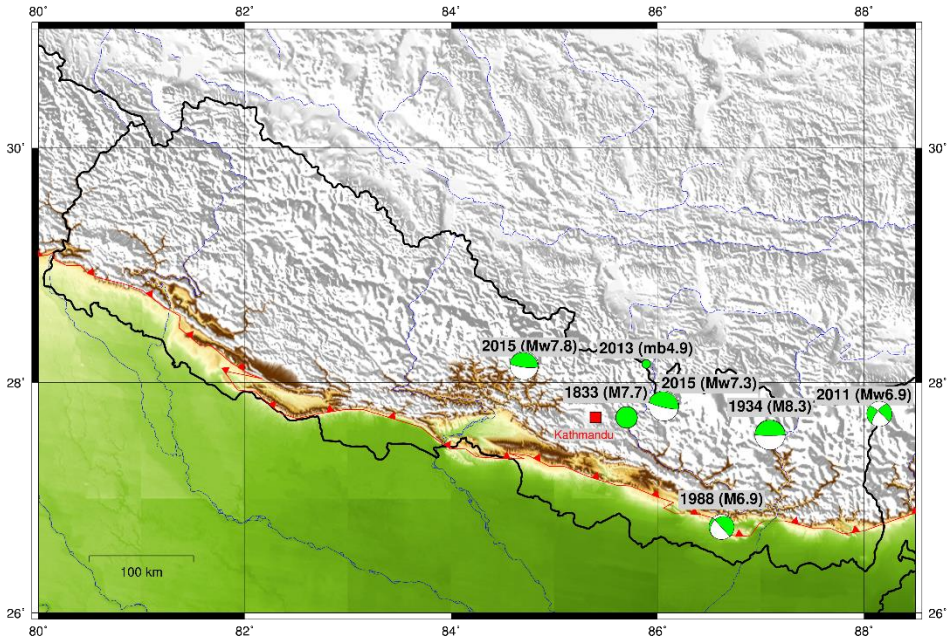

Figure 3. 2 Epicentres of earthquakes around the Kathmandu Basin mentioned in the text. Earthquakes without focal mechanism are shown as only a green circle. The red line is the MFT drawn as in Lave and Avouac [8].

3.2.1. August 26th, 1833 Earthquake (M 7.7)

There are varying accounts about this earthquake's epicentre. Some researchers pointed to the west of Kathmandu whereas some have pointed to east of Kathmandu [12,16-18]. The reported magnitude of this earthquake ranges from M 7.3 to M_w 7.8 depending on the calculation by different authors [12,17-19]. Though, there are no focal mechanism and depth information available, one can infer that this earthquake occurred due to thrusting as other large earthquakes in the Lesser Himalaya do.

Two large foreshocks were reported before the main quake [18] and might have contributed to low number of casualties as foreshocks worked as warning to people. Records mention damage to many houses and temples in Kathmandu, Bhaktapur, and Lalitpur as well as in Banepa, a town east of the Kathmandu Basin [12,17]. Number of casualties in Kathmandu were 414 but about 18,000 buildings were reported damaged [15]. The seismic intensity of this earthquake is considered to be VIII and IX in the Kathmandu Basin [12].

3.2.2. Jan 15th, 1934 Nepal-Bihar Earthquake (M 8.3)

This earthquake is most probably the largest and also the latest one to occur before the 2015 Gorkha earthquake [20]. The confusion about its epicentre remained for about 50 years [21] as some researchers considered the epicentre to be around Bihar, north India [16] due to lot of damage there, whereas other researchers pointed to east Nepal [22-27].

The magnitude of this earthquake ranges from M_w 8 to M_w 8.4 in different literatures [10,22,23,28,29]. Only one instrumental record in India is available where velocity of the earthquake was recorded as 8 m/s which might have been larger in the Kathmandu Basin. The mechanism of the earthquake is

calculated as low-angle thrust similar to other earthquakes in the region [22]. Though exact depth is not available, it can be inferred that the depth was ~30 km as it occurred in the MFT root zone. The MFT in Patu Khola section in Terai plain of east Nepal shows evidence of surface rupture for this earthquake [27,30].

The loss of human life and damage to buildings are clearly recorded [31] for this earthquake. There were 8,519 deaths in Kathmandu (out of 15,000 deaths in Nepal and India). The southern part of Kathmandu and Bhaktapur city in east suffered the heaviest damage (Figure 3.3).

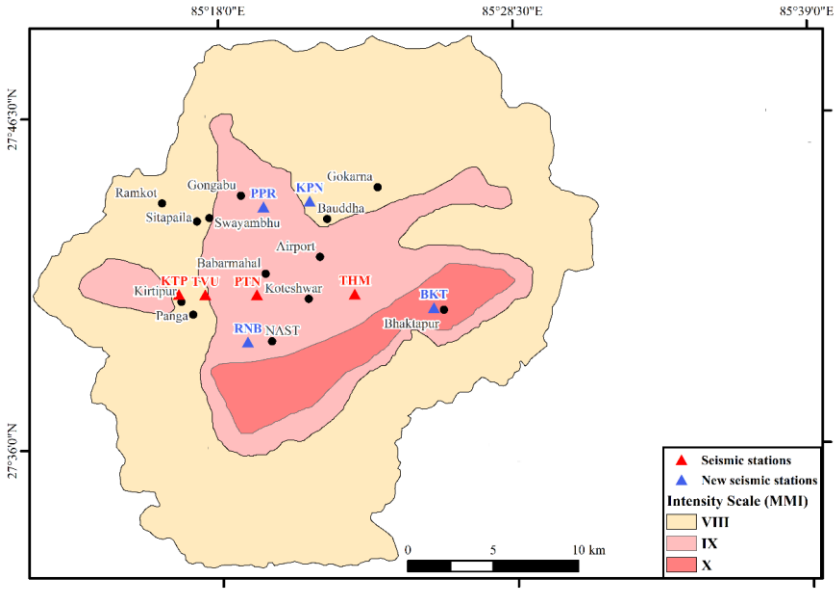

Figure 3. 3 Seismic Intensity (MMI) distribution map of Kathmandu with seismic stations of present study based on Rana [31] and Roy, et al. [32].

3.2.3. August 20th, 1988 Udaypur Earthquake (M_w 6.9)

Most of the earthquakes in the Nepal Himalaya occur in the Lesser Himalayan region but this earthquake occurred in the Siwalik region of south Nepal. The area around the epicentre might be the only active zone in the Siwalik region [33]. The cluster of smaller earthquakes in this area specifies a NE-SW trending major tectonic feature that is oblique to the regional thrusts [33-35]. The size of the earthquake is Ml 6.5 [33] and M_w 6.9 [36] and regarding the depth of this intra-plate earthquake, there are mentions of it being an upper mantle event [33] as well as being a crustal event [35,37].

East Nepal, the Kathmandu Basin, and north and east India suffered most damage during this earthquake including 721 deaths, 6,553 injuries, and 4,470 damaged buildings in Nepal [38]. Bhaktapur city alone had around 1,000 damaged buildings and seven lost lives. Though liquefaction in Terai region were reported at few places, no accounts of liquefaction in the Kathmandu Basin were mentioned [38].

3.2.4. September 18th, 2011 Sikkim Earthquake (M_w 6.9)

The epicentre of this earthquake is Nepal-India border in east Nepal, and was felt in Kathmandu. The magnitude of this earthquake was M_w 6.9 and it occurred at 50 km depth (USGS). It had strike-slip fault focal mechanism and is considered to have occurred in one of the major transverse fault [39]. Many transverse faults found in the Sikkim region [40] can produce large earthquake of this magnitude. Damage to buildings and occurrence of landslides were reported from east Nepal. Inside the Kathmandu Basin, one person lost his life when a wall collapsed as the result of the earthquake.

3.2.5. April 25th, 2015 Gorkha Earthquake (M_w 7.8)

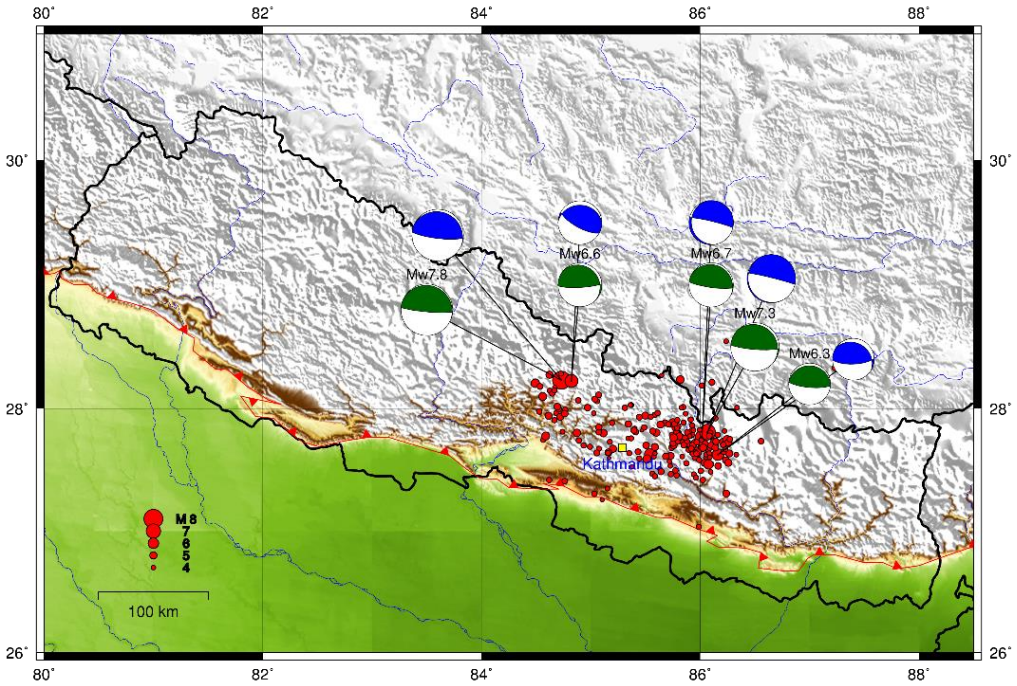

Figure 3. 4 Epicentres of main shock and aftershocks of the 2015 Gorkha Earthquake. Focal mechanisms are shown for the main shock and the major aftershocks. The focal mechanisms in green are as calculated by GCMT [41], and blue as calculated by USGS.

The epicentre of this M_w 7.8 earthquake was in Gorkha district about 80 km west of the Kathmandu Basin. Many authors had shown possibility of a large earthquake in the seismic gap of western Nepal [13,17,42]. The earthquake occurred in a shallow depth of ~8 km. The focal mechanism indicates north dipping thrust at <10° [6,36]. The rupture propagated eastward [43,44] at velocity of ~ 2.9 km/s [45] with multistage rupture [46] and stopped around 90 km east of the Kathmandu Basin where many aftershocks are clustered (Figure 3.4). The earthquake have produced 495 aftershocks larger than Ml 4.0 [47]. The largest one (M_w 7.3) occurred two week later at Sindhupalchowk district, east of Kathmandu.

During the rupture propagation, most of the energy—as well as the slip—were concentrated in the north of Kathmandu [45,48]. The records in GPS stations inside Kathmandu show that the basin experienced a permanent tectonic displacement of 135 cm towards south-southwest (SSW) direction and a vertical uplift of 63 cm [48-50], which is very similar to the displacement records obtained in KTP [51].

The earthquake caused widespread damage in central and east Nepal. Whereas, due to the eastward propagation of the rupture, there were negligible damage in west Nepal. The regions around epicentre of the mainshock and the largest aftershock, Gorkha and Sindhupalchowk, along with the Kathmandu Basin suffered heavy damages. More than 8,000 lives were lost throughout the country. In the Kathmandu Basin alone, about 13% buildings were reported completely damaged and 1,739 people lost their lives [52]. There were reports of ground fissures, avalanches, and landslide in different parts of the country.

Bilham [53] compared this earthquake with the 1833 earthquake and indicated that the 3.5 m slip in the decollement zone (MFT) as a result of this earthquake matches the 180 years' worth of stress accumulation after the 1833 earthquake at a rate of 18 mm/yr.

3.3 STRONG- MOTION CHARACTERISTICS OF THE KATHMANDU BASIN

The location in a seismically active region and the wave amplification due to thick soft sediments, have made the Kathmandu Basin susceptible to seismic damage. An in-depth study of strong-motion characteristics is necessary to address this susceptibility, nevertheless only a few detailed research were carried out before the Gorkha earthquake.

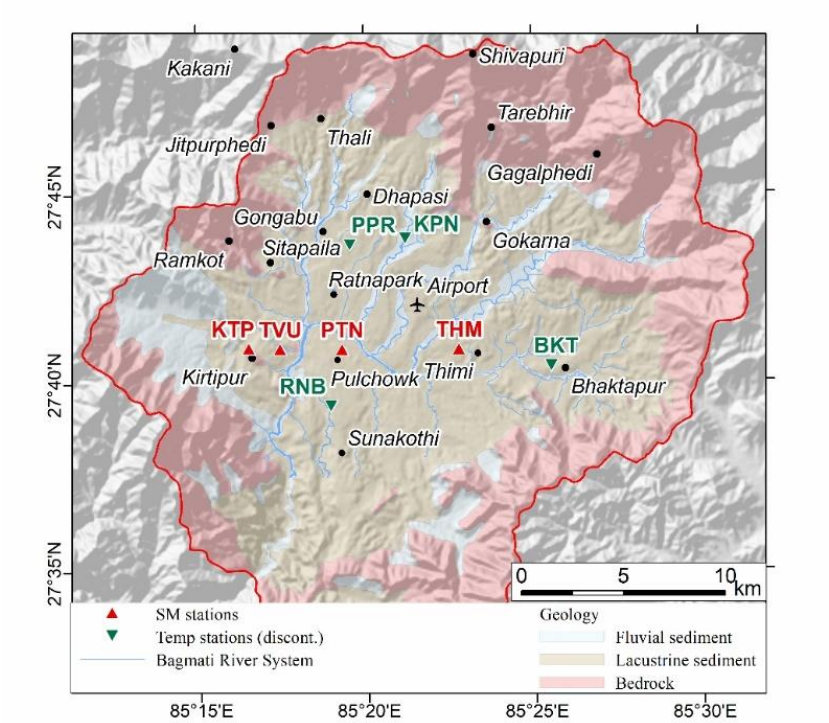

Figure 3. 5 Location map indicating general geology (Shrestha et al1998) and seismic stations in the Kathmandu Basin. Red line marks the boundary of Kathmandu (Bagmati watershed).

In this background, to analyse the strong-motion characteristics of the Kathmandu Basin, four continuous recording accelerometers (Mitsutoyo JEP-6A3-2) were installed in the Kathmandu Basin in 2011 [51] namely KTP, TVU, PTN, and THM in a W-E profile. Bolted to the ground floor of buildings ranging from 1 to 4 story, these accelerometers operate at 100 Hz with GPS time calibration. They recorded a number of earthquakes including the main shock of the Gorkha earthquake on April 25th, 2015 and subsequent aftershocks. After the occurrence of the Gorkha earthquake, four temporary stations; BKT, RNB, PPR, and KPN were deployed (Figure 3.5) for 3 months (May 8th- August 6th, 2015) to observe the aftershock activity. The station KTP is installed over the bedrock site whereas other stations, including the temporary ones, are installed over sediment sites.

3.3.1. Strong- motion observation in the Kathmandu Basin

Though the Kathmandu Basin is filled with soft sediment, the uneven basement topography has a big role in the strong-motion characteristics. The waveform of earthquakes recorded in the basin show high amplification in the sediment site.

If we were to look at the velocity waveform of a moderate earthquake (mb 4.9) of August 30th, 2013 that occurred ~80 km NE of Kathmandu (Figure 3.2), we can see the long excitation of waves in the sedimentary sites. The PGV's are small, nevertheless one can observe the amplification of the waves in the sediment sites (Figure 3.6) when compared to that of the rock site, KTP.

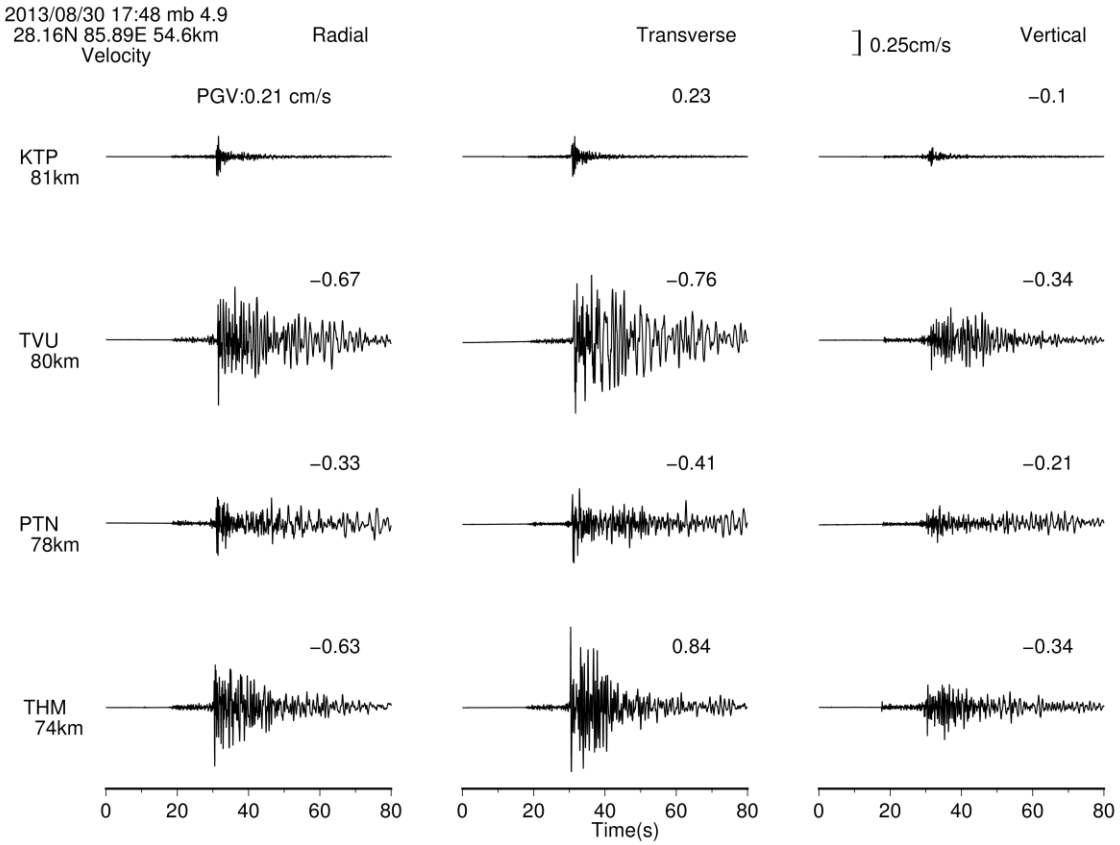

Figure 3. 6 Velocity waveform of the mb 4.9 earthquake.

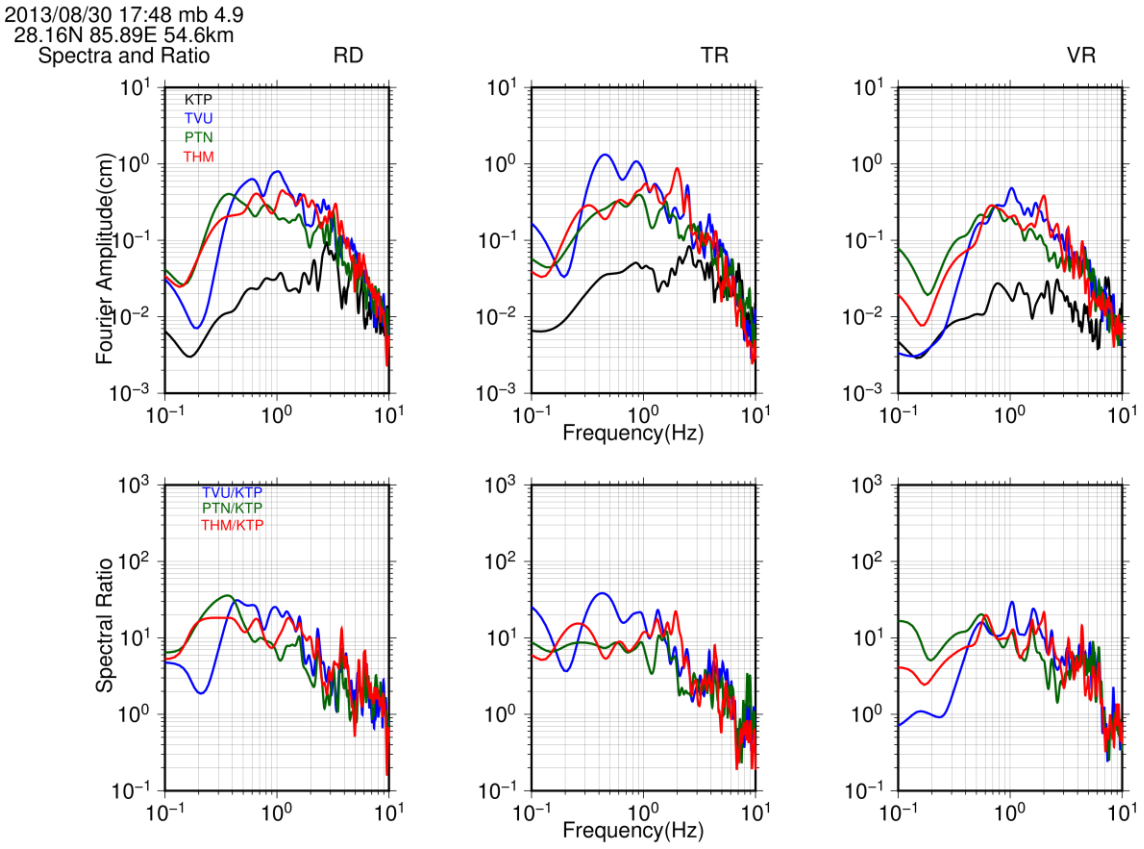

Figure 3. 7 Fourier spectra and Spectral ratio of velocity waveform of the mb 4.9 earthquake.

The Fourier spectra of these records (Figure 3.7) show amplification of low frequency waves in the sedimentary sites. The rapid increase in the slope of Fourier spectra of sediment sites is also noteworthy. The spectral ratio, i.e. the ratio of Fourier spectrum of sedimentary site to that of the rock site also show the wave amplification in longer periods i.e. ~0.4 Hz, ~0.35 Hz, and 0.3 Hz respectively for TVU, PTN, and THM . Similar results are observed when H/V spectral ratio of the ambient noise was used to calculate resonant frequencies: 0.43 Hz, 0.35 Hz, and 0.29 Hz for TVU, PTN, and THM respectively [54].

The main shock of 2015 Gorkha earthquake has an interesting feature. Normally, peak ground accelerations are higher in the sedimentary sites as a result of ground amplification. But, the rock site KTP recorded the highest PGA (Figure 3.8) during this earthquake. However, in the velocity waveform (Figure 3.9), the sedimentary site TVU had the highest PGV. This high PGA value is due to an isolated large ground acceleration spike in KTP record in fault parallel direction, i.e. N117°E (Figure 3.10). We can see that the spike with a frequency of ~4 Hz is not present in other directional components. This spike can be a result of a small event triggered by a large velocity pulse beneath KTP [55] in the fault plane.

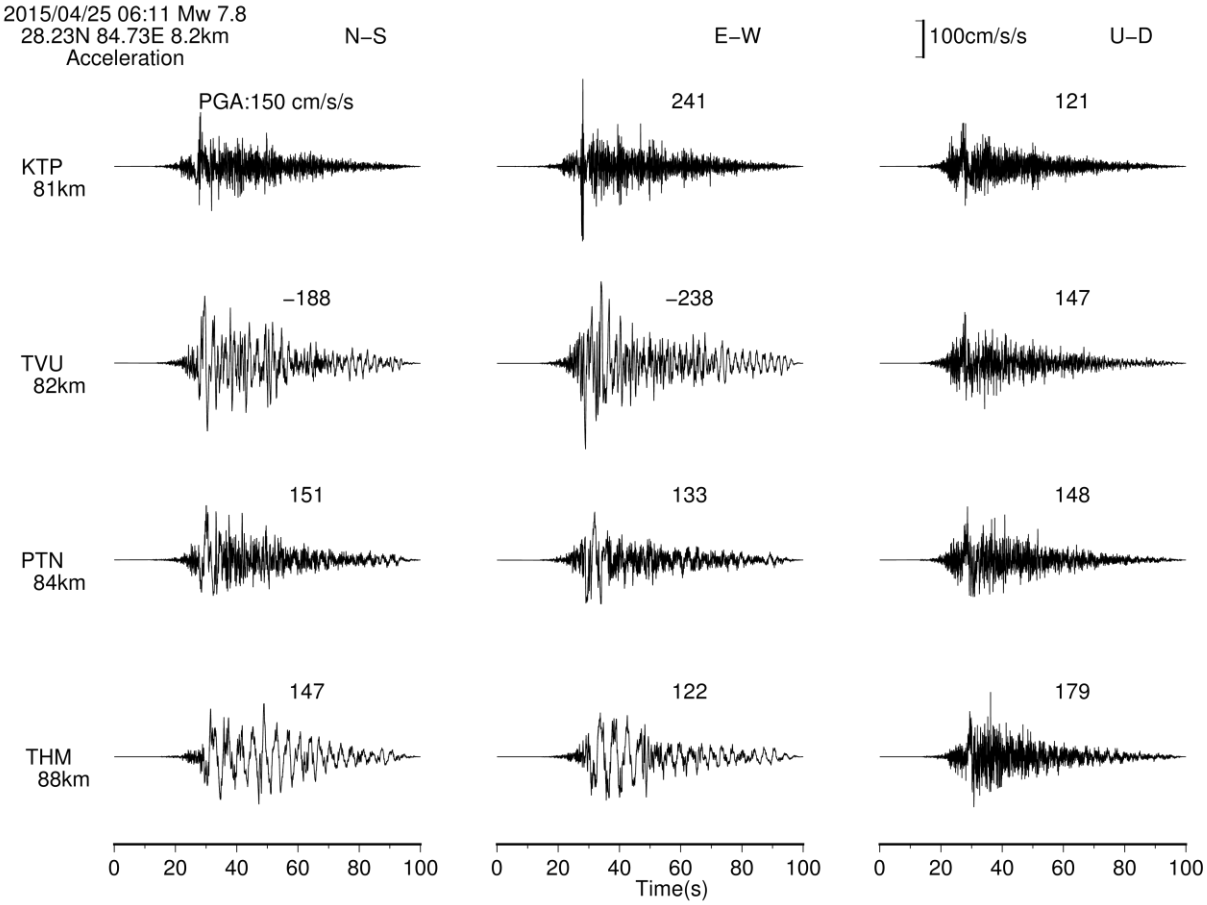

Figure 3.8 Acceleration waveform of main shock of the 2015 Gorkha earthquake (M_w 7.8).

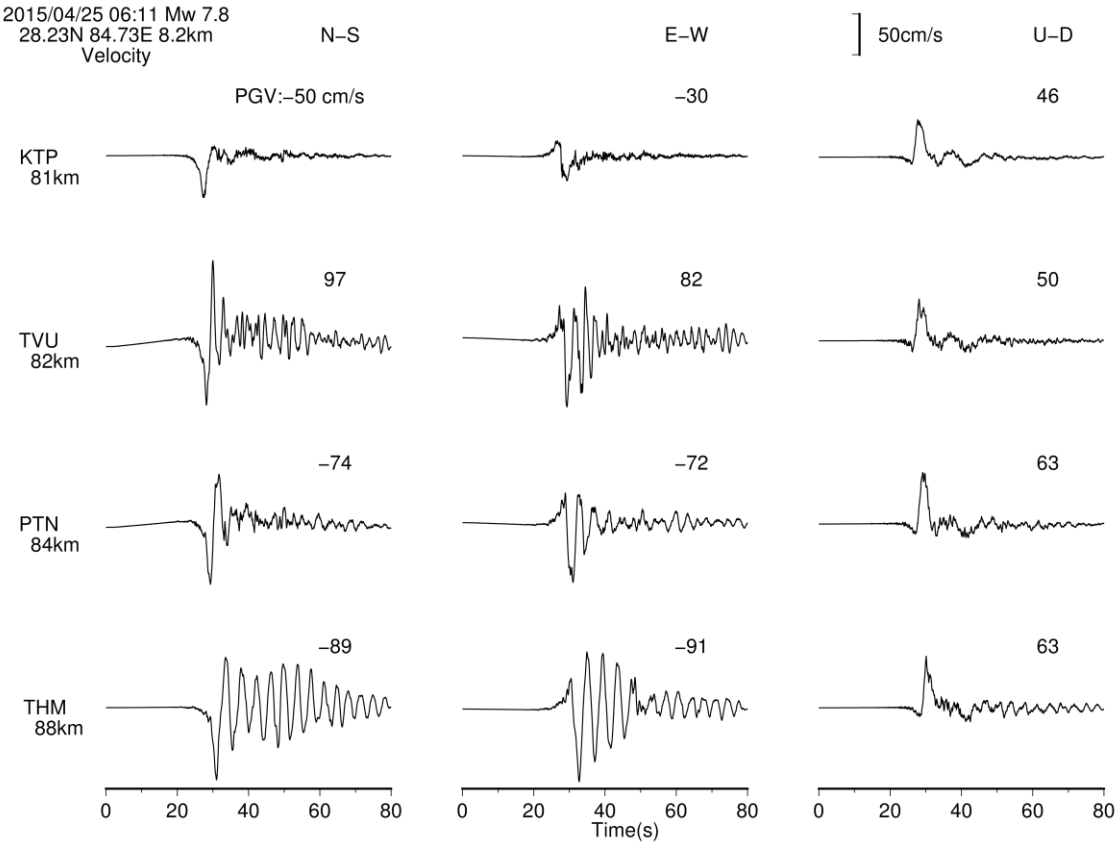

Figure 3. 9 Velocity waveform of main shock of the 2015 Gorkha earthquake.

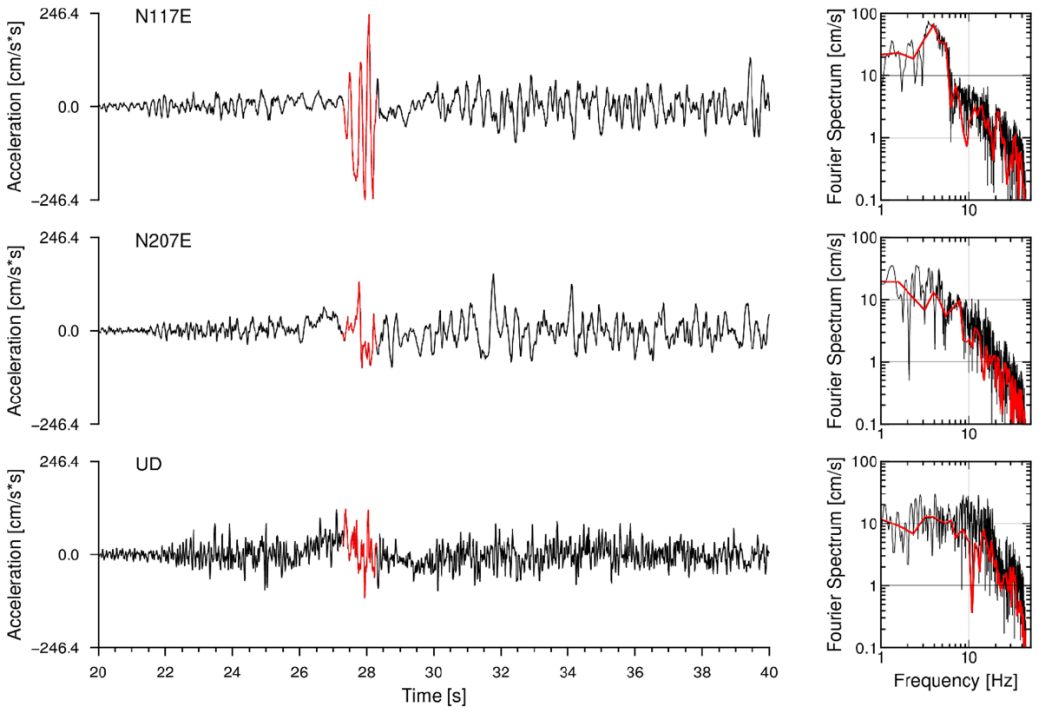

Figure 3. 10 Large isolated acceleration spike in KTP during main shock of the 2015 Gorkha earthquake [55].

Though the acceleration as well as velocity waveform show wave oscillation in sedimentary sites in the horizontal components, the vertical component (UD) looks very similar for all the sites including the rock site KTP (Figure 3.8, 3.9). The velocity waveform show sharp velocity pulse in all stations which can be effect of forward rupture directivity of the tectonic offset [51,56]. The Fourier spectra and spectral ratio (Figure 3.11) of the main shock show significant amplification in the sediment sites in the horizontal component. Nevertheless, amplification is not so prominent in the vertical component. This indicates complicated long-period basin response in the Kathmandu Basin [51].

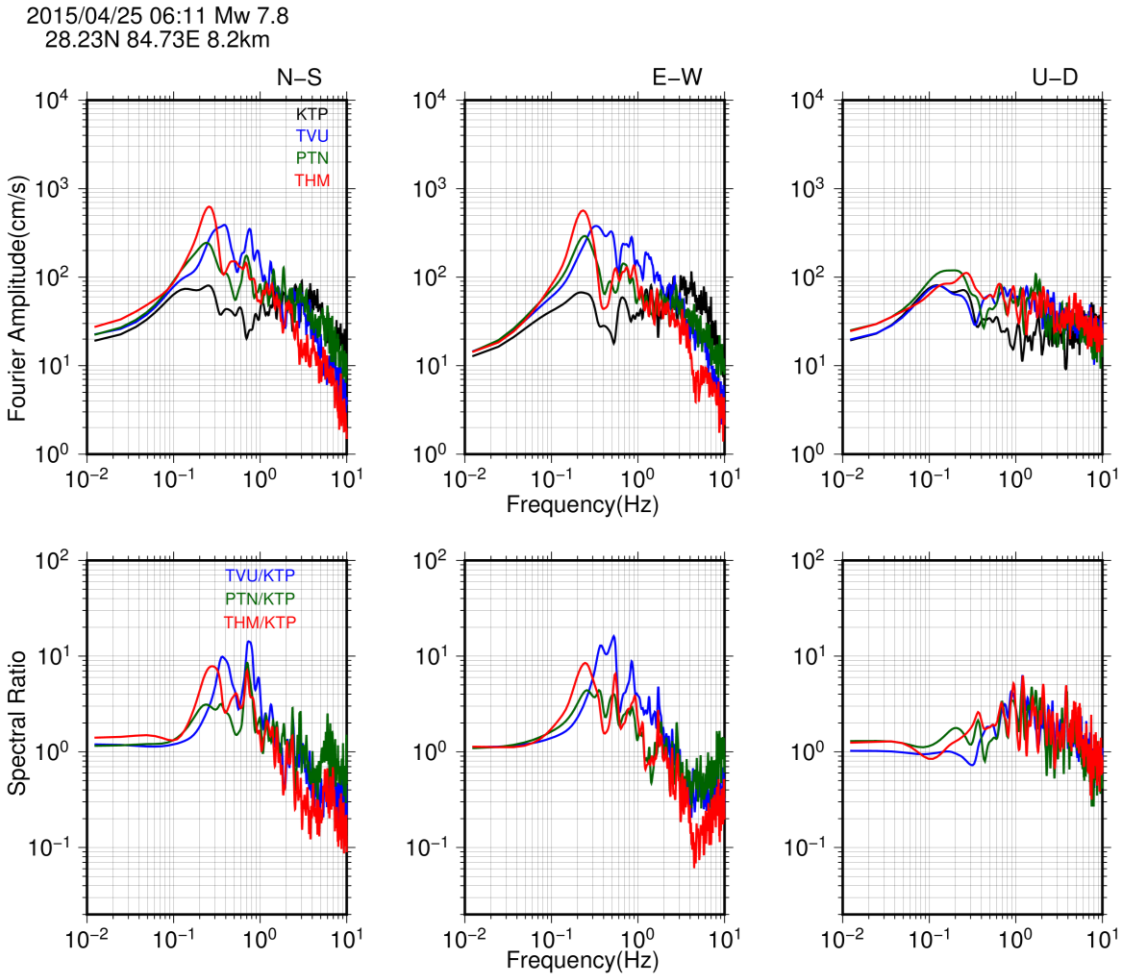

Figure 3. 11 Fourier spectra and spectral ratio of acceleration waveform of main shock of the Gorkha Earthquake (M_w 7.9).

The largest aftershock (M_w 7.3) occurred on May 12th, 2015 after temporary stations were employed so there are records from eight accelerometers for this earthquake (Figure 3.12). The epicentre is about 70 km east of the Kathmandu Basin. The highest PGA (189 cm/s/s) is recorded at the temporary site RNB, south Kathmandu. The envelope of PTN record is rather flat when compared to that of other stations. This phenomenon is also seen in the mb 4.9 earthquake (Figure 3.6). The Fourier spectra and spectral ratio show significant amplification of sedimentary sites in frequencies <0.2 Hz (Figure 3.13). The site KPN (north Kathmandu) however has low amplification in the low frequency range indicating a variation in site effect.

The unevenness of the basin topography is also clear by the fact that despite KTP and TVU being less 2 km apart, their response to earthquake varies widely. The S-wave arrival during mb 4.9 and M_w 7.8 (main shock) earthquakes at KTP is visibly faster than expected [54,57] as the waves have to pass through thick sediments to reach TVU. At KTP, being a rock site, the S-waves arrives faster than they do at TVU.

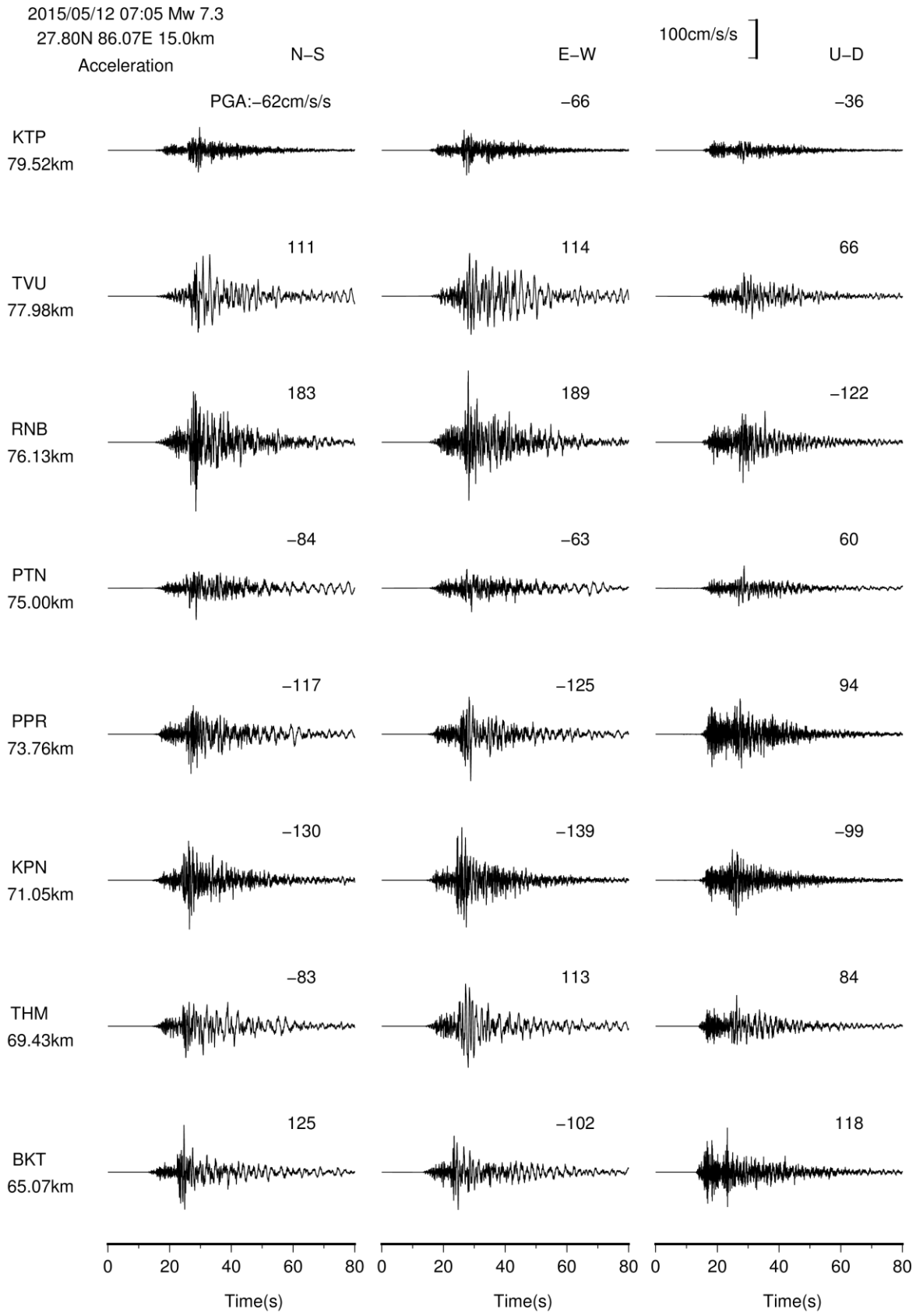

Figure 3. 12 Acceleration waveform of all eight stations during the largest aftershock (M_w 7.3).

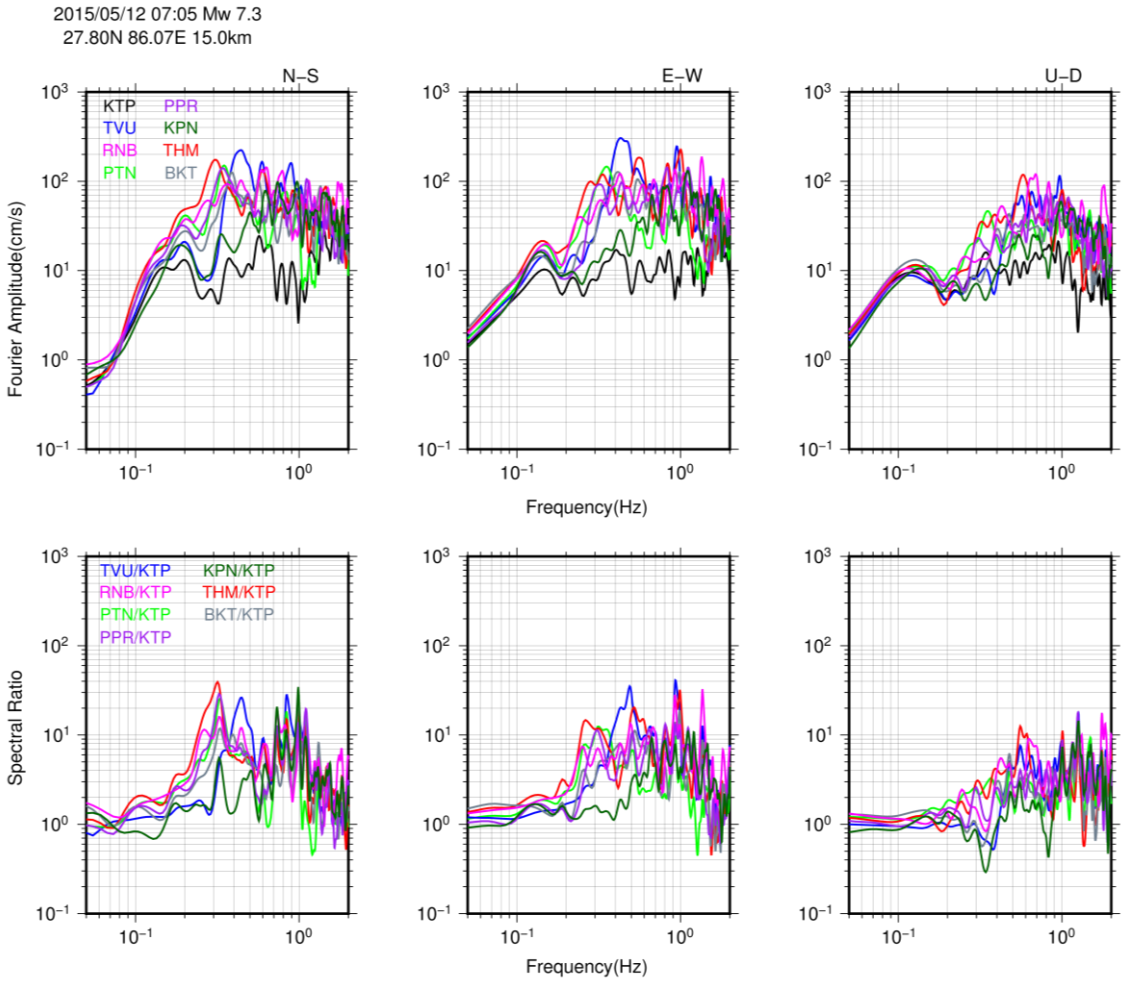

Figure 3. 13 Fourier spectra and spectral ratio of acceleration waveform of the M_w 7.3 earthquake.

3.3.2. Nonlinearity of soil in the Kathmandu Basin

When seismic waves pass from bedrock to the overlying soil layers, they get amplified. Nevertheless, the phenomenon can be different during propagation of strong seismic waves. The strong ground-motion increase shear strain in the soil layers causing reduction of shear rigidity and increase of damping factor as seismic response characteristics of soil becomes nonlinear. It results in reduction of shear wave velocity (V_s) as well as the amplitude of high frequency waves due to augmented damping factor. This phenomenon is termed nonlinearity. The nonlinearity occurs when strong seismic waves propagate through soft and thick layers during large earthquakes. The observation of nonlinearity has been reported in many places around the world during large earthquakes [58,59]. Few authors have reported nonlinearity in Kathmandu during the 2015 Gorkha Earthquake (M_w 7.8) [55,60,61].

The comparison of Fourier spectra of earthquake records from borehole seismometer with those from the surface seismometer directly above can reveal the nonlinearity by showing the damping of higher frequencies in the surface records. The nonlinearity of a soil profile can also be identified by comparison of S-wave horizontal to vertical spectral ratio (S-H/V) of weak-motions with that of a strong-motion [59,62]. This method is useful to examine the nonlinearity in sites lacking a pair of surface and borehole seismometers. Since the Kathmandu Basin doesn't have borehole seismometers to compare the spectra, the S-H/V ratio method is employed. The S-H/V for a number of ~M5 aftershocks (Table 3.1) of the Gorkha earthquake is compared with that of the main shock in the four stations. The time window for weak-motion was selected as 10.24 s after S-wave arrival whereas 20.48 s was considered for the main shock.

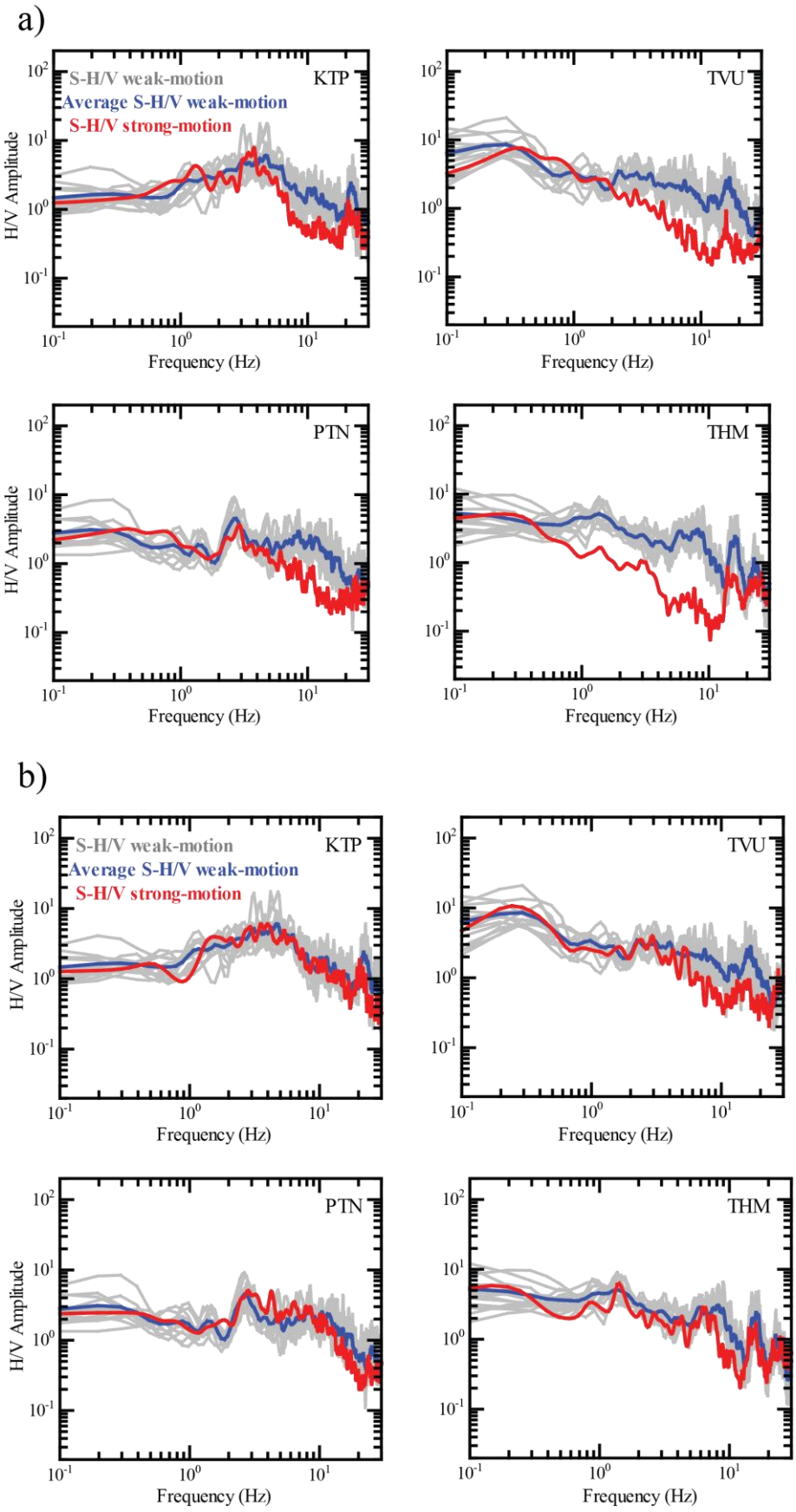

Figure 3. 14 Comparison of S-H/V of strong-motion and weak-motion for a) the main shock M_w 7.8, and b) the largest aftershock (M_w 7.3).

Table 3. 1 Weak- motions (~M 5) earthquakes considered for checking presence of nonlinearity.

SN	Date	Lat	Lon	Dep (km)	Mag.
1	2015-04-25 06:37	27.74N	85.83E	10.0	mb 5.1
2	2015-04-25 06:56	27.88N	85.75E	10.0	mb 5.5
3	2015-04-25 12:44	28.10N	84.56E	10.0	mb 5.2
4	2015-04-25 17:42	28.24N	85.83E	10.0	M_w 5.1
5	2015-04-25 23:16	27.80N	84.87E	13.6	M_w 5.1
6	2015-05-12 07:17	27.71N	86.22E	13.0	mb 5.5
7	2015-05-12 07:34	27.75N	86.24E	10.0	mb 5.4
8	2015-05-12 08:06	27.72N	86.02E	15.0	mb 5.0
9	2015-05-12 08:13	27.76N	85.75E	15.0	mb 5.1
10	2015-05-12 08:21	27.73N	86.13E	15.0	mb 5.2
11	2015-05-12 21:25	27.78N	86.64E	10.0	mb 5.2
12	2015-05-13 21:38	27.72N	86.05E	8.4	mb 5.0
13	2015-05-16 11:34	27.56N	86.07E	7.0	M_w 5.5

It can be clearly observed that the amplitude in the high frequency (> 3 Hz) range in the S-H/V spectra of strong-motion decreased significantly when compared to that of the weak-motions (Figure 3.14a). A parameter 'Degree of nonlinearity of site response (DNL)' is used to quantify the nonlinearity (Equation 3.1). This parameter is summation of difference between S-H/V of strong motion (R_{strong}) and the weak motions (R_{weak}) [59]. The DNL of the main shock is highest in THM (12.7), followed by TVU (11.9) and PTN (8.4). KTP shows the least non-linearity (6.7) which is also apparent from the figure (Figure 3.14a).

$$DNL = \sum \left| \log\left(\frac{R_{strong}}{R_{weak}}\right) \right| . \Delta f \qquad (3.1)$$

The comparison of S-H/V of weak-motions and that of the largest aftershock (M_w 7.3) didn't reveal significant nonlinearity (Figure 3.14b) in TVU, PTN, and THM like during the main shock. The DNL of both the earthquakes along with average horizontal PGA for all four sites are tabulated in Table 3.2. The average PGA in KTP without the large isolated acceleration spike (Figure 3.10) is mentioned in the bracket with an asterisk. Figure 3.15) illustrates larger value of DNL during main shock (M_w 7.8) than during the M_w 7.3 earthquake. The *KTP** in the figure indicates the value of average PGA of KTP without the large isolated acceleration spike. A high value of DNL in the rock site KTP during the main shock necessitates a detailed investigation and discussion regarding the site as well as the source effect.

Table 3. 2 Average horizontal PGA and Degree of Nonlinearity of permanent stations during M_w 7.8 and M_w 7.3 earthquake.

Station	M_w 7.8		M_w 7.3	
	Av. PGA (m/s^2)	DNL	Av. PGA (m/s^2)	DNL
KTP	199 (151*)	6.7	64	2.2
TVU	211	11.9	113	6.9
PTN	138	8.4	74	3.4
THM	139	12.7	98	4.7

The identification of nonlinearity during the mainshock in Kathmandu can also explain the less-than-anticipated damage inside the basin as the higher frequencies affecting the medium- and low-rise buildings were dampened. The main shock records show decreased high-frequency waves and the PGA

estimate from GMPE's were higher than observed PGA [51] which can point towards nonlinearity of the Kathmandu Basin sediments.

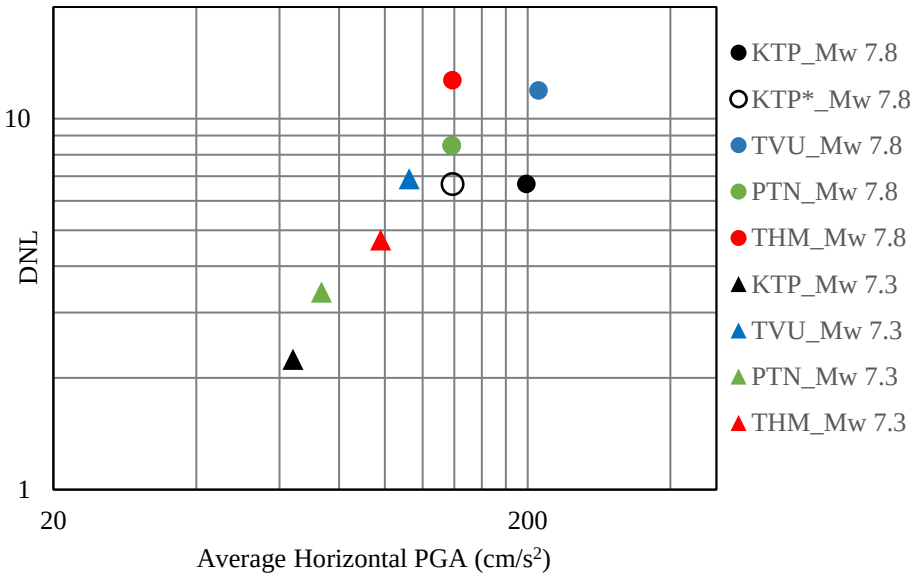

Figure 3. 15 Average Horizonal PGA vs DNL for M_w 7.8 and M_w 7.3 earthquake.

3.4 BUILDING DAMAGE ASSESSMENT AROUND THE SEISMIC STATIONS

The visual damage assessment around the stations helps to compare the direct relationship of strong-motion characteristics and the effect of an earthquake. On May 6th and May 7th, 2015, between the main shock and the largest aftershock, rapid visual damage assessments of buildings in an area inscribed by 200 m radius from the seismic stations was carried out. A few buildings outside the 200 m radius were also considered at some of the sites. The comparison of damage status and strong-motion waves gives the relationship between site response and the situation of damage around the stations. Though this was the first damage assessment of buildings around earthquake stations in Nepal, similar studies were carried out after the 1994 Northridge earthquake, USA [63], 2011 Christchurch earthquake, New Zealand [64], and the 2014 South Napa earthquake, USA [65].

Broadly the buildings in Kathmandu can be classified as load-bearing masonry and RC infill-frame structures. Kathmandu has a fair share of vernacular architectural structures as well as contemporary RC infill-frame structures. The old settlements of Kathmandu have old buildings and monuments built of bricks held together with mud mortar. Though construction practice has changed a lot with time, brick are still predominant construction material: newer buildings use cement as mortar instead of mud. These load-bearing masonry wall structures have low tensile strength and, without adequate members to resist lateral forces, get damaged by out-of-plane as well as in-plane failure of the walls. Construction of RC infill-frame structures started after late 1970s [66] in Nepal and has been the default construction technique for most of the buildings. The RC infill-frame buildings found in Nepal are either designed according to the Mandatory Rules of Thumb (MRT) of the Nepal Building Code (NBC 1994)[67], according to the Indian Building Code, or are poorly designed without engineering supervision. A seismic vulnerability study carried out before the Gorkha earthquake concluded that the poorly designed RC infill-frame buildings were highly vulnerable to earthquakes [66].

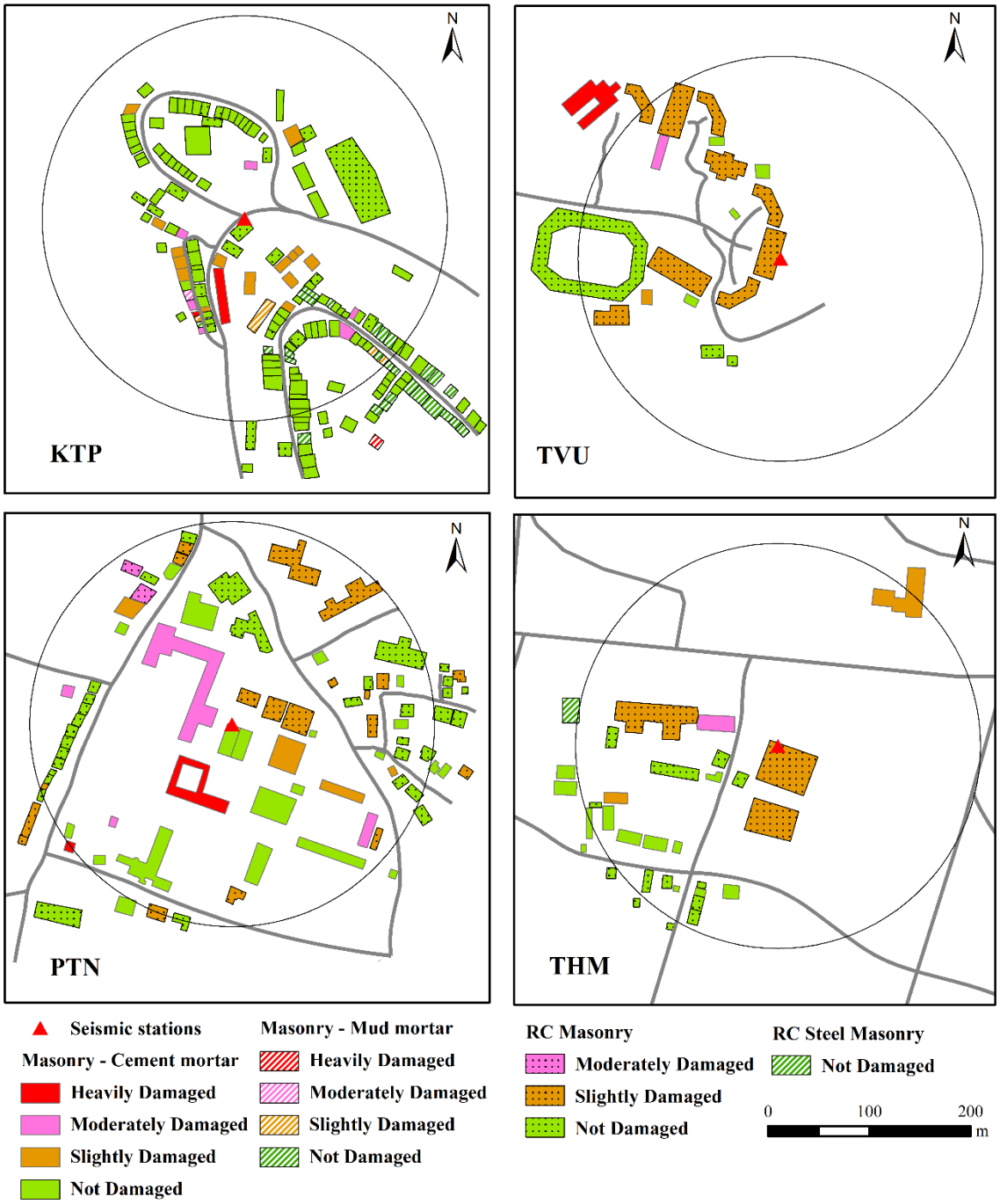

Figure 3. 16 Damage distribution of buildings around the seismic stations.

The damage assessment was carried out by method defined by European Macroseismic Scale 1998 (EMS98) [68]. The extent of damage was evaluated separately for masonry and RC infill-frame structures. The sampled buildings were classified into four categories: load-bearing masonry mud mortar, load-bearing masonry cement mortar, RC infill-frame, and RC steel masonry. The damage extent were differentiated into four classes: 'slightly damaged', 'moderately damaged', 'heavily damaged', and 'completely damaged'. The age of buildings, use, location, number of story, and surrounding topography were also noted.

The damage was mostly seen in masonry structures whereas RC infill-frame structures suffered little to no damage in most places (Figure 3.16). Around KTP, majority of buildings (~94%) remained unscathed. One masonry mud mortar building was heavily damaged (Figure 3.17a) and there were few instances of cracks in the inner walls of some buildings (Figure 3.17b). Around TVU, which is inside

university premise, there are mostly RC infill-frame structures. Statistically speaking, this site suffered the most damage (~10%) (Figure 3.16). A load-bearing masonry building was heavily damaged (Figure 3.17c) and few RC infill-frame structures also were slightly damaged (Figure 3.17d).

About 9% of buildings around PTN suffered slight to moderate damages (Figure 3.16). Two masonry buildings were damaged and shear cracks were observed in a multistory RC infill-frame building (Figure 3.17e, f). As the area around THM is relatively new, it suffered the least damage (Figure 3.16). A masonry school building suffered moderate damage (Figure 3.17g) and compound walls were collapsed (Figure 3.17h).

Figure 3. 17 Damaged structures around the seismic stations.

The result of assessment can be compared with the strong-motion records at the respective stations. The acceleration response spectra of single degree of freedom with 5% damping ratio in average horizontal direction display high response in short periods (<1 s) in rock site KTP (Figure 3.18). In case of sediment sites, the response is high in long-periods. THM has the highest response in periods longer than 3s. The response in TVU has the highest peaks in the 1-2 s than other stations. It has other peaks at 0-1 s and in periods longer than 3 s. Similarly, response of PTN is high in 0-1 s and 1-2 s.

The seismic design coefficient based on Nepal Building Code NBC -105[67] is much lower than the response of the earthquake record (Figure 3.18). The NBC-105 is in allowable stress design levels and is determined as function of basic seismic coefficient, seismic zone factor (based on Probabilistic Seismic Hazard Assessment map), importance of building, and structure performance. When comparing with the design requirement of Building Standard Law of Japan [69] for the same soil types, the design coefficient is higher than earthquake response and so is the limit curve for engineering bedrock according to Building Standard Law of Japan (MLIT 2000) [70], except in KTP for very short periods.

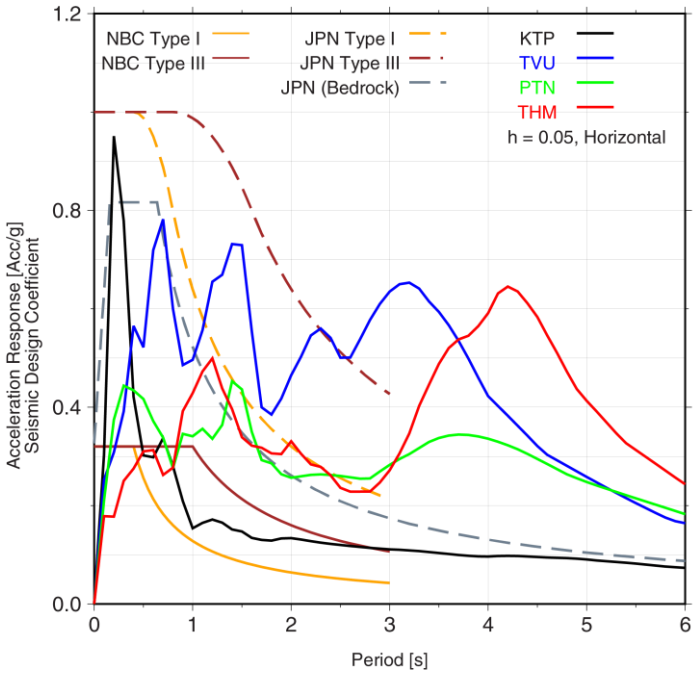

Figure 3. 18 Acceleration response spectra of the main shock. Also shown are the design spectra according to NBC-105[67], AIJ-1993[69], and MLIT-2000[70].

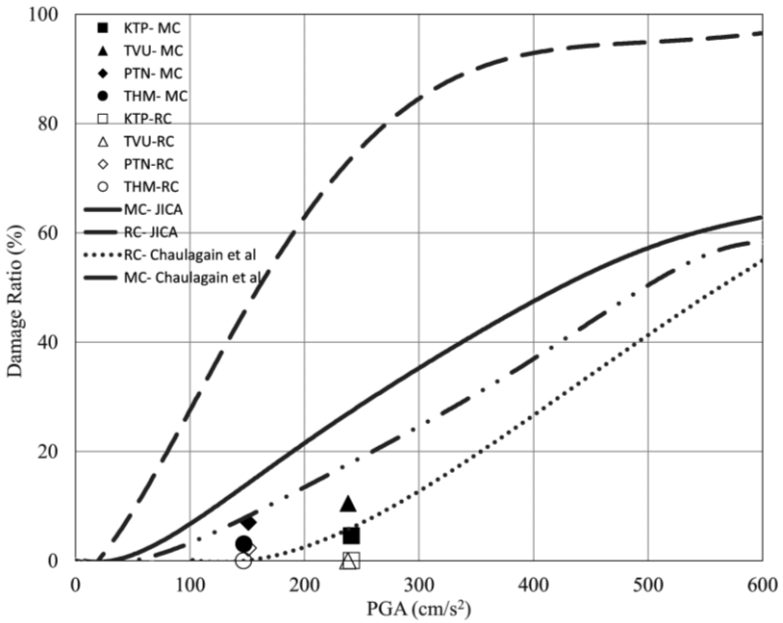

Figure 3. 19 Comparison of fragility curve and damage ratio.

The comparison of fragility curves and damage ratio (Figure 3.19) shows that though the damage ratio is higher in the masonry structures than in the RC infill frame-structure, they remained under the respective curves meaning the damage was less than expected by these curves. The damage ratio is the percentage of moderate and heavily damaged buildings to total number of buildings studied around a station. The fragility curves used were for load-bearing masonry cement mortar and RC infill frame structures [71] [72]. Since, load-bearing masonry mud mortar structures were found only in KTP, it couldn't be compared with damage at other sites. The fragility curves considered were from two different sources and the difference in values in the curves for the same type of buildings can be attributed to the difference in method of fragility curve construction.

Table 3. 3 Summary of damage situation around the stations.

Site	I* (1-2s)	I_H (1-2s)	PGA (cm/s^2)	Damage situation	No of buildings	Damage (%)
KTP	4.28	16.80	241	Majority of buildings unharmed with less than 2% buildings heavily damaged	174	5.74
TVU	5.54	34.14	238	Cracks in RC building foundations, one masonry building completely collapsed	19	10.52
PTN	5.04	31.52	151	Few masonry and RC structures developed cracks	85	9.41
THM	5.03	38.00	147	Very few damage except in an old school masonry building	32	3.13

A study in Japan [73] proposed an earthquake intensity based on the acceleration response between 1-2 s period (I*) to explain damage to infrastructures asserting that JMA Instrumental Intensity could not explain the damage properly. This parameter was referred for present study and it was found that I* was highest in TVU (Table 3.3). It is worth noting that response of TVU is higher than those of other sites not only in 1-2 s period but in a broad range of 0.5-3 s. The building damage may not be related to the predominant period of the building alone, as most of the low-rise and medium-rise buildings in Kathmandu have a predominant period of 0.1–0.2 s [74], but the response of TVU in the 0.1–0.2 s range is not the highest. The site TVU suffered the heaviest damage among the four stations, and the parameter I* can directly be associated with the building damage. On the other hand, even though the Housner Spectral Intensity (IH) [75] calculated from the pseudo-velocity spectrum over the 1–2 s period range is the highest (38.00) for THM, the percentage of damaged buildings is lower in THM than around other stations. Figure 3.20 shows the positive correlation between intensity I* and the number of slightly damaged (Ds), moderately damaged (Dm), and heavily damaged (Dh) buildings. The direct effect of site amplification can be clearly understood as the area around KTP suffered less damage despite having old masonry buildings, whereas comparatively new RC structures suffered damage in the area around TVU and PTN.

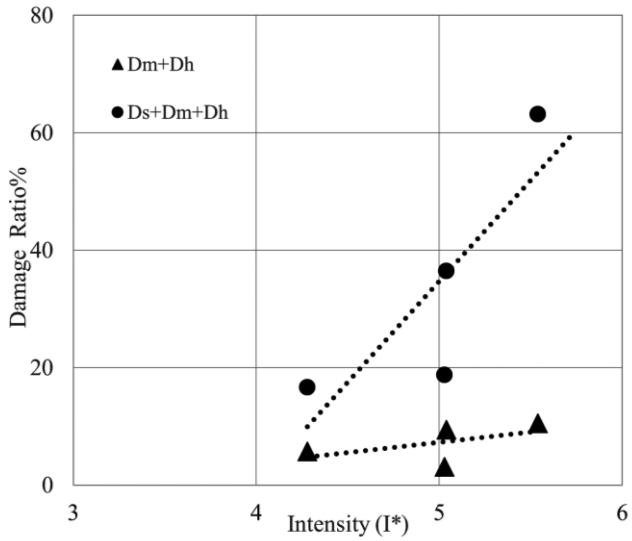

Figure 3. 20 Correlation between earthquake intensity (I) and damage ratio of slightly damaged (Ds), moderately damaged (Dm), and heavily damaged (Dh) buildings.*

Figure 3. 21 Damage to buildings in a) Bhaktapur, b) Gongabu, c) Sitapaila, and d) Ramkot.

Many buildings in different parts of the Kathmandu Basin, like Bhaktapur, Gongabu, Sitapaila, Ramkot (Figure 3.21), Sankhu, and Panga suffered heavy damage. Old masonry buildings in Bhaktapur and RC infill structures in Gongabu were completely collapsed and cases of liquefaction were reported. A team of researchers traced an extension of a localised lineament [76] in area south-west of THM. The worst hit areas of Kathmandu though didn't have seismic stations nearby, so similar study couldn't be carried out due to lack of strong-motion data to compare the damage. As basin topography and sediment in the Kathmandu Basin is heterogeneous, the response of sites merely few hundred meters apart varies a lot, so generalizing the response might not produce accurate results.

The high response of the earthquake in longer periods indicate the dominance of low-frequency waves during the Gorkha earthquake. The natural frequency of the low-rise buildings are high and they do not resonate with the low frequency wave [74]. The nonlinear property of Kathmandu sediments also dampened the higher frequencies. These might explain the low damage that occurred in the Kathmandu Basin, which is less catastrophic than previously anticipated [77]. Nevertheless, the low strength of load-bearing masonry structures and lack of regular maintenance can be the cause of damage to vernacular structures in different parts of Kathmandu. The earthquake was more likely to seriously damage high-rise buildings and base isolated structures that have longer natural period, had there been any inside the Kathmandu Basin.

References

[1] Pandey, M. R., Tandukar, R. P., Avouac, J. P., Lavé, J. & Massot, J. P. Interseismic strain accumulation on the Himalayan crustal ramp (Nepal). *Geophysical Research Letters* **22**, 751-754, doi:10.1029/94GL02971 (1995).

[2] Avouac, J.-P., Ayoub, F., Leprince, S., Konca, O. & Helmberger, D. V. The 2005, Mw 7.6 Kashmir earthquake: Sub-pixel correlation of ASTER images and seismic waveforms analysis. *Earth and Planetary Science Letters* **249**, 514-528, doi:10.1016/j.epsl.2006.06.025 (2006).

[3] Armijo, R., Tapponnier, P., Mercier, J. & Tonglin, H. Quaternary extension in southern Tibet: field observations and tectonic implications. *Journal of Geophysical Research* **91**, 13803-13872 (1986).
[4] Nakata, T. Active faults of the Himalaya of India and Nepal. *Geological Society of America Special Papers* **232**, 243-264, doi:10.1130/SPE232-p243 (1989).
[5] de la Torre, T. L., Monsalve, G., Sheehan, A. F., Sapkota, S. & Wu, F. Earthquake processes of the Himalayan collision zone in eastern Nepal and the southern Tibetan Plateau. *Geophysical Journal International* **171**, 718-738, doi:10.1111/j.1365-246X.2007.03537.x (2007).
[6] GCMT. *Global CMT Catalog Search*, <http://www.globalcmt.org/> (2015).
[7] Rajaure, S. *et al.* Double difference relocation of local earthquakes in the Nepal Himalaya. *Journal of Nepal Geological Society* **46**, 133-142 (2013).
[8] Lave, J. & Avouac, J. P. Active folding of fluvial terraces across the Siwaliks Hills, Himalayas of central Nepal. *J Geophys Res-Sol Ea* **105**, 5735-5770, doi:10.1029/1999jb900292 (2000).
[9] Avouac, J. P. Mountain building, erosion, and the seismic cycle in the Nepal Himalaya. *Advances in Geophysics* **46**, 1-80, doi:10.1016/S0065-2687(03)46001-9 (2003).
[10] Bollinger, L., Avouac, J. P., Cattin, R. & Pandey, M. R. Stress buildup in the Himalaya. *Journal of Geophysical Research: Solid Earth* **109**, n/a-n/a, doi:10.1029/2003jb002911 (2004).
[11] Jackson, M. & Bilham, R. GPS Measurement across the Himalaya. *Geophysical Research Letters* **21**, 1169-1172 (1994).
[12] Bilham, R. Location and magnitude of the 1833 Nepal Earthquake and its relation to the rupture zones of contiguous great Himalayan earthquakes. *Current Science* **69**, 101-128 (1995).
[13] Bilham, R. & Wallace, K. Future Mw >8 earthquakes in the Himalaya: implications form the 26th Dec 2004 Mw = 9.0 earthquake on India's eastern plate margin. *Geological Survey of India Special Publication* **85**, 1-14 (2005).
[14] Avouac, J. P. in *Treatise on Geophysics* (ed Gerald Schubert) 377-439 (Elsevier, 2007).
[15] Dixit, A. M., Yatabe, R., Dahal, R. K. & Bhandary, N. P. Initiatives for earthquake disaster risk management in the Kathmandu Valley. *Natural Hazards* **69**, 631-654, doi:10.1007/s11069-013-0732-9 (2013).
[16] Seeber, L. & Armbruster, J. G. in *Earthquake Prediction* 259-277 (American Geophysical Union, 1981).
[17] Ambraseys, N. N. & Douglas, J. Magnitude calibration of north Indian earthquakes. *Geophysical Journal International* **159**, 165-206, doi:10.1111/j.1365-246X.2004.02323.x (2004).
[18] Szeliga, W., Hough, S., Martin, S. & Bilham, R. Intensity, Magnitude, Location, and Attenuation in India for Felt Earthquakes since 1762. *Bulletin of the Seismological Society of America* **100**, 570-584, doi:10.1785/0120080329 (2010).
[19] Khattri, K. N. & Tyagi, A. K. Seismicity patterns in the Himalayan plate boundary and identification of areas of high seismic potential. *Tectonophysics* **96**, 281-297 (1983).
[20] Pant, M. R. in *Adarsha* Vol. 2 29-60 (2002).
[21] Hough, S. & Bilham, R. Site response of the Ganges basin inferred from re-evaluated macroseismic observations from the 1897 Shillong, 1905 Kangra, and 1934 Nepal earthquakes. *J Earth Syst Sci* **117**, 773-782, doi:10.1007/s12040-008-0068-0 (2008).
[22] Chen, W. P. & Molnar, P. Seismic moments of major earthquakes and the average rate of slip in central Asia. *Journal of Geophysical Research* **82**, 2945-2469 (1977).
[23] Molnar, P. & Deng, Q. Faulting associated with large earthquakes and the average rate of deformation in central and eastern Asia. *Journal of Geophysical Research* **89**, 6203, doi:10.1029/JB089iB07p06203 (1984).
[24] Pandey, M. R. & Molnar, P. The distribution of intensity of the Bihar-Nepal Earthquake 15 January 1934 and bounds of the extent of the rupture zone. *Journal of Nepal Geological Society* **5**, 22-24 (1988).
[25] Bilham, R., Gaur, V. K. & Molnar, P. Earthquakes. Himalayan seismic hazard. *Science (New York, N.Y.)* **293**, 1442-1444, doi:10.1126/science.1062584 (2001).
[26] Avouac, J. P., Bollinger, L., Lavé, J., Cattin, R. & Flouzat, M. Le-cycle sismique en Himalaya. *C. R. Acad. Sci.* **333**, 513-529 (2001).

[27] Sapkota, S. N. *et al.* Primary surface ruptures of the great Himalayan earthquakes in 1934 and 1255. *Nature Geoscience* **6**, 71-76 (2013).
[28] Geller, R. J. & Kanamori, H. Magnitudes of great shallow earthquakes form 1904 to 1952. *Bulletin of Seismological Society of America* **67**, 587-598 (1977).
[29] Abe, K. Magnitudes of large shallow earthquakes from 1904 to 1980. *Physics of Earth and Planetary Interiors* **27**, 72-92 (1981).
[30] Bollinger, L. *et al.* Estimating the return times of great Himalayan earthquakes in eastern Nepal: Evidence from the Patu and Bardibas strands of the Main Frontal Thrust. *Journal of Geophysical Research: Solid Earth* **119**, 7123-7163, doi:10.1002/2014jb010970 (2014).
[31] Rana, B. S. *Mahabhukampa (The Great Earthquake)*. (B.S. Rana, 1935).
[32] Roy, S. C., Dunn, J. A., Auden, J. B. & Ghosh, A. M. N. The Bihar-Nepal Earthquake of 1934. *Memoirs of Geological Society of India,* **73**, 391 (1939).
[33] Pandey, M. R., Tandukar, R. P., Avouac, J. P., Vergne, J. & Heritier, T. Seismotectonics of the Nepal Himalaya from a local seismic network. *Journal of Asian Earth Sciences* **17**, 703-712 (1999).
[34] Monsalve, G. *et al.* Seismicity and one-dimensional velocity structure of the Himalayan collision zone: Earthquakes in the crust and upper mantle. *Journal of Geophysical Research* **111**, doi:10.1029/2005jb004062 (2006).
[35] Ghimire, S. & Kasahara, M. Source process of the Ms=6.6, Udayapur earthquake of Nepal–India border and its tectonic implication. *Journal of Asian Earth Sciences* **31**, 128-138, doi:10.1016/j.jseaes.2007.04.007 (2007).
[36] USGS. *Earthquake Hazards Program*, <http://earthquake.usgs.gov/> (2015).
[37] Bilham, R., Bendick, R. & Wallace, K. Flexure of the Indian plate and intraplate earthquakes. *J Earth Syst Sci* **112**, 315-329, doi:10.1007/BF02709259 (2003).
[38] Dixit, A. M. Geological effects and intensity distribution of the Udaypur (Nepal) Earthquake of August 20, 1988. *Journal of Nepal Geological Society* **7**, 1-17 (1991).
[39] Arora, B. R., Prajapati, S. K. & Reddy, C. D. Geophysical Constraints on the Seismotectonics of the Sikkim Himalaya. *Bulletin of the Seismological Society of America* **104**, 2278-2287, doi:10.1785/0120130254 (2014).
[40] Joshi, A., Kumari, P., Singh, S. & Sharma, M. L. Near-field and far-field simulation of accelerograms of Sikkim earthquake of September 18, 2011 using modified semi-empirical approach. *Natural Hazards* **64**, 1029-1054, doi:10.1007/s11069-012-0281-7 (2012).
[41] Ekstrom, G., Nettles, M. & Dziewonski, A. M. The global CMT project 2004-2010: Centroid-moment tensors for 13,017 earthquakes. *Physics of Earth and Planetary Interiors* **200-201**, 1-9, doi:10.1016/j.pepi.2012.04.002 (2012).
[42] Bilham, R. in *Himal Magazine* Vol. 7 26-30 (Kathmandu, 1994).
[43] Avouac, J.-P., Meng, L., Wei, S., Wang, T. & Ampuero, J.-P. Lower edge of locked Main Himalayan Thrust unzipped by the 2015 Gorkha earthquake. *Nature Geoscience*, doi:10.1038/ngeo2518 (2015).
[44] Yagi, Y. & Okuwaki, R. Integrated seismic source model of the 2015 Gorkha, Nepal, earthquake. *Geophysical Research Letters* **42**, 6229-6235, doi:10.1002/2015GL064995 (2015).
[45] Fan, W. & Shearer, P. M. Detailed rupture imaging of the 25 April 2015 Nepal earthquake using teleseismic P waves. *Geophysical Research Letters* **42**, doi:10.1002/2015GL064587 (2015).
[46] Denolle, M. A., Fan, W. & Shearer, P. M. Dynamics of the 2015 M7.8 Nepal Earthquake. *Geophysical Research Letters*, doi:10.1002/2015gl065336 (2015).
[47] NSC. *Aftershocks of Gorkha Earthquake*, <http://www.seismonepal.gov.np/index.php?action=earthquakes&show=recent> (2018).
[48] Galetzka, J. *et al.* Slip pulse and resonance of Kathmandu basin during the 2015 Mw 7.8 Gorkha earthquake, Nepal imaged with geodesy. *Science (New York, N.Y.)*, doi:10.1126/science.aac6383 (2015).
[49] ARIA. *M7.8 Gorkha, Nepal Earthquake, April 25, 2015*, <http://aria.jpl.nasa.gov/node/43> (2015).
[50] Survey Department. *Survey Department Press Release (in Nepali)*, <http://dos.gov.np/notice/%E0%A4%AA%E0%A5%8D%E0%A4%B0%E0%A5%87%E0%

A4%B6-%E0%A4%B5%E0%A4%BF%E0%A4%9C%E0%A5%8D%E0%A4%9E%E0%A4%AA%E0%A5%8D%E0%A4%A4%E0%A4%BF/> (2015).
[51] Takai, N. *et al.* Strong Ground Motion in the Kathmandu Valley during the 2015 Gorkha, Nepal, Earthquake. *Earth, Planets and Space* **68**, doi:10.1186/s40623-016-0383-7 (2016).
[52] Government of Nepal. *Nepal Disaster Risk Reduction Portal*, <http://drrportal.gov.np/> (2015).
[53] Bilham, R. *Mw = 7.8 earthquake central Nepal (25 April 2015)*, <http://cires1.colorado.edu/~bilham/2015%20Nepal/Nepal_2015_earthquake.html> (2015).
[54] Bijukchhen, S. *et al.* A comparative study of strong ground motion records from 30 August 2013 south Tibet earthquake on the rock and soil sites of Kathmandu Valley. *Journal of Nepal Geological Society* **48**, 48 (2015).
[55] Takai, N., Shigefuji, M., Bijukchhen, S., Ichiyanagi, M. & Sasatani, T. in *16 World Conference on Earthquake Engineering* 12 (Santiago, Chile, 2017).
[56] Hisada, Y. & Bielak, J. A theoretical method for computing near-fault ground motions in layered half-spaces considering static offset due to surface faulting, with a physical interpretation of fling step and rupture directivity. *Bulletin of Seismological Society of America* **93**, 1154-1168 (2003).
[57] Bijukchhen, S. M. *Strong Ground-Motion characteristics in the Kathmandu Basin (Strong-motion observation and damage assessment of 2015 Gorkha, Nepal Earthquake)* Masters thesis, Hokkaido University, (2015).
[58] Beresnev, I. A. & Wen, K. L. Nonlinear Soil Response-A Reality? *Bulletin of Seismological Society of America* **86**, 1964-1978 (1996).
[59] Noguchi, S. & Sasatani, T. in *14th World Conference on Earthquake Engineering* (Beijing, China, 2008).
[60] Dhakal, Y. P. *et al.* in *JAEE International Symposium on Earthquake Engineering* (Tokyo, 2015).
[61] Rajaure, S. *et al.* Characterizing the Kathmandu Valley sediment response through strong motion recordings of the 2015 Gorkha earthquake sequence. *Tectonophysics* **714-715**, 146-157, doi:10.1016/j.tecto.2016.09.030 (2017).
[62] Wen, K.-L. Non-Linear Soil Response in Ground Motions. *Earthquake Engineering & Structural Dynamics* **23**, 559-608 (1994).
[63] Applied Technology Council. ATC- 38 Database on the Performance of Structures near Strong-Motion Recordings: 1994 Northridge Earthquake. (ATC, California, USA, 2000).
[64] Iizuka, H., Sakai, Y. & Koketsu, K. Strong Ground Motions and Damage Conditions Associated with Seismic Stations in the February 2011 Christchurch, New Zealand, Earthquake. *Seismol Res Lett* **82**, 875-881, doi:DOI 10.1785/gssrl.82.6.875 (2011).
[65] Applied Technology Council. Performance of Buildings and Nonstructural Components in the 2014 South Napa Earthquake FEMA P-1024. (ATC, Washington D.C., USA, 2015).
[66] Chaulagain, H., Rodrigues, H., Jara, J., Spacone, E. & Varum, H. Seismic response of current RC buildings in Nepal: A comparative analysis of different design/construction. *Engineering Structures* **49**, 284-294 (2013).
[67] NBC-105. (ed Department of Buildings HMG of Nepal Ministry of Housing and Physical Planning) (Kathmandu, 1995).
[68] Grunthal, G. *European Macroseismic Scale 1998*. (Centre Europèen de Géodynamique et de Séismologie, 1998).
[69] Architectural Institute of Japan (AIJ). *Earthquake motion and Ground Conditions: in commemoration of the 20th anniversary of the research subcommittee on earthquake ground motion, the Architectural Institute of Japan*. (AIJ, 1993).
[70] MLIT. (ed Infrastructure and Transport Ministry of Land) (MLIT, Japan, 2000).
[71] JICA. The study of earthquake disaster mitigation in the Kathmandu valley, Kingdom of Nepal. (Japan International Cooperation Agency and Ministry of Home Affairs Nepal, Kathmandu, 2002).
[72] Chaulagain, H., Rodrigues, H., Silva, V., Spacone, E. & Varum, H. Earthquake loss estimation for the Kathmandu Valley. *Bulletin of Earthquake Engineering* **14**, 59-88, doi:10.1007/s10518-015-9811-5 (2016).

[73] Sakai, Y., Kanno, T. & Koketsu, K. Proposal of instrumental seismic intensity scale from response spectra in various period ranges. *Journal of Structural and Construction Engineering (Transaction of AIJ)* **585**, 71-76 (2004).
[74] Parajuli, R. R. & Kiyono, J. Ground Motion Characteristics of the 2015 Gorkha Earthquake, Survey of Damage to Stone Masonry Structures and Structural Field Tests. *Frontiers in Built Environment* **1**, doi:10.3389/fbuil.2015.00023 (2015).
[75] Housner, G. W. in *Proceedings of the Symposium on Earthquake and Blast Effects on Structures* 20-36 (Earthquake Engineering Research Institue, 1952).
[76] Angster, S. *et al.* Field Reconnaissance after the 25 April 2015 M 7.8 Gorkha Earthquake. *Seismol Res Lett* **86**, 1506-1513, doi:10.1785/0220150135 (2015).
[77] Hough, S. E. Introduction to the Focus Section on the 2015 Gorkha, Nepal, Earthquake. *Seismol Res Lett* **86**, 1502-1505, doi:10.1785/0220150212 (2015).

CHAPTER IV
ESTIMATION OF 1-D VELOCITY MODELS BENEATH STRONG-MOTION OBSERVATION SITES USING STRONG-MOTION RECORDS

CHAPTER IV. ESTIMATION OF 1-D VELOCITY MODELS BENEATH STRONG-MOTION OBSERVATION SITES USING STRONG-MOTION RECORDS

4.1 INTRODUCTION

The manifestation of an earthquake effect is a combination of source, path, and site characteristics. In addition to the earthquake magnitude, site conditions play a vital role in the effect of earthquakes on infrastructure. An earthquake with seemingly no effect above hard ground can be felt as a strong tremor that can cause severe damage in areas above soft or unconsolidated sediments due to the amplification of seismic waves. There are accounts of more than 20 devastating earthquakes occurring in or near the Nepal Himalaya after the 13th century [1]; the 2015 Gorkha Earthquake is the most recent. A location in a seismically active region, and the presence of thick sediments that amplify seismic waves, have made the Kathmandu Basin a seismically vulnerable region. Moreover, the increasing tendency for haphazard building construction without proper engineering considerations has added to the potential for catastrophe.

A thorough study of ground motion amplification is required to prepare safe and up-to-date building codes that reduce loss of life and property during an earthquake. Characterizing subsurface velocity structures is a necessary precondition for achieving that goal. Previously, there was a study of 1-D velocity models in a few places in Kathmandu based on micro-tremors [2]. A subsurface velocity model was prepared based on geological maps [3] and borehole logs collected during an earthquake disaster mitigation study [4]. Piya [5] used available borehole data and geological information to prepare soil profiles of the basin sediment for liquefaction hazard analysis. The borehole logs available are predominantly from the groundwater wells in the Kathmandu Basin. The velocity logging below depths of 30 m is not available. A study of basement structure using microtremor recordings from different locations in the Kathmandu Basin, some of which lie in vicinity of the sites described in the present study, was carried out in 2012 [6]. Sugimura, et al. [7] have prepared an atlas of geological cross-section of the Kathmandu Basin based on available borehole logs, geological maps, and geological fieldwork.

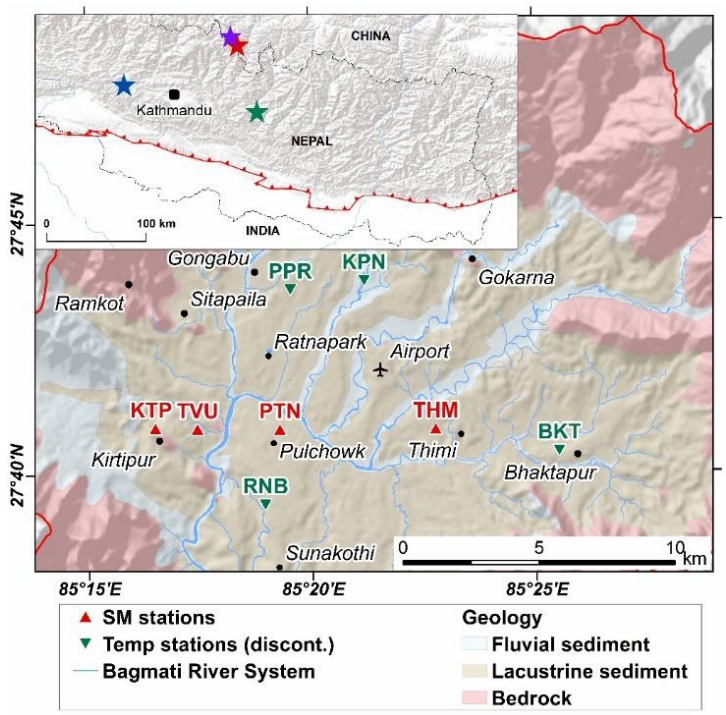

Figure 4. 1 Location map of the strong-motion seismometers. Inset: Map of central and eastern Nepal showing epicentres of four earthquake used in this study.

In this study, the seismic records of moderate earthquakes obtained from an array of strong-motion accelerometers (Figure 4.1) are used to estimate 1-D velocity models of the stations by forward

modelling of low-frequency S-waves. A similar 1-D velocity model was prepared for seismic station KATNP, maintained by the United States Geological Survey (USGS), in Kathmandu using the mainshock of the Gorkha Earthquake [8]. Furthermore the velocity models thus constructed are examined by comparing observed H-to-V spectral ratio with the theoretical H-to-V spectral ratio obtained from the models. This 1-D velocity models are to be used in construction of a 3-D subsurface model of the Kathmandu Basin.

As already mentioned in Chapter II, the tectonic basin of Kathmandu is filled with fluvio-lacustrine deposit and surrounded by hills on all sides. It was a lake until 10 ka after which it dried out leaving a sediment filled basin [9] now drained by the Bagmati River system. The sediment thickness is estimated to be more than 600 m [10,11] at the centre. The sediments inside the basin have their origin in the basement rocks of the surrounding mountains. Geologically, the sediment in the Kathmandu Basin have coarser sediment in the bottom and fringes of the basin which were deposited by proto-Bagmati River system [11]. These sediments give way to finer sediments in the upper and central part. The layers can be generalised as coarse sand and gravel at the bottom superimposed with layers of sand and clay of lacustrine facies; fluvial deposits from the Bagmati River system makeup the topmost layers [3,12-14].

Furthermore, borehole logs [4,5,14] demonstrate a number of different layers and lenses formed due to varying depositional environment. The basin is highly undulated and several rock outcrops are exposed inside the basin as they breach through these sediments. The variation in basement topography, geology, and the depositional environment make it difficult to generalise the subsurface geologic structures and ground response of the basin. The lack of proper data on subsurface geology, velocity logs, and soil profiles makes the task challenging.

4.2 SEISMIC RECORDS CONSIDERED FOR THE STUDY

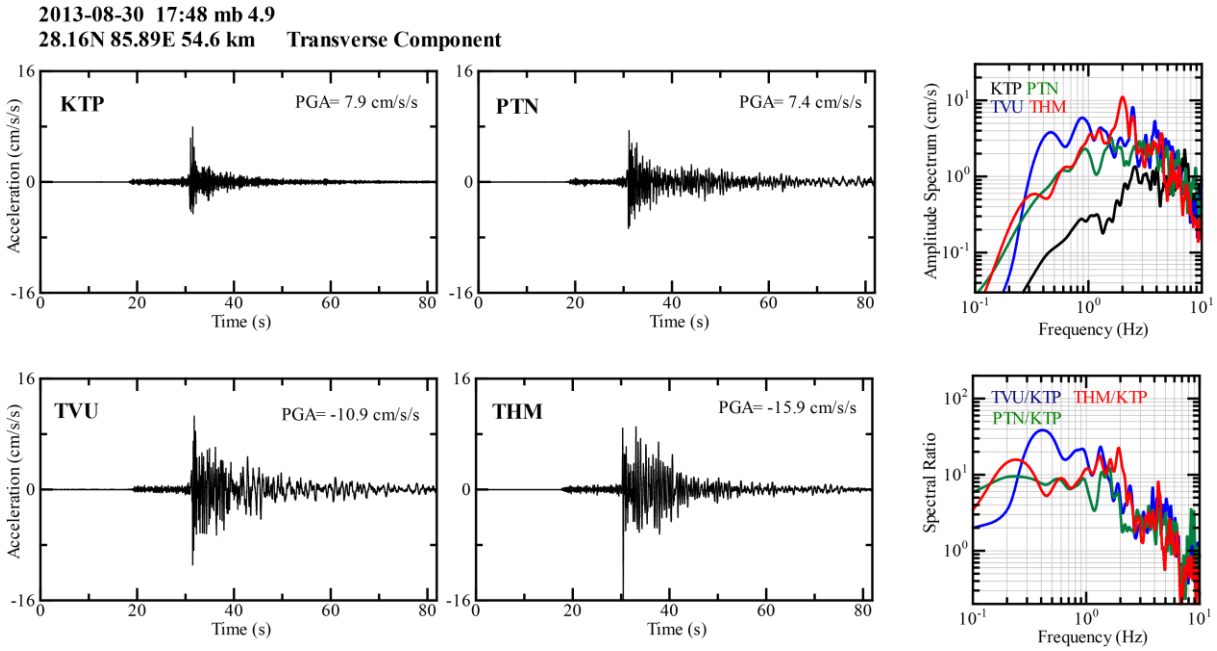

Figure 4. 2 Acceleration waveform, Fourier spectra, and spectral ratio of transverse component of the mb 4.9 earthquake (2013-08-30 17:48).

For this study, four moderate sized earthquakes are considered. The earthquake records are from the strong-motion stations KTP, TVU, PTN, and THM. One earthquake amongst the four occurred when four temporary stations (BKT, RNB, PPR, and KPN) were also in operation, so there are eight records for this earthquake.

The first earthquake (mb 4.9) occurred near the Nepal-Tibet border about 80 km NE of Kathmandu (represented by a red star in Figure 4.1 inset) on August 30th, 2013. As mentioned earlier the sedimentary

sites TVU, PTN, and THM show high amplification during this earthquake (Figure 3.7). The Fourier spectra of the transverse component demonstrate the presence of low-frequency waves and significant amplification compared to that of the rock site KTP. This amplification is further confirmed by the spectral ratio of the sedimentary sites.

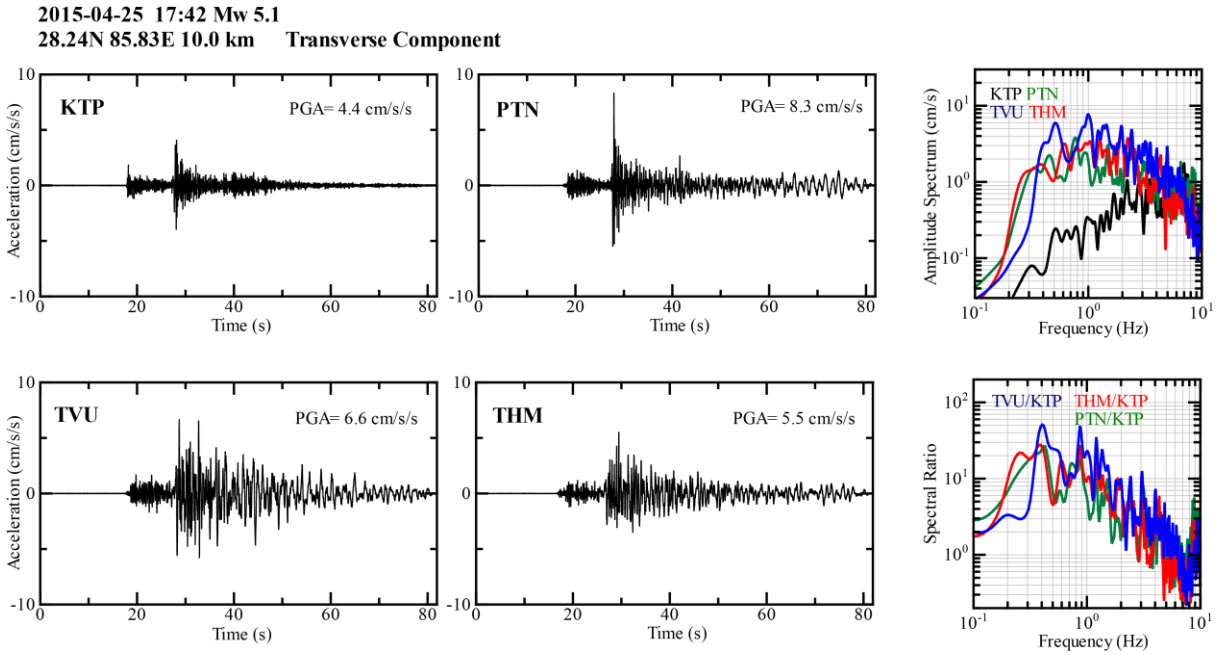

Figure 4. 3 Acceleration waveform, Fourier spectra, and spectral ratio of transverse component of the M_w 5.1 earthquake (2015-04-25 17:42).

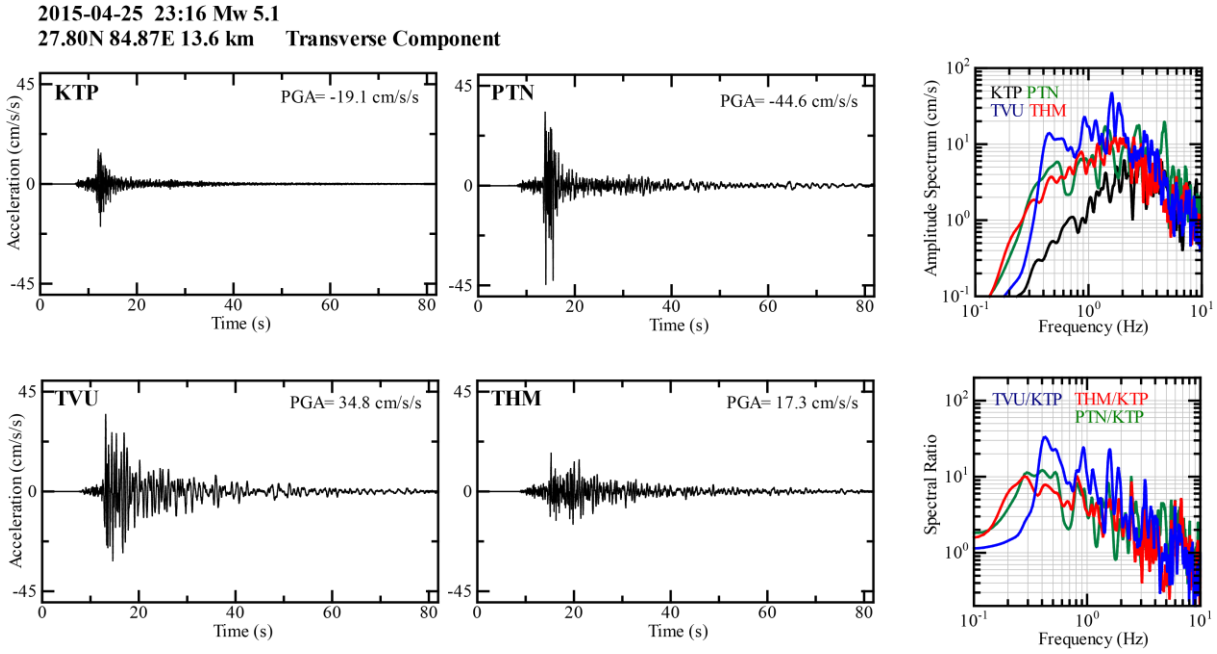

Figure 4. 4 Acceleration waveform, Fourier spectra, and spectral ratio of transverse component of the M_w 5.1 earthquake (2015-04-25 23:16).

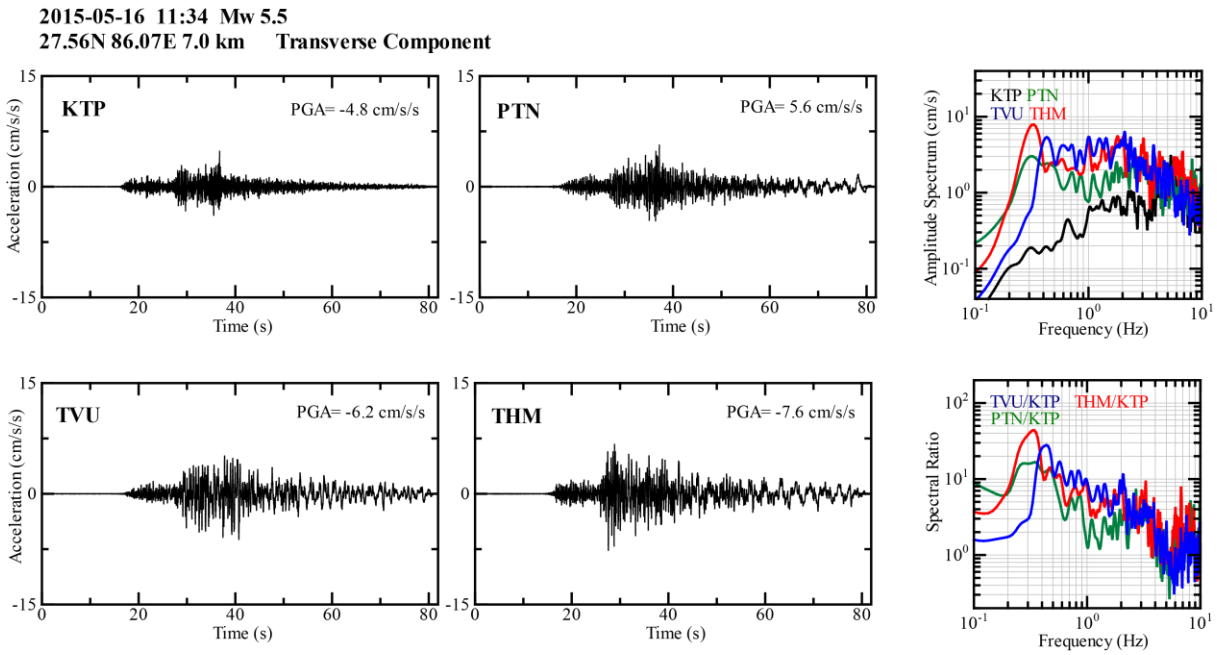

Figure 4. 5 Acceleration waveform, Fourier spectra, and spectral ratio of transverse component of the M_w 5.5 earthquake (2015-05-16 11:34) in four permanent stations.

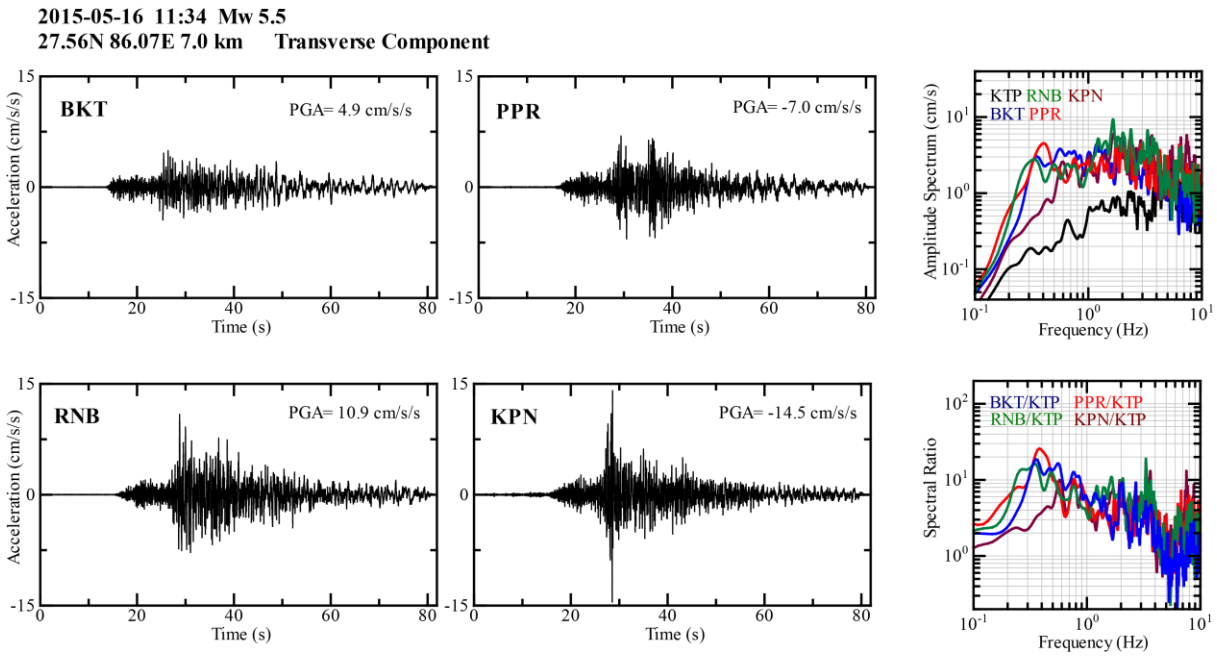

Figure 4. 6 Acceleration waveform, Fourier spectra, and spectral ratio of transverse component of the M_w 5.5 earthquake (2015-05-16 11:34) recorded in temporary stations.

The three other earthquakes considered are aftershocks of the 2015 Gorkha earthquake. Two of them, both M_w 5.1, occurred on the same day as the main shock (April 25th, 2015). The first one (blue star, Figure 4.1 inset) occurred at 17:42 UTC with an epicentre ~80km north-east of Kathmandu (Figure 4.3). The other one had an epicentre about 45 km west of Kathmandu (light blue star, Figure 4.1 inset) and occurred at 23:16 UTC (Figure 4.4). The four temporary sites were added a week after the main shock, so they lack records of all three earthquakes. Therefore, an earthquake (M_w 5.5) that occurred on May 16, 2015 about 75 km east of Kathmandu (green star, Figure 4.1 inset) which was recorded at all eight stations was also considered (Figure 4.5, 4.6).

The forms of the Fourier spectra of the rock site (KTP) depend on f^2 for low frequencies (f < 1 Hz) except for the M_w 5.5 event. This spectral form resulted from incidence of the low-frequency S-wave beneath the KTP site. The higher frequencies (f > 1 Hz) do not depend on f^0. This might be due to site amplification or the effect of a weathered rock layer at the top. The spectra of the sedimentary sites show larger amplitudes in 0.2 < f < 2 Hz than those at KTP. There is sharp increase in amplitude at low frequencies between 0.2 and 0.4 Hz at the sedimentary sites for all earthquakes which has also been mentioned in Chapter III. It should be noted that as the window length for the spectral analysis in Figure 4.2 – Figure 4.6 is 80 s, the high amplitude observed is pertinent to S-wave amplification as well as excitation of basin induced surface waves.

4.3 METHODOLOGY

The response of a laterally heterogeneous sedimentary basin to incident S-waves is to produce S-wave amplification and basin-induced surface waves. The direct long-period S-wave from a 3-D simulation for a deep basin structure is essentially same as that from 1-D simulation for a flat-layered structure beneath the site [15,16]. As an initial step in the 3-D simulation of the Kathmandu Basin, a 1-D velocity structure estimation was conducted using forward modelling of an observed long-period S-wave from the mb 4.9 earthquake.

For the task, available borehole data [4,5,14], geological maps [3,17], and geological cross-sections [7] were synthesized to create the initial 1-D subsurface models. The shear wave velocity data for Kathmandu is not available. So, in the earthquake disaster mitigation report [4], average shear wave velocity of different sediment types were derived based on the N-value of the soil. This information was consulted for the preparation of 1-D initial subsurface model. The number of layers were based on the geological cross-sections where geological formations with similar lithotype were considered as same layer.

Table 4. 1 Physical properties of the underground structure considered for estimation of velocity models

V_p (m/s)	V_s (m/s)	ρ (kg/m3)	Q
500	200	1500	20
750	300	1600	30
875	350	1700	35
1000	400	1700	40
1250	500	2000	50
1750	700	2000	70
5500	3200	2400	200

The station KTP, which lies in Kirtipur, west Kathmandu is a rock site. The shear wave velocity (Vs) of the shallow subsurface layer measured during installation of the stations shows Vs~ 700 m/s at KTP, whereas other three sedimentary sites, TVU, PTN, and THM showed ~200 m/s [18]. The absence of prominent peaks in the average H/V ratio of microtremors at KTP and early arrival of S-wave at KTP compared to other sites during earthquakes [19] indicate KTP as a rock site. The low shear wave velocity though points that there likely is a weathered and fractured layer of exposed bedrocks overlying the basement rock at depth. Since the basin was gradually turned into the lake by damming of the proto-Bagmati river, the basement rocks were most probably exposed a long time before being overlain by sediments of the river. That's why the 1-D models were prepared with a thin layer of weathered rock (Vs= 700 m/s) overlying the bedrocks. The shear wave velocity of the basement layer or bedrock was fixed as 3.2 km/s from a regional velocity model of the Himalaya [20,21]. Table 4.1 shows the physical properties of the underground structure considered for the 1-D velocity model estimation.

The forward modelling was carried out by the Propagator Matrix method [22] which relates the incident wave to its surface displacement, in 1-D simulation of the theoretical long period S-wave. When the

waveform incident at angle *j* propagates through a layer with density ρ, the motion stress vector *f(z)* at a depth *z* can be related to the motion stress vector at the surface $f(z_0)$ with a matrix **P**, known as the Propagator Matrix.

$$\boldsymbol{f}(z) = \boldsymbol{P}(z, z_0)\boldsymbol{f}(z_0) \tag{4.1}$$

For the horizontal component of S-wave, the Propagator Matrix for a layer is

$$\boldsymbol{P}(\boldsymbol{z}, \boldsymbol{z_0}) = \begin{bmatrix} \boldsymbol{cos}[\boldsymbol{\omega\eta}(\boldsymbol{z}-\boldsymbol{z_0})] & (\boldsymbol{\omega\mu\eta})^{-1}\boldsymbol{sin}[\boldsymbol{\omega\eta}(\boldsymbol{z}-\boldsymbol{z_0})] \\ -(\boldsymbol{\omega\mu\eta})\,\boldsymbol{sin}[\boldsymbol{\omega\eta}(\boldsymbol{z}-\boldsymbol{z_0})] & \boldsymbol{cos}[\boldsymbol{\omega\eta}(\boldsymbol{z}-\boldsymbol{z_0})] \end{bmatrix} \tag{4.2}$$

where, $\eta = \frac{\cos j}{V_s}$ and $\mu = \rho {V_s}^2$.

For, *n* layers above a half space, equation (4.1) becomes

$$\boldsymbol{f}(\boldsymbol{z_n}) = \boldsymbol{P}(\boldsymbol{z_n}, \boldsymbol{z_{n-1}})\boldsymbol{P}(\boldsymbol{z_{n-1}}, \boldsymbol{z_{n-2}}) \ldots . \boldsymbol{P}(\boldsymbol{z_1}, \boldsymbol{z_0})\boldsymbol{f}(\boldsymbol{z_0})$$

$$\boldsymbol{f}(\boldsymbol{z_n}) = \widehat{\boldsymbol{P}}(\boldsymbol{z_n}, \boldsymbol{z_0})\boldsymbol{f}(\boldsymbol{z_0}) \tag{4.3}$$

The motion stress vector ***f****(z)*, can be written in terms of amount of down-going wave $\grave{S}$ and amount of up-going wave $\acute{S}$ as

$$\boldsymbol{f}(\boldsymbol{z_n}) = \boldsymbol{F}(\boldsymbol{z_n})\begin{pmatrix} \grave{\boldsymbol{S}} \\ \acute{\boldsymbol{S}} \end{pmatrix} \tag{4.4}$$

From equation (4.3) and (4.4), we obtain

$$\begin{pmatrix} \grave{\boldsymbol{S}} \\ \acute{\boldsymbol{S}} \end{pmatrix} = \boldsymbol{E^{-1}}(\boldsymbol{z_n})\widehat{\boldsymbol{P}}(\boldsymbol{z_n}, \boldsymbol{z_0})\begin{pmatrix} \boldsymbol{l_0} \\ \boldsymbol{0} \end{pmatrix}_{\boldsymbol{z=z_0}} \tag{4.5}$$

where, $\boldsymbol{E}^{-1}(z_n)$ is defined as

$$\boldsymbol{E^{-1}}(\boldsymbol{z_n}) = \begin{bmatrix} \frac{\boldsymbol{1}}{\boldsymbol{2}} & \frac{-\boldsymbol{i}}{\boldsymbol{2\omega\mu\eta}} \\ \frac{\boldsymbol{1}}{\boldsymbol{2}} & \frac{\boldsymbol{i}}{\boldsymbol{2\omega\mu\eta}} \end{bmatrix}$$

From equation (4.5), we obtain

$$\begin{pmatrix} \grave{\boldsymbol{S}} \\ \acute{\boldsymbol{S}} \end{pmatrix} = \boldsymbol{B}(\boldsymbol{z_n}, \boldsymbol{z_0})\begin{pmatrix} \boldsymbol{l_0} \\ \boldsymbol{0} \end{pmatrix} \tag{4.6}$$

When the incident wave is known, its surface displacement l_0, after passing through *n* layers, can be estimated with

$$\boldsymbol{l_0} = \frac{\acute{\boldsymbol{S}}}{\boldsymbol{B_{21}}} \tag{4.7}$$

The long period transverse component of the acceleration waveform from the rock site (KTP) during the mb 4.9 earthquake was considered as the incident wave and simulated waveforms at the three sediment sites were calculated using equation (4.7). Although the bedrock at KTP is overlain with a shallow weathered rock layer, this material has little or no effect on the long period waves being used in this study. As this earthquake originated at > 50 km depth, it has been assumed that the seismic waves impinged on the bedrock beneath the basin perpendicularly. The information regarding damping of soil

layers in the Kathmandu Basin is not available, so a frequency independent Q = 0.1 V_s (V_s in m/s) is considered which is commonly used for long period strong motion simulation [23,24].

A pulse of band-pass filtered (0.1-0.5 Hz) acceleration waveform from KTP record was used as the input motion passing through the initial models to obtain simulated ground motions at the sediment sites. The bandwidths were chosen considering the spectral ratio in the low frequency range for all earthquakes. The thickness of the layers were then adjusted using trial-and-error to match the simulated waveforms with observed ones. The adjusted 1-D velocity models were then used to simulate the long period S-waves of the three aftershocks, two M_w 5.1 and a single M_w 5.5, of the Gorkha earthquake. These simulated S-waves were compared with the observed ones to verify the adjusted models. In case of these aftershocks though, since they have shallow hypocentres, the incident angle was considered to be 30°, also based on trial-and-error.

As a method of verifying the velocity models estimated by modeling long-period S-waves by Propagator Matrix method, H-to-V spectral ratio (HVSR) method was implemented. This method uses the horizontal-to-vertical spectral ratio of observed earthquakes for inversion of layered structures based on the diffused field theory for plane body waves [25,26]. The following equation relates the H/V ratio of plane body waves to transfer functions of horizontal motion and vertical motion on the surface due to vertically incident S-wave and P-wave, respectively:

$$\frac{\boldsymbol{H(\omega)}}{\boldsymbol{V(\omega)}} = \sqrt{\frac{\boldsymbol{\alpha_H}}{\boldsymbol{\beta_H}}} \frac{\boldsymbol{|TF_1(\omega)|}}{\boldsymbol{|TF_3(\omega)|}} \qquad (4.8)$$

where α_H and β_H are, respectively, the P-wave and S-wave velocities of bedrock. TF_1 is the transfer function for horizontal motion on the surface due to a vertically incident S wave at bedrock, and TF_3 is transfer function for vertical motion on the surface due to a vertically incident P wave.

Equation (4.8) is used to estimate the theoretical H/V ratio using the adjusted velocity models. The value of Q was set to 0.1 V_s for this method as well. The P-wave velocities of the layers were estimated as a function of shear wave velocity based on previous studies in the Himalayan region: V_p/V_s = 1.73 for basement rocks [20] and V_p/V_s = 2.5 for sedimentary layers [27] (Table 4.1). Ten moderate aftershocks (M5-M5.5) of the Gorkha Earthquake (Table 4.2) were selected and their observed average H/V ratios were compared with the theoretical H/V ratios from equation (4.8).

Table 4. 2 Moderate earthquakes considered for the HVSR method for fixed stations.

SN	Date	Lat	Long	Dep (km)	Magnitude
1	2015-04-25 06:37	27.74N	85.83E	10.0	mb 5.1
2	2015-04-25 06:56	27.88N	85.75E	10.0	mb 5.5
3	2015-04-25 12:44	28.10N	84.56E	10.0	mb 5.2
4	2015-04-25 17:42	28.24N	85.83E	10.0	M_w 5.1
5	2015-04-25 23:16	27.80N	84.87E	13.6	M_w 5.1
6	2015-05-12 07:17	27.71N	86.22E	13.0	mb 5.5
7	2015-05-12 07:34	27.75N	86.24E	10.0	mb 5.4
8	2015-05-12 08:21	27.73N	86.13E	15.0	mb 5.2
9	2015-05-12 21:25	27.78N	86.64E	10.0	mb 5.2
10	2015-05-16 11:34	27.56N	86.07E	7.0	M_w 5.5

The HVSR method has been used to generate a 1-D velocity structures in Tohoku, Japan [26], confirming that the method could be employed to estimate the 1-D structures at the present study sites. The temporary stations added after the main shock do not have records of the m4.9 earthquake, so the HVSR method is employed for the 1-D velocity model estimation.

The initial 1-D velocity models of the temporary stations were prepared using the geological cross-sections, as it was done for the permanent stations. Then these initial models were adjusted by the HVSR method. For the process, the observed average H/V ratios from eight moderate (M5-M5.5) aftershocks

(Table 4.3) were considered. The observed H/V ratios were then compared with the theoretical H/V ratios for the velocity models using trial-and-error. Finally, the adjusted models were used to simulate the theoretical long-period S-waves from the aftershock (M_w 5.5) of the Gorkha Earthquake applying the Propagator Matrix method for all seven sites.

Despite the availability of a number of aftershock records, many were small and had low-energy in the long period range, so they were not considered in this study. Moreover, a number of moderate sized aftershocks in the database were affected by continuous smaller aftershocks occurring for several seconds. The quality of the records was a constraint in choosing the earthquake for the modeling of the observed long-period S-wave. In case of larger earthquakes, because they are affected by the nonlinear site response of basin sediment [8,28,29], the nonlinear response needs to be taken into account if they were to be used for similar calculations.

Table 4. 3 Earthquakes considered for the HVSR method for four temporary stations.

SN	Date	Lat Long	Dep (km)	Magnitude
1	2015-05-12 07:17	27.714N 86.218E	13.0	mb 5.5
2	2015-05-12 07:34	27.746N 86.245E	10.0	mb 5.4
3	2015-05-12 08:06	27.722N 86.061E	15.0	mb 5.0
4	2015-05-12 08:13	27.760N 86.760E	15.0	mb 5.1
5	2015-05-12 08:21	27.730N 86.132E	15.0	mb 5.2
6	2015-05-12 21:25	27.783N 86.638E	10.0	mb 5.2
7	2015-05-13 21:38	27.720N 86.050E	8.4	mb 5.0
8	2015-05-16 11:34	27.560N 86.073E	7.0	M_w 5.5

4.4 RESULTS

The velocity models were adjusted by matching the simulated long-period S-wave with the observed records from the mb 4.9 earthquake (Figure 4.7). The calculation using adjusted velocity models (Figure 4.8), estimated by modelling the long-period S-wave returned simulated waveforms with good agreement to the observed ones from the earthquakes. The model for KTP was considered as a bedrock site overlain by a layer of weathered rock and those for TVU, PTN, and THM are adjusted 1-D velocity models. It can be seen that the site THM has the thickest sediment. The black dashed lines in the figure indicate the initial velocity model prepared based on geological maps, cross-sections, and borehole logs nearby. The initial and adjusted 1-D velocity models of TVU, PTN, and THM are tabulated in Table 4.4. The simulated S-waves using the adjusted velocity models for both M_w 5.1 aftershocks (Figure 4.9, Figure 4.10) had good fits at PTN, whereas at TVU and THM, there are discrepancies in the amplitude though frequency match is better. In contrast, the simulated S-waves for the M_w 5.5 earthquake (Figure 4.11) were in better agreement at THM and PTN. The waveform matching is conducted for the time windows indicated by the red arrows in the Figures 4.7, 4.9, 4.10, and 4.11. Also shown in the figures are simulation results from initial models (in grey). The difference between the simulation results using the initial velocity models and adjusted models can be clearly observed. These observed waveforms have larger amplitudes compared with the simulated ones in the later phases, as the complex 3-D basement topography have played a role in their amplification, which cannot be simulated properly with only 1-D structures.

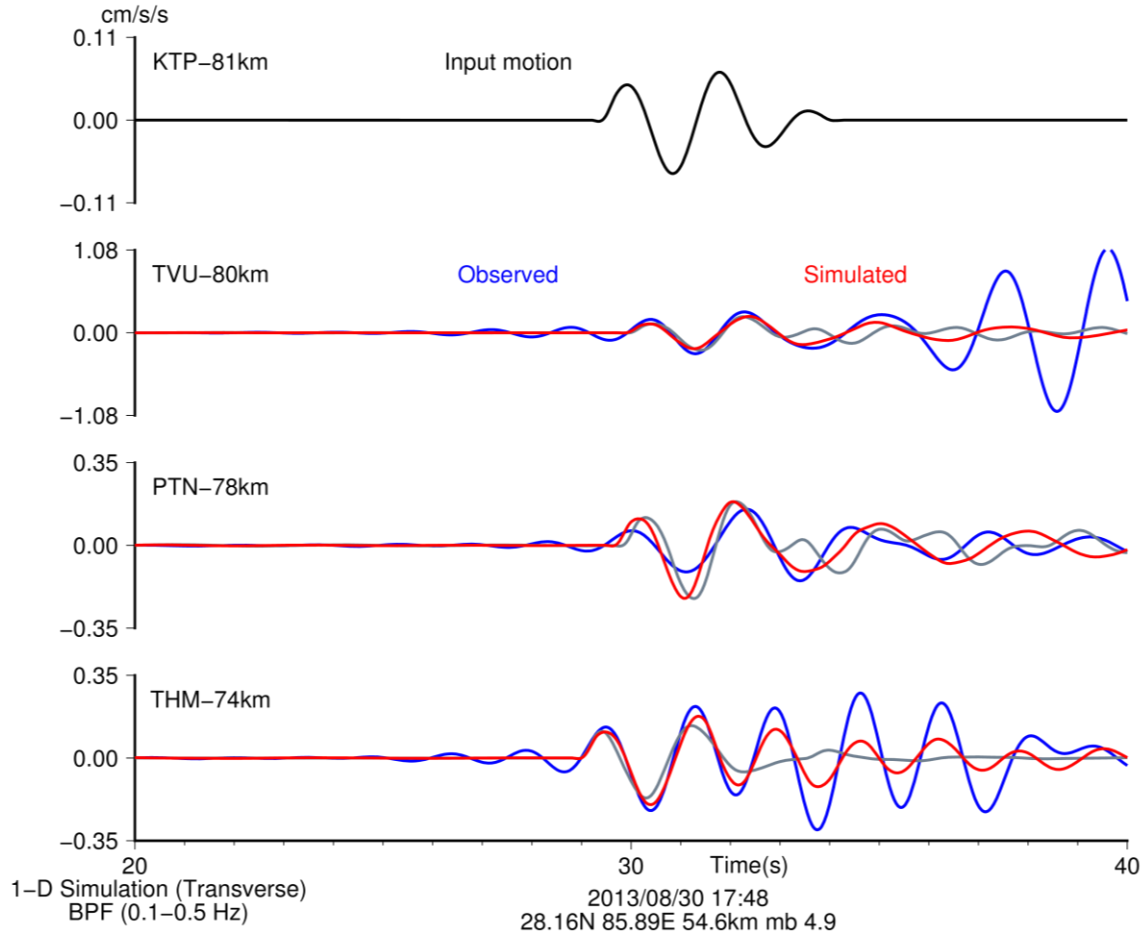

Figure 4. 7 Comparison between simulated and observed waveform for the mb 4.9 earthquake. Comparison is carried out only for the part shown by red arrows.

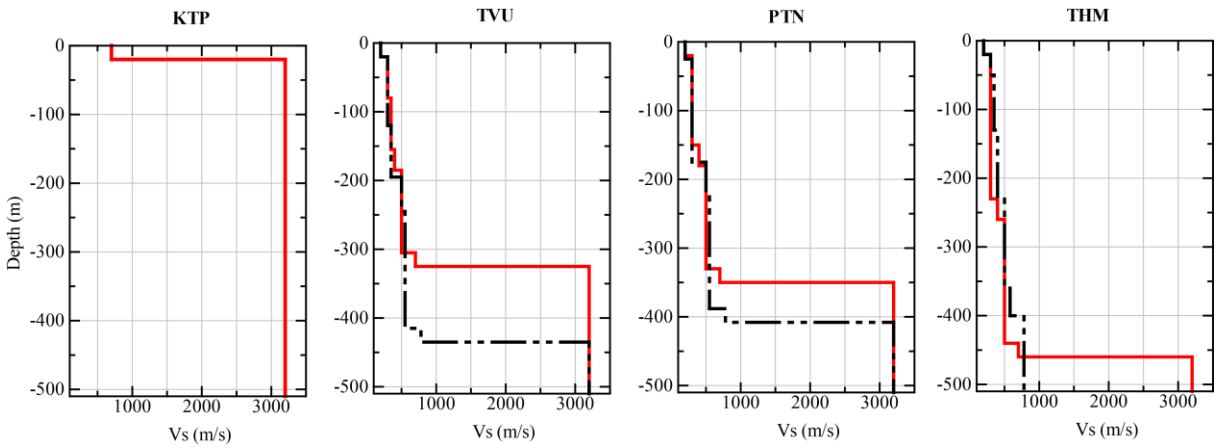

Figure 4. 8 1-D velocity models for four permanent stations.

The comparison of the average H/V ratios from observed records and the theoretical H/V ratios (the HVSR method) shows agreement in the low-frequency (long-period) range (Figure 4.12). The fundamental peaks of the H/V ratios range from 0.25 to 0.4 Hz for the sedimentary sites. The figure also shows the difference between results from the initial velocity model and adjusted velocity model. The fundamental frequencies of the observed and theoretical H/V ratio (the HVSR method) at TVU show considerably better agreement than those at the other sites. However, there are discrepancies in the high

frequency range, suggesting that velocity models need adjustments for higher frequencies. Both the H/V ratios at KTP are similar in shape, a flat profile with no clear peak, in the in the low-frequency range (< 1 Hz), while they are not similar in shape in the high-frequency range (> 1 Hz).

Table 4. 4 Initial and adjusted velocity models of three permanent sedimentary stations

Initial 1-D model				Adjusted 1-D model			
V_s (m/s)	Layer thickness (m)			V_s (m/s)	Layer thickness (m)		
	TVU	PTN	THM		TVU	PTN	THM
200	20	25	20	200	20	20	20
300	100	150	30	300	60	130	210
350	75	0	80	350	75	0	0
500	50	48	100	400	30	30	30
550	170	165	130	500	120	150	180
580	-	-	40	-	-	-	-
780	20	20	>100	700	20	20	20

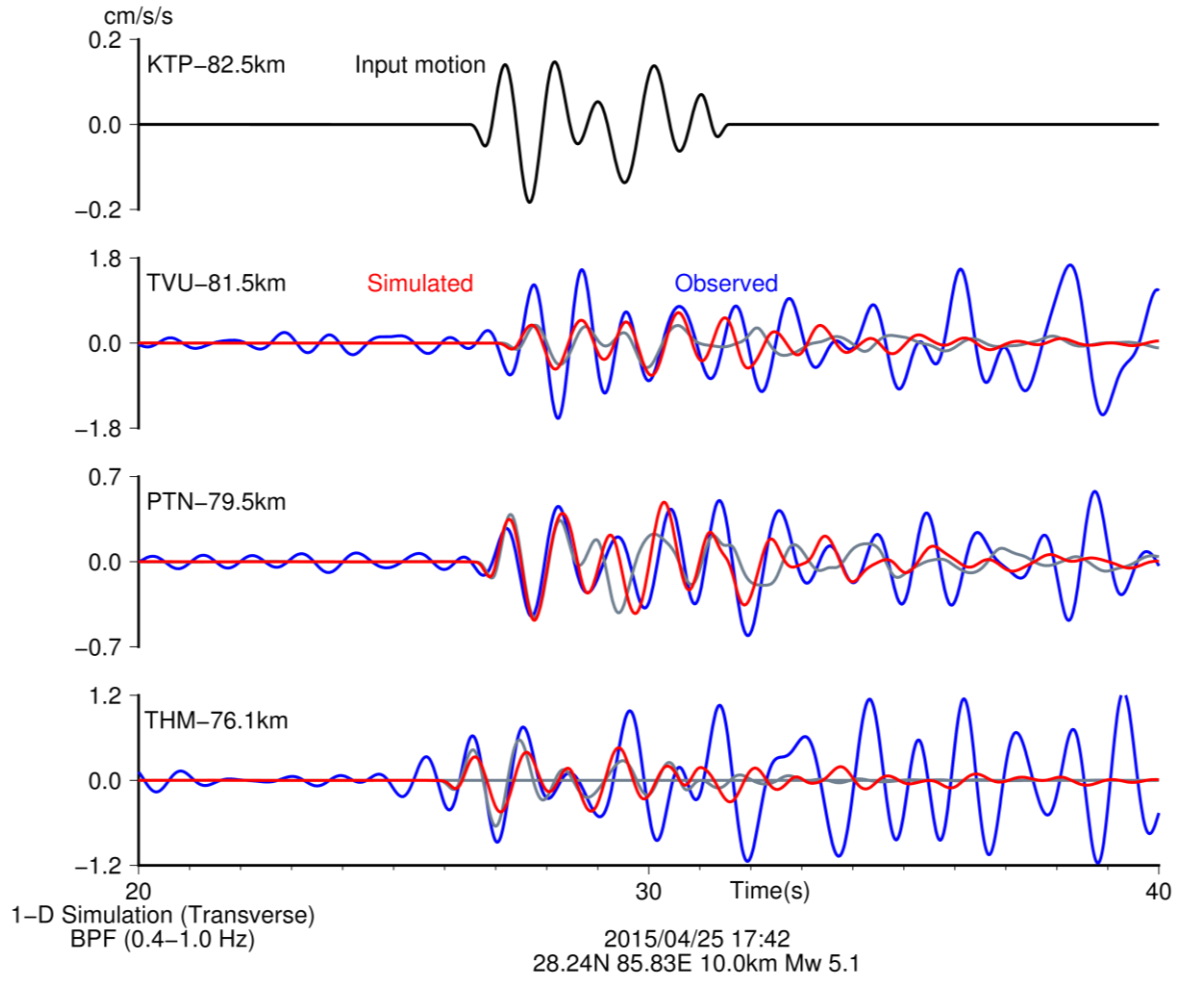

Figure 4. 9 Simulation of M_w 5.1 earthquake suing the adjusted 1-D velocity models. Comparison of waves for the part indicated by red arrows.

The 1-D velocity models for the four temporary sites were adjusted using the HVSR method (Figure 4.13). Similar to the four permanent stations, the fundamental frequency and amplitude in the lower frequency range show better agreement with the observed H/V ratio. The fundamental frequencies for the sites range from 0.3-0.7 Hz. The 1-D velocity models for the temporary sites (Figure 4.14) are also tabulated in Table 4.5. The simulated waveform for the M_w 5.5 earthquake using the 1-D velocity model provided encouraging results (Figure 4.15). The simulated and observed waveforms for sites RNB and KPN show better agreement in both frequency and amplitude. However, the BKT site needs finer tuning; the presence of a pond near the BKT site might have some effect on the observed waveform. In general, we found that we can use the HVSR method to determine the subsurface structure of the Kathmandu Basin.

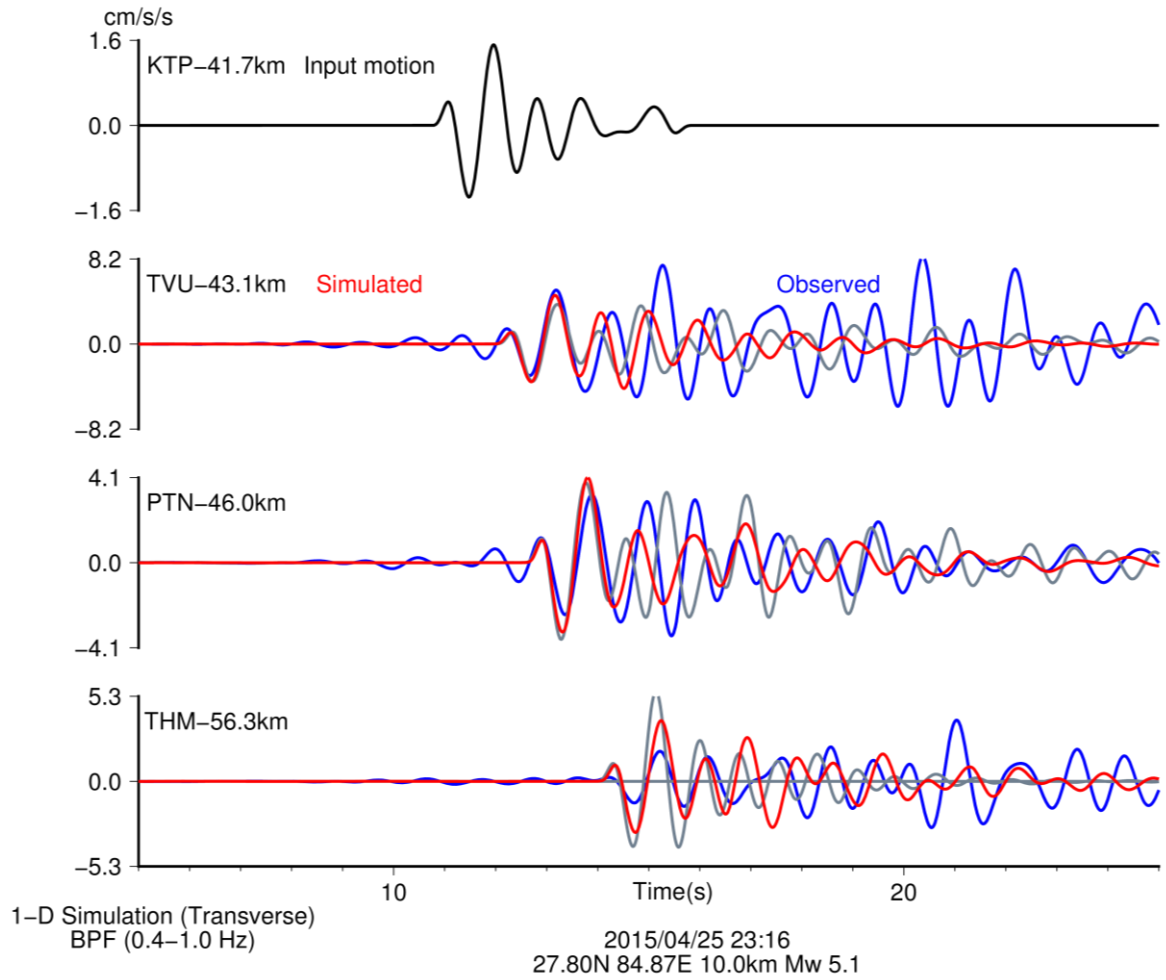

Figure 4. 10 Comparison of simulated waveform and observed waveform in four permanent stations for Mw 5.1 earthquake.

The 1-D velocity models (Figure 4.8, Figure 4.14) of the sediment show varying sediment thicknesses (bedrock depths) for the sites in the Kathmandu Basin. The depth of bedrock varies from 155 m at KPN to 440 m at THM. Because THM is not at the centre of the basin, the depth definitely is more at the centre. As indicated previously, the dominant clay layer in the central part transitions to a sandy layer in the north; this observation has been taken into account while adjusting the velocity models for the northern sites, PPR and KPN (Figure 4.13). As the models were based on the geological cross-sections and borehole logs near the PPR site [4], which showed the dominance of sandy layer with lenses of clay layers, the adjusted models (Figure 4.14, Table 4.5) show a velocity inversion at PPR. An important

feature of the velocity models (Figure 4.8, Figure 4.14) is a large velocity contrast at the bedrock depth. This is due to a geological unconformity in the lithological sequence, where the proto-Bagmati River and initial lake sediments deposited over the layer of weathered basement rock during the basin formation.

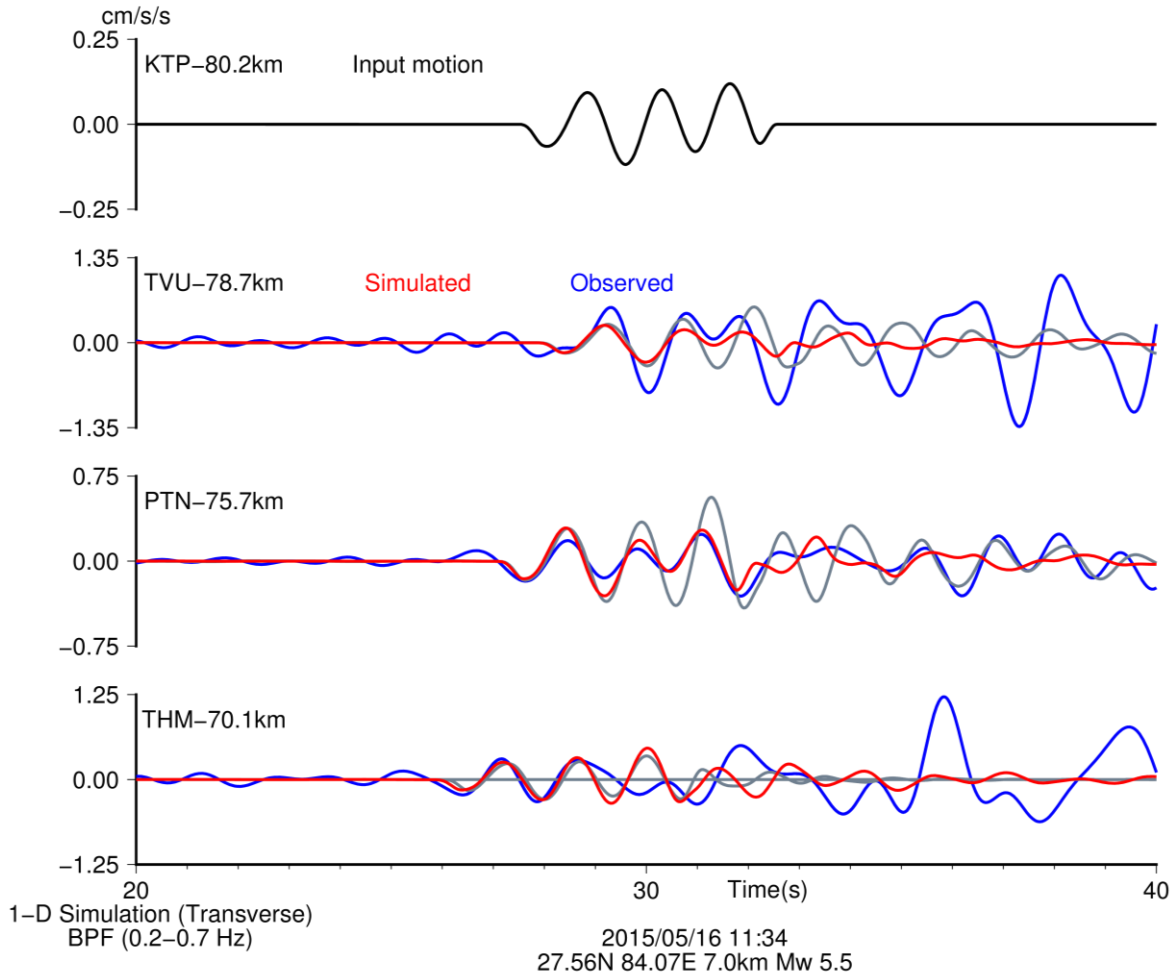

Figure 4. 11 Simulation of M_w 5.5 earthquake in four permanent sites using adjusted velocity models.

A previous study using 1-D modelling near the central Kathmandu showed that sediment depth was ~ 450 m [2,8]. The depth of basement rock calculated using an empirical relationship with the fundamental frequency of ambient seismic noise [30] indicated that bedrock depth at the centre is 347 m. While some of the ambient noise measurement sites from the study [30] lie in the vicinity of the present stations, the previously calculated sediment thicknesses are less than those calculated in the present study. This study estimates sediment thickness beneath TVU as 325 m, and the ambient noise study indicated a thickness of 65 m-138 m beneath two nearby sites. Nevertheless, it clearly shows that the basin has an undulating topography. The 1-D velocity structures and their respective theoretical amplification obtained from the Propagator Matrix method (Figure 4.16) shows the variation between the sites in the form of a difference in fundamental frequency. There is significant amplification in the low-frequency range. The variation in amplification indicates uneven basement topography, which makes generalizing the effects of earthquakes difficult.

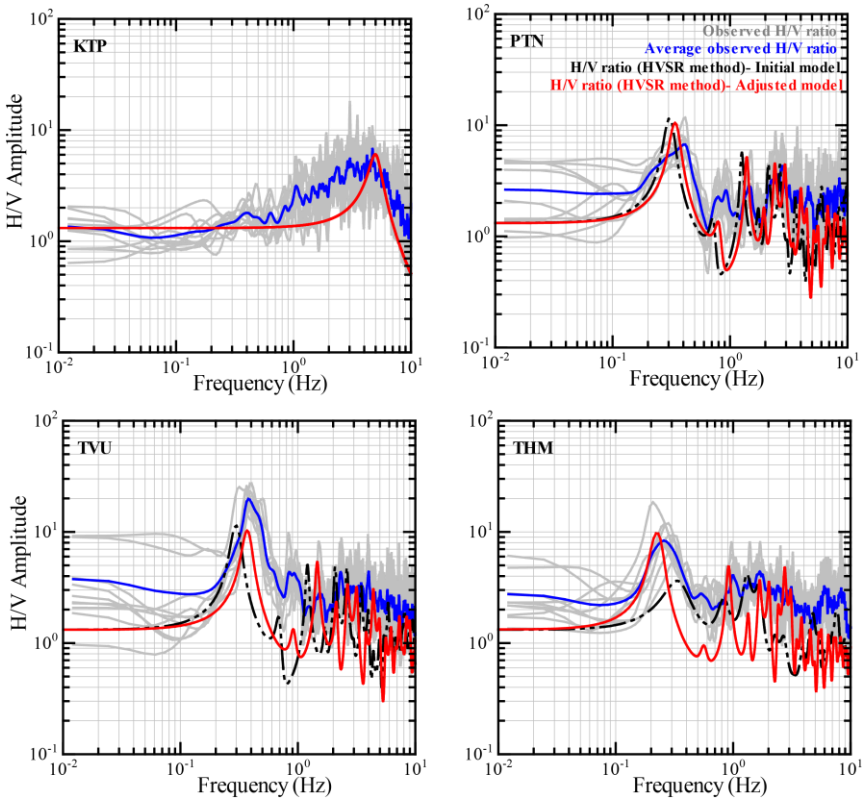

Figure 4. 12 Comparison of the observed average H/V ratio with the theoretical H/V ratio calculated by HVSR method in permanent stations.

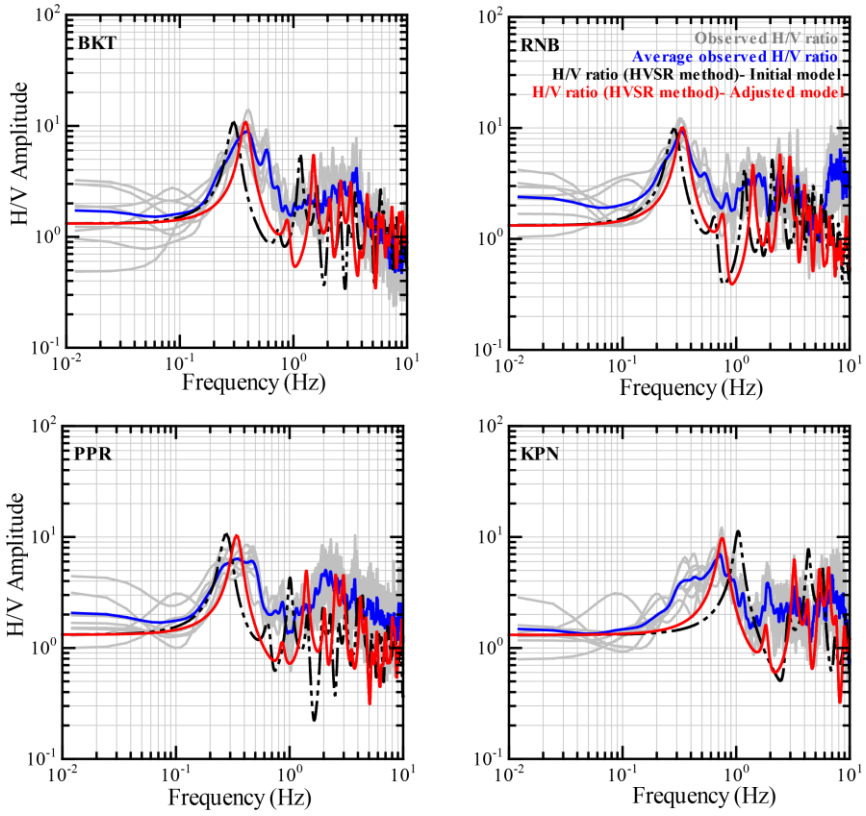

Figure 4. 13 Comparison of the observed and theoretical H/V ratios for four temporary sties.

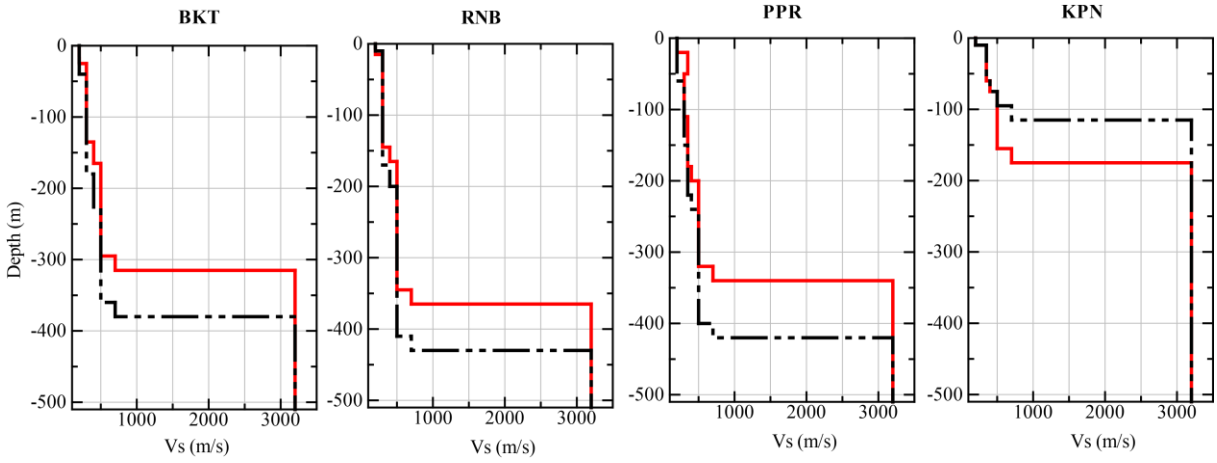

Figure 4. 14 1-D velocity models for four temporary stations adjusted using HVSR method. Also shown are initial models in black dashed line.

Table 4. 5 Initial and adjusted 1-D velocity models of the temporary stations. The asterisk (350) indicate the velocity inversion at PPR.*

Initial 1-D model					Adjusted 1-D model				
Vs (m/s)	Layer thickness (m)				Vs (m/s)	Layer thickness (m)			
	BKT	RNB	PPR	KPN		BKT	RNB	PPR	KPN
200	40	10	60	10	200	25	15	20	10
-	-	-	-	-	350*	-	-	30	-
300	140	160	90	0	300	110	130	60	0
350	0	0	70	50	350	0	0	70	50
400	50	30	20	15	400	30	20	20	15
500	130	210	160	20	500	130	180	120	80
700	20	20	20	20	700	20	20	20	20

4.5 CONCLUSION

This study estimated 1-D velocity models for seven sites in the Kathmandu Basin using strong-motion records from moderate sized earthquakes. First, the initial 1-D velocity models were constructed based on available geological data, borehole logs, and cross-sections. Second, the velocity models were adjusted from the initial models, by using forward modelling of the observed long-period S-wave from mb 4.9 deep earthquake. In this modelling, the observed long-period S-wave at the rock site was assumed as incident wave at the bedrock beneath the sedimentary sites. Third, the adjusted velocity models were verified by comparing the long-period simulated S-waves with the observed ones for three aftershocks (M_w 5.1, M_w 5.1, and M_w 5.5) of the 2015 Gorkha Earthquake (M_w 7.8). The results thus obtained have fairly good agreement between the observed and simulated waveforms.

Finally, the horizontal-to-vertical spectral ratios (H/V ratios) of earthquake ground motion were examined to verify the adjusted velocity models estimated by forward modelling of the observed long-period S-wave. The observed H/V ratios agreed with the theoretical H/V ratios [25] calculated from the adjusted velocity models in the low frequency range; however, there were discrepancies in the high frequency range. It can be hypothesized that the HVSR method can also be used to estimate the subsurface geology in the Kathmandu Basin where the velocity contrast between the bottom sediment

layer and the bedrock is rather high. The HVSR method is also a tool to validate 1-D velocity models. The adjusted 1-D velocity models estimated by this study show the variation of sediment thickness beneath the sites. The bedrock depth varies from 155-440 m indicating an undulating basement topography of the Kathmandu Basin. The models show a high velocity contrast at the bedrock depth which results in significant S-wave amplification at the sediment sites. The information from these 1-D velocity models are used to estimate a 3-D underground velocity model of the basin along with information from geological maps, cross-sections, borehole logs, and gravitational survey data.

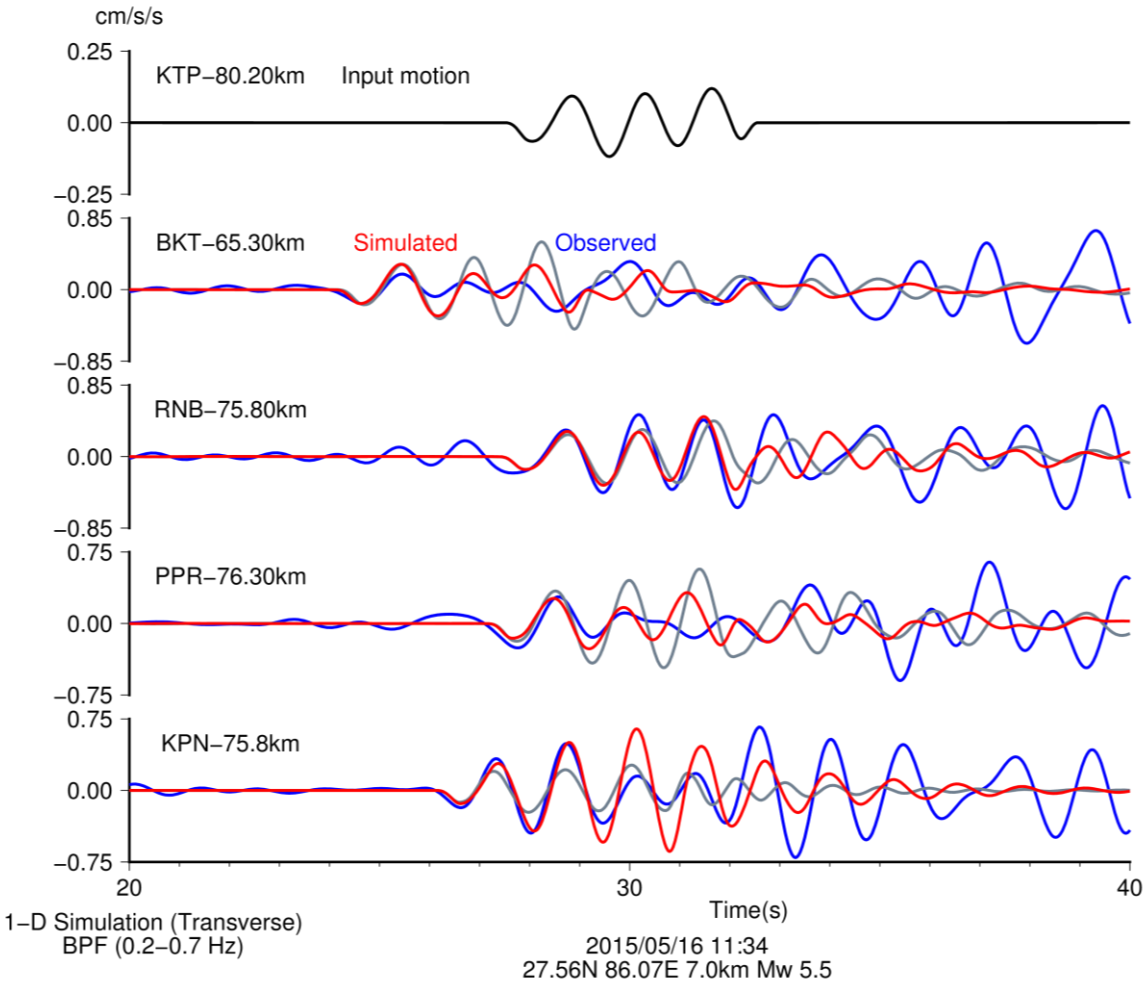

Figure 4. 15 Comparison of simulated and observed waveform at the temporary sites for M_w 5.5 earthquake.

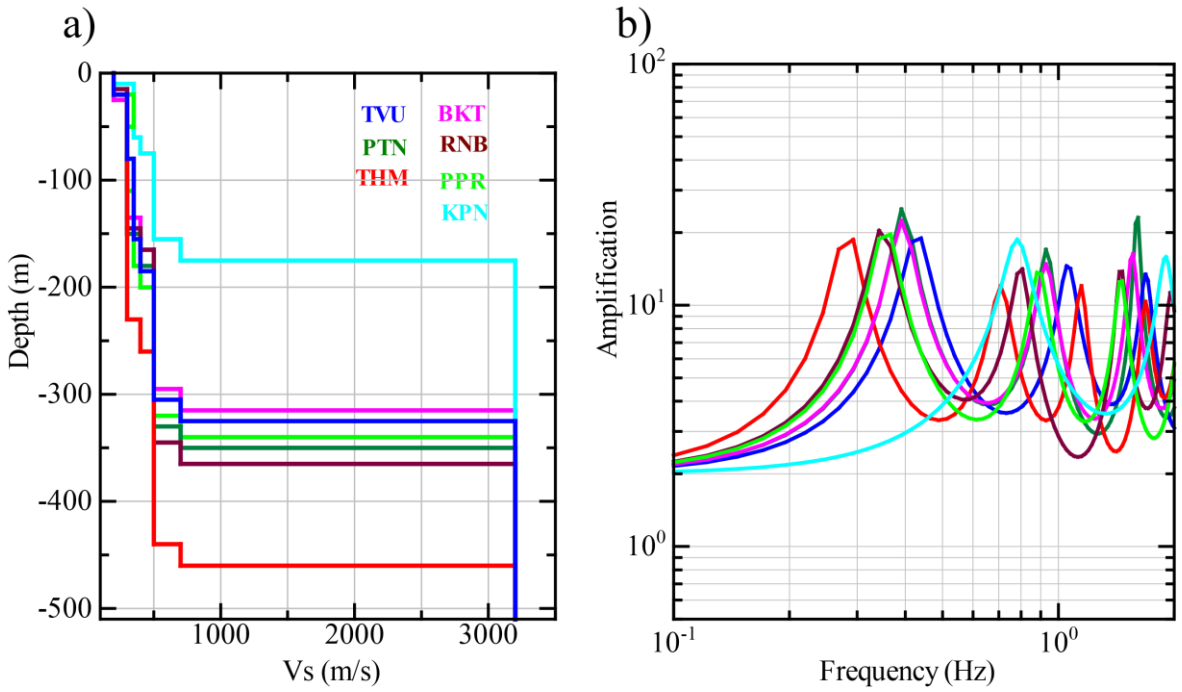

Figure 4. 16 a) Adjusted 1-D velocity structures, and b) Theoretical amplification factors for sedimentary sites calculated by Propagator Matrix method.

References

[1] Dixit, A. M., Yatabe, R., Dahal, R. K. & Bhandary, N. P. Initiatives for earthquake disaster risk management in the Kathmandu Valley. *Natural Hazards* **69**, 631-654, doi:10.1007/s11069-013-0732-9 (2013).

[2] Pandey, M. R. in *12th World Conference on Earthquake Engineering* (Auckland, New Zealand, 2000).

[3] Shrestha, O. M. *et al.* (Department of Mines and Geology, Kathmandu, 1998).

[4] JICA. The study of earthquake disaster mitigation in the Kathmandu valley, Kingdom of Nepal. (Japan International Cooperation Agency and Ministry of Home Affairs Nepal, Kathmandu, 2002).

[5] Piya, B. K. *Generation of a geological database for the liquefaction hazard assessment in Kathmandu valley* M.Sc thesis, International Institute for Geo-Information and Earth Observation (ITC), (2004).

[6] Paudyal, Y. R., Yatabe, R., Bhandary, N. P. & Dahal, R. K. A study of local amplification effect of soil layers on ground motion in the Kathmandu Valley using microtremor analysis. *Earthquake Engineering and Engineering Vibration* **11**, 257-268, doi:10.1007/s11803-012-0115-3 (2012).

[7] Sugimura, Y. *et al.* (Japan Social Fund, Kathmandu, 2012).

[8] Dhakal, Y. P. *et al.* Analysis of strong ground motions and site effects at Kantipath, Kathmandu, from 2015 Mw 7.8 Gorkha, Nepal, earthquake and its aftershocks. *Earth, Planets and Space* **68**, doi:10.1186/s40623-016-0432-2 (2016).

[9] Sakai, H., Fujii, R. & Kuwahara, Y. Changes in the depositional system of the Paleo-Kathmandu Lake caused by uplift of the Nepal Lesser Himalayas. *Journal of Asian Earth Sciences* **20**, 267-276, doi:http://dx.doi.org/10.1016/S1367-9120(01)00046-3 (2002).

[10] Moribayashi, S. & Maruo, Y. Basement topography of the Kathmandu valley, Nepal- An application of gravitational method of the survey of a tectonic basin in the Himalayas *Journal of Japan Society of Engineering Geology* **21**, 30-37 (1980).

[11] Sakai, H. Stratigraphic division and sedimentary facies of the Kathmandu Basin Group, central Nepal. *Journal of Nepal Geological Society* **25**, 19-32 (2001).

[12] Yoshida, M. & Igarashi, Y. Neogene to Quaternary lacustrine sediments in the Kathmandu valley, Nepal. *Journal of Nepal Geological Society* **4**, 73-100 (1984).
[13] Dongol, G. M. S. Geology of the Kathmandu fluviatile lacustrine sediments in the light of new vertebrate fossil occurrences. *Journal of Nepal Geological Society* **31**, 43-57 (1985).
[14] Sakai, H., Fujii, R., Kuwahara, Y., Upreti, B. N. & Shrestha, S. D. Core drilling of the basin-fill sediments in the Kathmandu valley for palaeoclimatic study: preliminary results. *Journal of Nepal Geological Society* **25**, 9-18 (2001).
[15] Dhakal, Y. P., Sasatani, T. & Takai, N. in *9 SEGJ International Symposium* (Sapporo, Japan, 2009).
[16] Dhakal, Y. P., Sasatani, T. & Takai, N. Validation of the Deep Velocity Structure of the Tokachi Basin Based on 3-D Simulation of Long-Period Ground Motions. *Pure and Applied Geophysics* **168**, 1599-1620, doi:10.1007/s00024-010-0237-3 (2011).
[17] Japan Water Agency. (ADB, JWA, 2012).
[18] Takai, N. *et al.* Shallow underground structure of strong ground motion observation sites in the Kathmandu valley. *Journal of Nepal Geological Society* **48**, 50 (2015).
[19] Bijukchhen, S. M. *Strong Ground-Motion characteristics in the Kathmandu Basin (Strong-motion observation and damage assessment of 2015 Gorkha, Nepal Earthquake)* Masters thesis, Hokkaido University, (2015).
[20] Monsalve, G. *et al.* Seismicity and one-dimensional velocity structure of the Himalayan collision zone: Earthquakes in the crust and upper mantle. *Journal of Geophysical Research* **111**, doi:10.1029/2005jb004062 (2006).
[21] Ichiyanagi, M. *et al.* Aftershock activity of the 2015 Gorkha, Nepal, earthquake determined using the Kathmandu strong motion seismographic array. *Earth, Planets and Space* **68**, doi:10.1186/s40623-016-0402-8 (2016).
[22] Aki, K. & Richards, P. G. *Quantitative Seismology*. Second edn, 700 (University Science Books, 2000).
[23] Olsen, K. B., Nigbor, R. & Konno, T. 3D viscoelastic wave propagation in the Upper Borrego Valley, California, constrained by borehole and surface data. *Bulletin of Seismological Society of America* **90**, 134-150 (2000).
[24] Satoh, T. in *13 World Conference on Earthquake Engineering* (Vancouver, Canada, 2004).
[25] Kawase, H., Sanchez-Sesma, F. J. & Matsushima, S. The Optimal Use of Horizontal-to-Vertical Spectral Ratios of Earthquake Motions for Velocity Inversions Based on Diffuse-Field Theory for Plane Waves. *Bulletin of the Seismological Society of America* **101**, 2001-2014, doi:10.1785/0120100263 (2011).
[26] Nagashima, F. *et al.* Application of Horizontal-to-Vertical Spectral Ratios of Earthquake Ground Motions to Identify Subsurface Structures at and around the K-NET Site in Tohoku, Japan. *Bulletin of the Seismological Society of America* **104**, 2288-2302, doi:10.1785/0120130219 (2014).
[27] Borah, K., Kanna, N., Rai, S. S. & Prakasam, K. S. Sediment thickness beneath the Indo-Gangetic Plain and Siwalik Himalaya inferred from receiver function modelling. *Journal of Asian Earth Sciences* **99**, 41-56, doi:10.1016/j.jseaes.2014.12.010 (2015).
[28] Takai, N., Shigefuji, M., Bijukchhen, S., Ichiyanagi, M. & Sasatani, T. in *16 World Conference on Earthquake Engineering* 12 (Santiago, Chile, 2017).
[29] Rajaure, S. *et al.* Characterizing the Kathmandu Valley sediment response through strong motion recordings of the 2015 Gorkha earthquake sequence. *Tectonophysics* **714-715**, 146-157, doi:10.1016/j.tecto.2016.09.030 (2017).
[30] Paudyal, Y. R., Yatabe, R., Bhandary, N. P. & Dahal, R. K. Basement topography of the Kathmandu Basin using microtremor observation. *Journal of Asian Earth Sciences* **62**, 627-637, doi:10.1016/j.jseaes.2012.11.011 (2013).

CHAPTER V
CONSTRUCTION OF A 3-D UNDERGROUND VELOCITY MODEL OF THE KATHMANDU BASIN AND GROUND MOTION SIMULATION

CHAPTER V.CONSTRUCTION OF A 3-D UNDERGROUND VELOCITY MODEL OF THE KATHMANDU BASIN AND GROUND MOTION SIMULATION

5.1 INTRODUCTION

The prevention of loss of life and property during an earthquake can be achieved by construction of earthquake resilient structures. To accomplish this goal, the response of ground to the seismic waves must be thoroughly known. The response of ground to seismic waves vary depending upon the geology, physical property of the underground material, and the path the waves travelled through. So, it is necessary to demarcate areas which are susceptible to earthquake disaster and formulate suitable building codes. The information regarding ground motion prediction in specific site becomes essential for the task. This can be carried out by construction of a 3-D basin structures and simulation of ground motion based on the structure so that the response of specific place can be understood. Thus, a 3-D basin structure is an indispensable prerequisite for strong-motion estimation.

The ground motion estimation in the Kathmandu Basin to mitigate earthquake disaster has become a necessity as a risk of a large earthquake occurring in the Nepal Himalaya [1] looms large. Past earthquakes, the most recent one being the 2015 Gorkha earthquake brought lot of damages to the Kathmandu Basin. The amplification of seismic waves by soft sediments was observed during the earthquake as we already discussed in the preceding chapters. The response of site to the seismic waves vary a lot in the Kathmandu Basin because of its uneven topography and sediment distribution. During the Gorkha earthquake, it was observed that the area around rock site KTP in Kirtipur didn't suffer damage when compared to nearby settlement of Panga (< 2 km south of KTP) where many buildings completely collapsed after the mainshock [2]. It has been mentioned earlier that the site around TVU which is also less than 2 km far from KTP suffered statistically more damage than KTP. So, to understand this varied ground response in Kathmandu, a 3-D underground velocity model was prepared based on which strong-ground motion simulation could be carried out. This chapter focuses on the methodology of construction of 3-D underground velocity structure of the Kathmandu Basin using gravity anomaly data, geological map, geological cross-sections, and shallow borehole logs. It will also focus on the ground motion simulations based on this 3-D velocity model. The waveforms thus obtained will then be compared with observed waveforms to check the accuracy of the velocity structure.

5.2 CONSTRUCTION OF THE 3-D UNDERGROUND VELOCITY STRUCTURE

A 3-D velocity structure is normally constructed based on geophysical methods like seismic explorations (reflection and refraction), micro-tremor array, and gravity survey and direct methods like deep bore holes. Many government and research institutions prepare 3-D structures of important areas to facilitate different research. In Japan, NIED has prepared 3-D velocity models for many parts of the country [3,4]. These structures not only help in strong-motion studies but also in geological studies. Unfortunately in Nepal, a 3-D underground velocity model of the Kathmandu Basin though essential, is lacking. In the present study, the construction of 3-D velocity model is based on available geological data, borehole, and gravity survey data, which are but few.

5.2.1. Sub-surface structure of the basin

There are few previous studies regarding the sub-surface structure of the Kathmandu Basin. A Bouguer anomaly study [5] revealed the undulation of basement topography and presence of thick sediments at the central part (~600 m). The geological studies and maps [6-10] of the Kathmandu Basin show variation in the soil types but most of these data are from the surface and underground information is lacking. A study based on microtremor array in Kathmandu [11] was carried out to prepared 1-D velocity structures of some places in of the basin. In 2001, Sakai carried out a geological study along with few deep boreholes and classified the sediments into different geological formations [9].

An earthquake disaster mitigation study of the Kathmandu Basin [12] produced potential seismic wave amplification and liquefaction potential map for different scenario earthquakes. The study classified the

basin into 500 m square grids and defined the geological columnar sections for each grid for the analysis. They based their study in geomorphological classification, geological maps, and existing drilling/borehole data. Piya [13] prepared geological cross-sections of the basin from borehole logs for liquefaction analysis. Paudyal, et al. [14] mapped the basement of the Kathmandu by ambient seismic noise observation. They collected ambient noise of Kathmandu at 172 sites in 1 km grid by a single seismometer and used empirical formula to estimate the basement depth from H/V spectra method. Their depth to bedrock map clearly shows the undulated nature of the basement topography. The geological map, fieldwork data, and borehole logs were used to prepare a geological map with several geological cross-sections of the Kathmandu Basin [15] for underground water prospecting study (Figure 5.1).

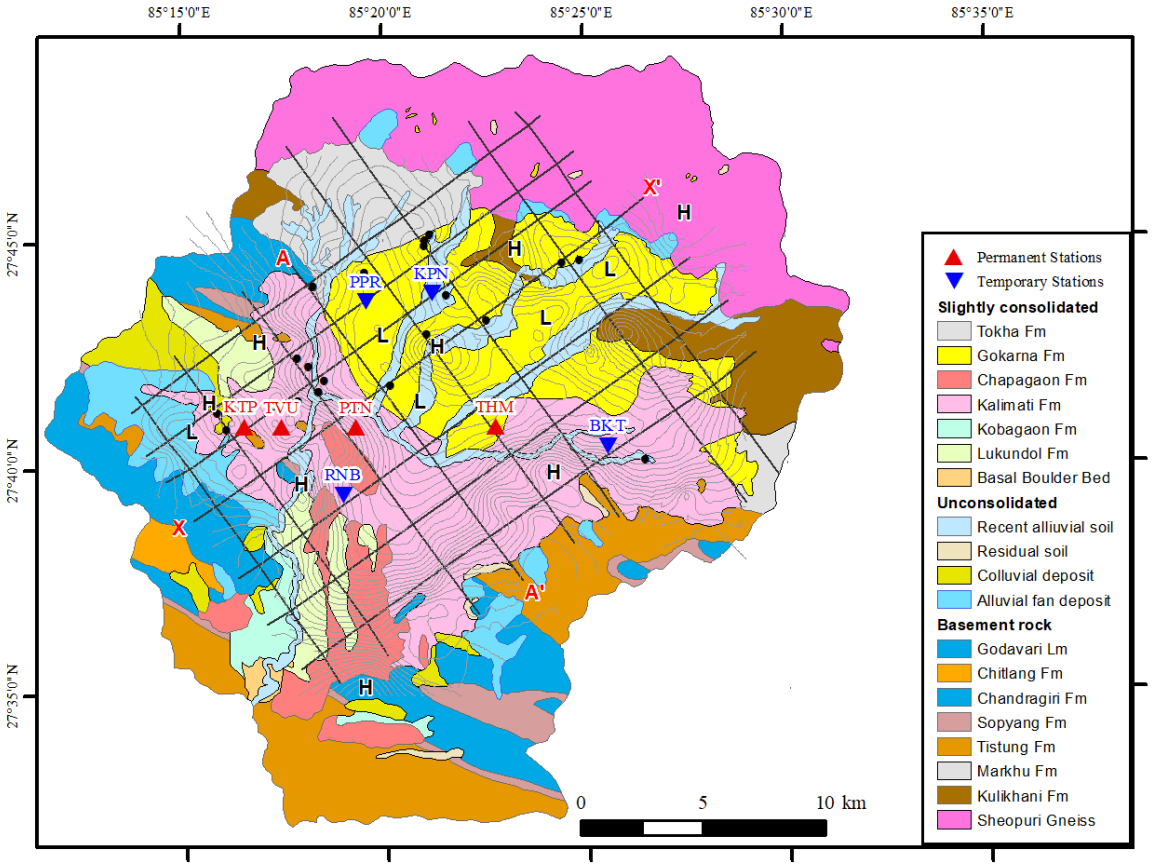

Figure 5. 1 Geological map of Kathmandu [8]. The black dots are the boreholes reaching the bedrock depth and the grid lines are the geological cross-sections [15]. The grey contours are the Bouguer anomaly contours [5] showing areas of High (H) and Low(L) gravity anomaly, indicating shallow and deep basement surface respectively.

The geological cross-sections (grid lines in Figure 5.1) show the undulation of the basin topography as well as the uneven distribution of geological formations. The cross-sections [15] are based on the gravity anomaly result [5], borehole data, geological maps [8,10], and geological field observations. Two cross-sections along X-X' and A-A' from Figure 5.1 can give a general picture of the 2-D structure of the Kathmandu Basin. The cross-section X-X' (Figure 5.2 a) shows the bedrock exposures at Pashupatinath and Gokarna forming smaller basins or sub-basins inside Kathmandu. The cross-section shows a number of faults formed during the mountain-building process and the abrupt exposure of the bedrocks can be a result of these faults. The cross-section A-A' (Figure 5.2 b) doesn't show the bed exposures but we can still see the undulation in the basin topography The deepest part of both the sections has a borehole reaching the bedrock at a depth of 550 m [16] from the surface. The sandy layers (yellow layers in Figure 5.2) replaces the black clay (purple layers) in the north-eastern part of the basin in X-X', but the clay layers are predominant in A-A' cross-section and the sandy layers are not observed. The bottom-most layer in both the cross-sections is the fluvial deposit of the proto-Bagmati River that overlies the bedrock

in almost all part of the Kathmandu Basin. Based on the general geological map and borehole data, these cross-sections cannot show the local heterogeneity which are undoubtedly present in a complex depositional environment of the paleo-Kathmandu Lake. The fault planes and local heterogeneities can have significant impact in the seismic response of those areas.

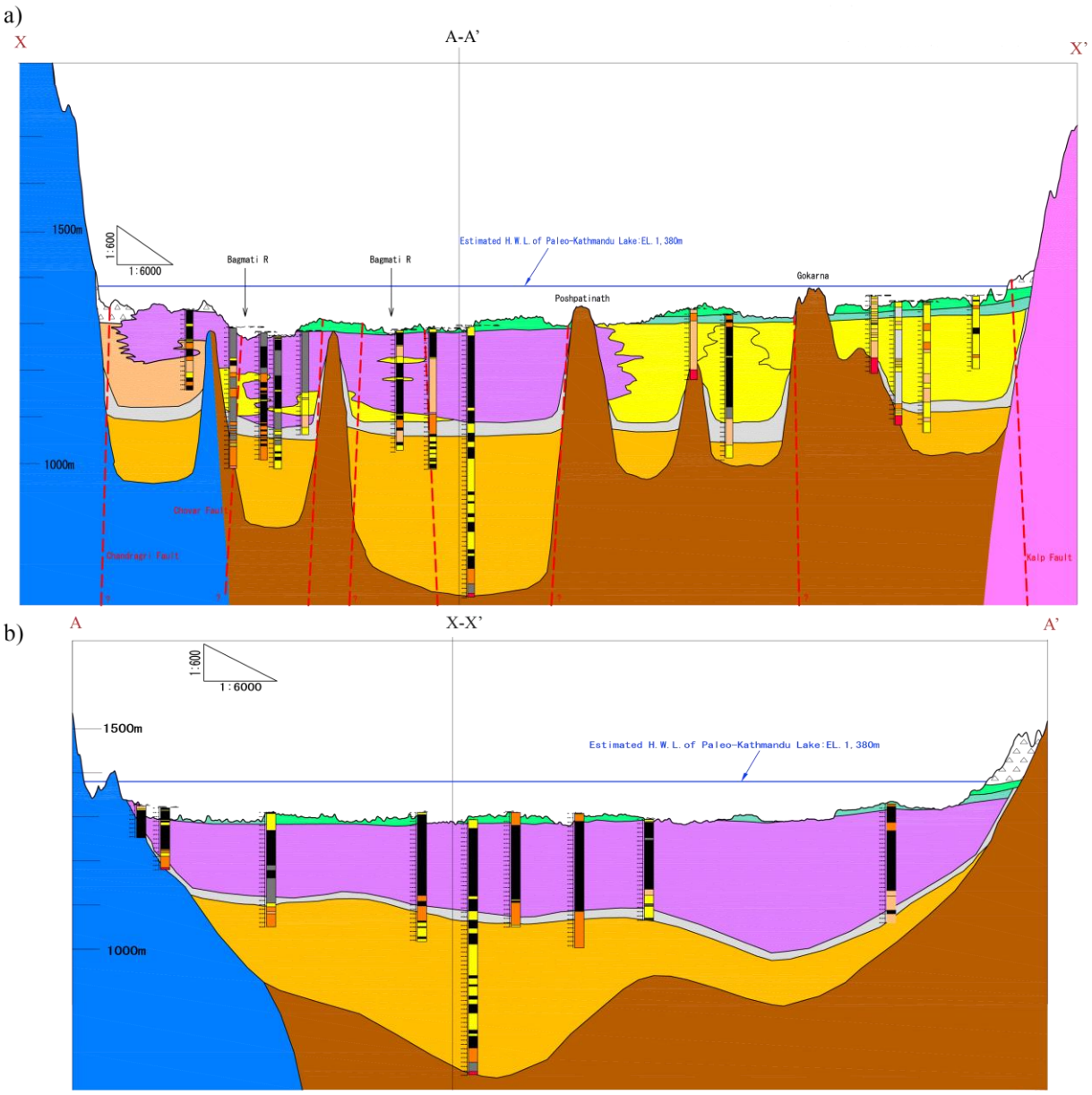

Figure 5. 2 Geological cross-sections [15] along a) X-X' and b) A-A' from Figure 5.1

5.2.2. Methodology

For the preparation of 3-D velocity structure, the geological maps, geological cross-sections [8,9,15], gravity anomaly data[5], and borehole logs [12,13] are considered. There are about 200 boreholes logs most of which were dug for groundwater prospecting so very few of them reach the bedrock. The borehole logs though lack P-S logging data as well as detailed lithological description.
The number of distinctive layers were decided according to the lithology. Though, the sediment of the basin have many heterogeneous layers and sediment lenses (Figure 5.2), these small scale heterogeneities cannot be accurately represented in detail in the 3-D velocity model. Instead, a more general approach is considered with distribution and extent of layers based on the type of the sediment.

The sediments in the basin show a fining upward sequence in general so the model has gravel, sand, and clay layers from bottom to the top.

As mentioned earlier, there is no available the P-S wave velocity data for the deep sediments. The P-S velocity logging for the shallow sediments (<30m) were carried out at five places during the disaster mitigation study [12]. The shear wave velocity (V_s) of the basin sediment layers were then calculated by an empirical formula based on the N-value of the soil type formulated during a study in Japan. The study points that the same empirical formula can be applied for the Kathmandu Basin as well. For the present study, the V_s for each layer is set by taking an average of the range mentioned in the JICA model. The JICA model though considers depth more than 100 m as engineering bedrock and set V_s=400 m/s but the basin sediments are indeed thicker than 100 m. The shear wave analysis carried out during installation of the strong-motion seismometers [17] show the top layer of sediment sites have V_s ~200 m/s whereas the rock-site KTP has V_s ~700 m/s, which is the weathered (exposed) bedrock layer. It can be considered that the similar weathered rock layer exposed at KTP is found at the bottom of the basin sediments, if not of the same lithology. Thus the pebbly coarse sand layer between V_s=400 m/s layer and the V_s= 700 m/s is considered to have V_s of 500 m/s. The top layer, which is clay of fluvial origin is considered to have V_s=200 m/s based on these previous studies.

The depth of the sediment layers are based on the gravity anomaly data, borehole logs, and geological cross-sections. The depth to the basement rock is largely based on the result of the Bouguer anomaly study [5]. For representation of the sediment layers, data from available borehole logs, and gravity anomaly data were compiled and then compared with the geological cross-sections [15]. A number of points were considered along the geological cross-sections (Figure 5.1) in SW-NE and NW-SE direction to properly characterise two dimensional variation of sediment distribution and their thickness. Depth to the layers and their thickness at these points were taken into account to represent the changes in the sediment distribution and the thickness. The points were considered in closer proximity where the variation in sediment distribution is abrupt and complex. Similarly at the borehole sites, the logs were correlated to differentiate and define similar layers and their thickness were computed. The differences between 1-D structures estimated using seismic records and the initial models (Chapter IV) were also considered for points at and around the seismic stations. All these points distributed around the basin were then interpolated to generate 3-D surface maps by Kriging method. The surface maps were generated individually for each layers with a uniform grid size of 100m x 100m using the kriging option in Surfer™ software. The kriging method generates an interpolated grid and estimates the values of spatially distributed points at the grid nodes [18]. Since, the interpolation by kriging was performed for individual layers separately, the boundaries of successive layers intersected each other at some places, which were then corrected to produce smoother 3-D surface layers.

This 3-D velocity model is used for the ground motion simulation by Finite Difference Method (FDM), which requires a planar top level, so the model is truncated at an altitude of 1,320 m above sea level. Since depressing the higher ground changes the basin shape, truncation is a viable option to keep the basin shape intact. This method though creates a filling effect for the regions below 1.320 m (mostly river terraces) by the topmost (V_s = 200 m/s) layer.

5.2.3. 3-D velocity model

The 3-D velocity model with 100 m x 100 m grid (Figure 5.3) has five distinct sedimentary layers superseding a thin weathered bedrock layer (Table 5.1) similar to the 1-D velocity models prepared in Chapter IV.

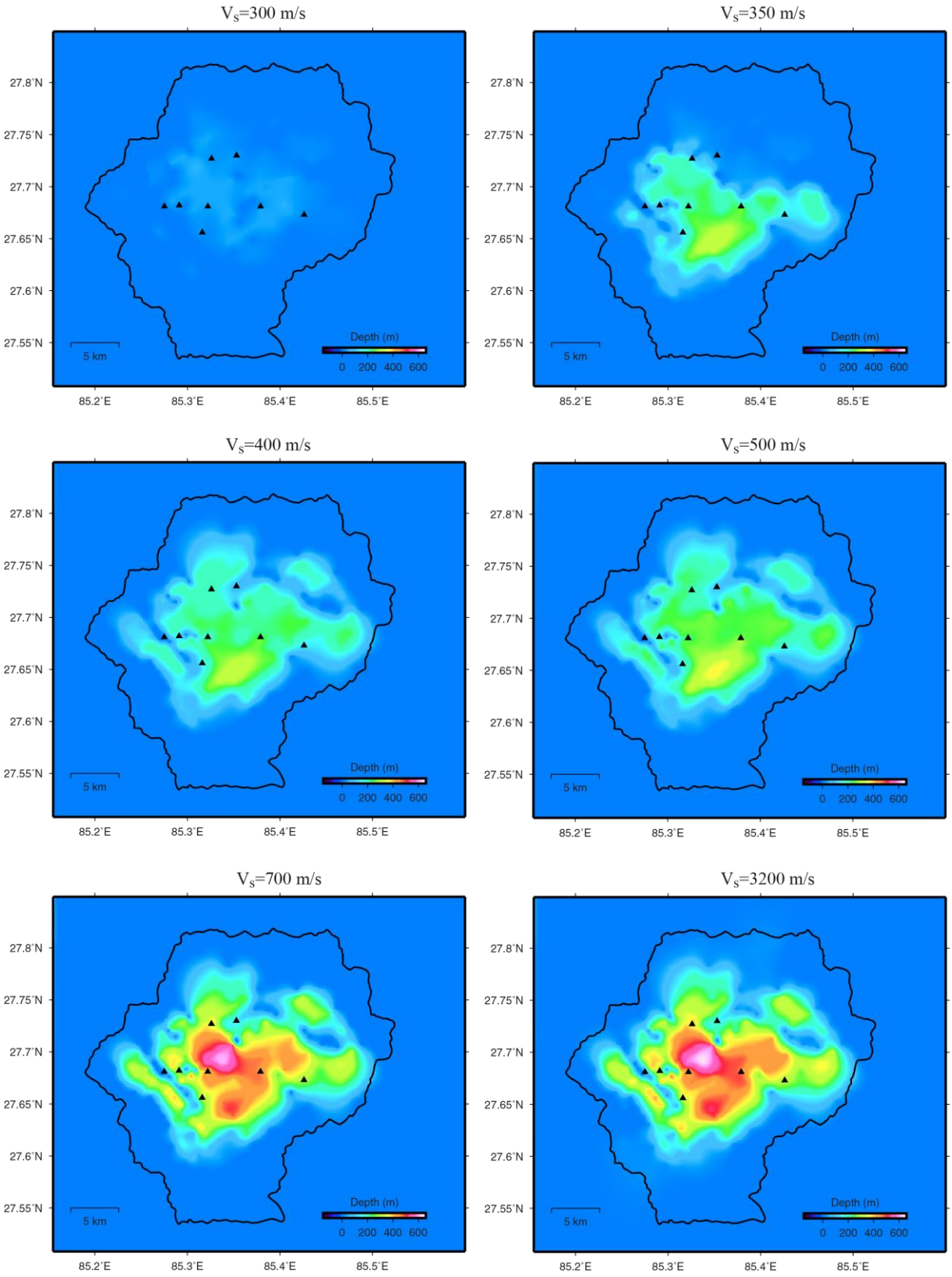

Figure 5. 3 Depth to the basin layers and bedrock of the Kathmandu Basin. The boundary of Kathmandu is shown in black. The black triangles are the location of eight strong-motion seismometers.

The topmost layer having a shear wave velocity of 200 m/s consists of fluvial clay and sand and represents the Patan Formation, the Thimi Formation, and recent fluvial deposits. It reaches to the depth of 50 m. A thick black clay layer (V_s = 300 m/s) represented by the Kalimati Formation and the Lukundol Formation forms the Layer 2 and is widely distributed reaching a depth up to 330 m. Layer 3 is the sandy and gravelly Gokarna Formation mostly distributed in north part of the basin. This layer has V_s = 350 m and reaches up to 330 m depth. The gravelly lignite formation (V_s=400 m/s) spans the whole of the basin and separates the lake deposit and the pebbly, coarse sandy layer (V_s=500 m/s) of proto-Bagmati depositional environment. The depth at the deepest part of the basin, at the centre is 612 m.

The thin bed (<40 m) of lignite (V_s = 400 m/s) separates the underlying proto-Bagmati sediments from the overlying lake sediments. Though this layer may not show significant effect during the ground motion simulation and thus seem unnecessary from engineering point of view, it is retained in the velocity model because of its importance from geological point of view. This ensures that the model can also be used for geological studies in the future.

For the present study it is considered that a layer (~20 m) of weathered rock (V_s=700 m/s) [17] overlies the bedrock (V_s = 3.2 km/s) at the basement. The physical properties of the bedrock is based on the 1-D velocity structure of the Nepal Himalaya [19]. During the formation of the Kathmandu Basin as a result of tectonic process, the rock at the base of the basin would have been exposed for quite some time and underwent weathering before gradually being covered by the river, and later the lake sediments. So, it would be reasonable to consider a layer of weathered rock overlain by river sediments creating a geological unconformity at the base of the Kathmandu Basin. This weathered rock layer is considered to span throughout the basin underlying the soft sediments (Figure 5.4) giving way to hard rock layer (V_s=3.2 km/s) as it approaches the surrounding mountains.

The cross-sections of the model clearly showed the undulation of the basin basement. The study attempts to represent the undulations based on the available geological and subsurface data. The site at KTP (Figure 5.4d) lies on a hillock of exposed bedrock while other sites lie over the sediments of varying depth. There are a number of smaller sub-basins formed by the uneven topography. These can be seen in the basement topography map (Figure 5.5). The site TVU also lies over such sub-basin.

Table 5. 1 Layers of the 3-D underground velocity models.

Layer	V_s (m/s)	Basic lithology	Geological unit	Max depth (m)
Layer 1	200	Clay, fine sand	Patan, Thimi Fm	50
Layer 2	300	Black clay, silt	Kalimati, Lukundol Fm	330
Layer 3	350	Sand, coarse sand	Gokarna Fm	330
Layer 4	400	Gravel, lignite	Basal Lignite	369
Layer 5	500	Boulder bed	Bagmati, Tarebhir Fm	612
Layer 6	700	Weathered bedrock	Tistung, Chandragiri Fm	632

An interesting feature is the high velocity contrast at the bottom of the basin. The shear wave difference between the bedrock (V_s = 3.2 km/s) and the weathered bedrock (V_s=700 m/s) is significant. This is due to the above mentioned geological unconformity where soft sediment were deposited directly over the erosional surface of the hard bedrocks. The result of 1-D forward modelling of seismic waves carried out at the seven station over sediment sites using this high velocity contrast model show good matching with the observed waves [20].

Since, the interpolation method for calculating surface by points can change the values, the 1-D velocity models of eight strong motion stations estimated in Chapter IV [20] were compared with the result after kriging (Figure 5.6) which indicates that there is very small difference between the 1-D model and the 3-D model below the seismic stations.

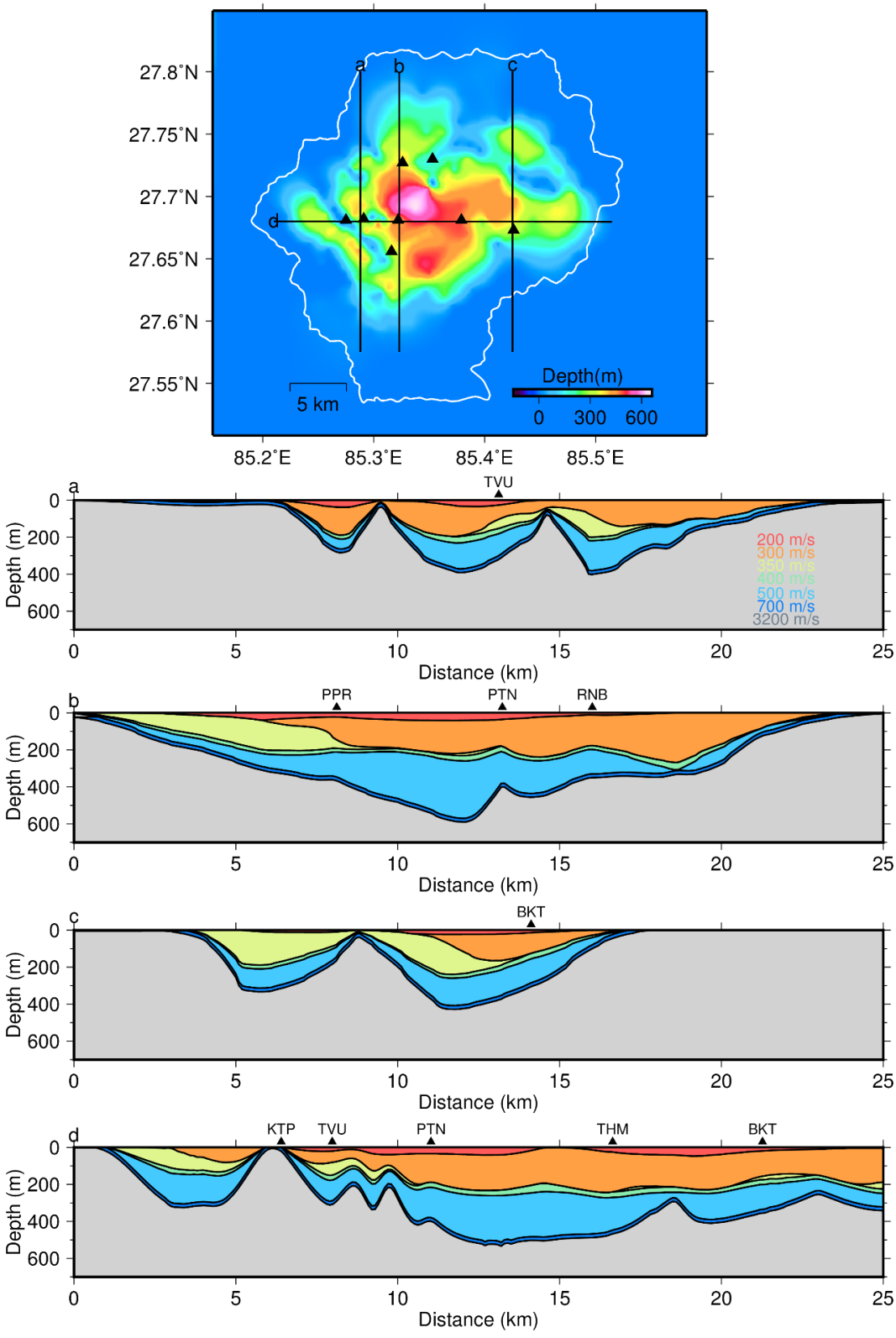

Figure 5. 4 Distribution of depth to the bedrock and (a-d) vertical cross-sections. Black triangles are the strong-motion seismometers. Notice the location of KTP on a hillock/ridge with sub-basin structures on both sides (section d).

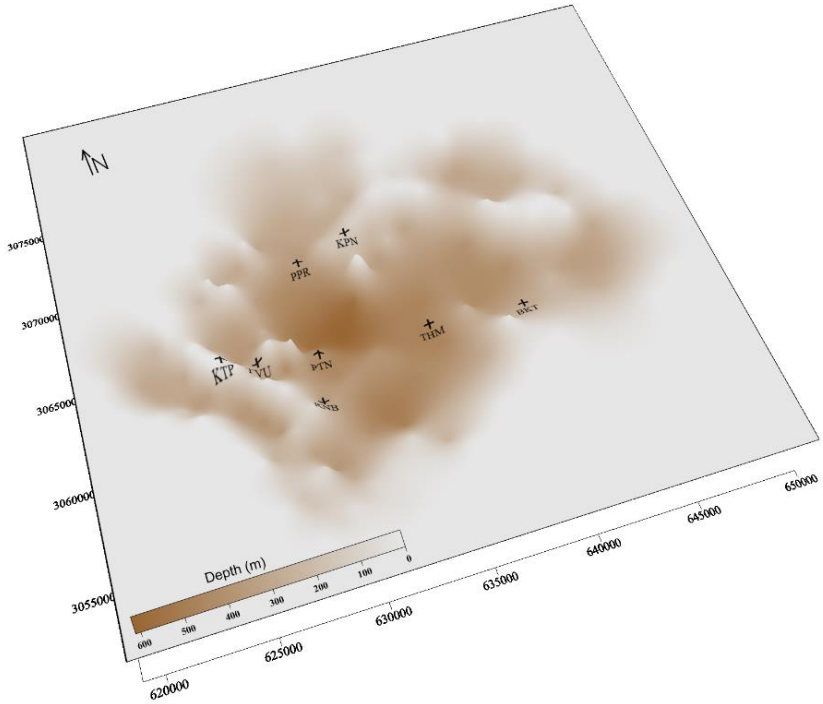

Figure 5. 5 Basin topography of the Kathmandu Basin. The sub-basin structures inside the basin can be clearly seen. The central part of the basin has the highest depth to the basement rocks.

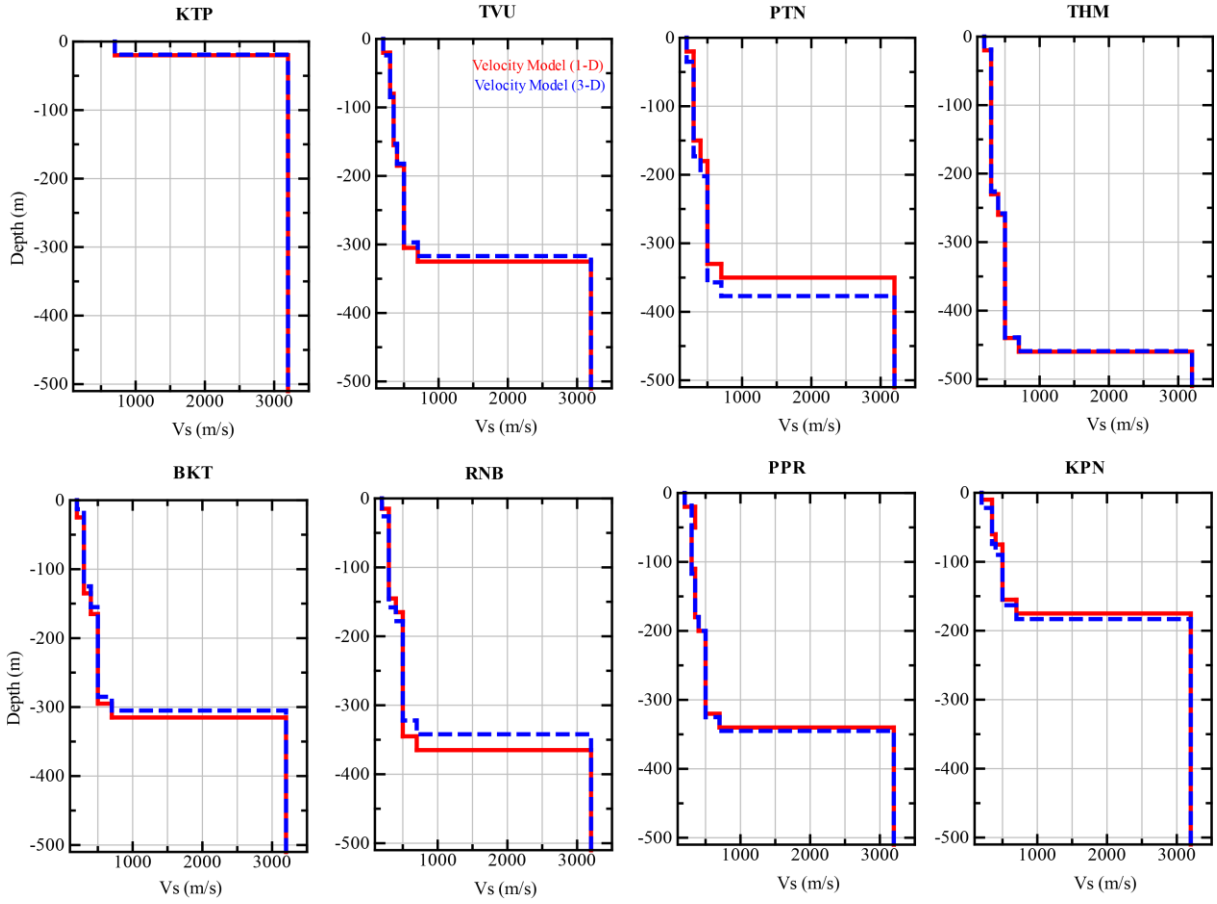

Figure 5. 6 Comparison of the velocity structures under the seismic station estimated by Propagator Matrix method (1-D) and the change in 3-D velocity model after kriging.

5.3 GROUND MOTION SIMULATION

The preparation of the 3-D velocity model of the Kathmandu Basin was to study the basin effect during earthquakes. The soft sedimentary layers not only amplify the earthquake waves but the shape of the basin prolongs the surface wave thereby increasing the effect of the earthquake. The conversion of S-waves into surface waves at the basin edges have also been observed in many basins around the world [21,22]. This basin edge effect was also reported in Kathmandu during the Gorkha earthquake [23,24]. These basin effect can be reproduced by 3-D wave simulations using the 3-D underground velocity models.

For present study, staggered-grid finite difference method [25] is employed for the ground motion simulation. This method is widely used to study the effect of basin structure during an earthquake [21-23,26,27]. There have been several studies trying to balance the trade-off of between ease and speed of calculation and evaluation of influence of slower surface layers [3,28]. The Ground Motion Simulation (GMS) program used for this study is developed by NIED, Japan and is based on the 3-D finite difference method (FDM) using discontinuous grids [3]. Instead of using the same grid-spacing all over the computational region, this method has two overlapping regions: the top one near the surface with finer grids and the region below with grid size three times that of the first region (Figure 5.7). The regions are overlapped in the vertical direction through a distance of *3h/2*, where *h* is the grid spacing of the first region. Aoi and Fujiwara [3] shows that this method not only significantly decreases the overall calculation time, but also help to compute the surface layers with slower velocity by using finer grids than those used for the higher velocity layers. They also showed that the comparison of results of continuous grid spacing to that from discontinuous grid spacing had very little misfit.

For the present work the GMS program was employed to synthesize the waveform from the 3-D velocity model by using discontinuous grid finite difference method with fourth-order accuracy. Two stability conditions have to be fulfilled in order to perform the calculation. In FDM, the number of grids per wavelength (n) is related to the size of grid (h), and the maximum frequency of wave that can be accurately modelled (f_{max}) based on the least velocity (V_{min}) of the layers [29] as shown by the Equation 5.1. For a fourth order accuracy at least 5 grids per wavelength are deemed necessary [30,31].

$$f_{max} = \frac{V_{min}}{nh} \qquad (5.1)$$

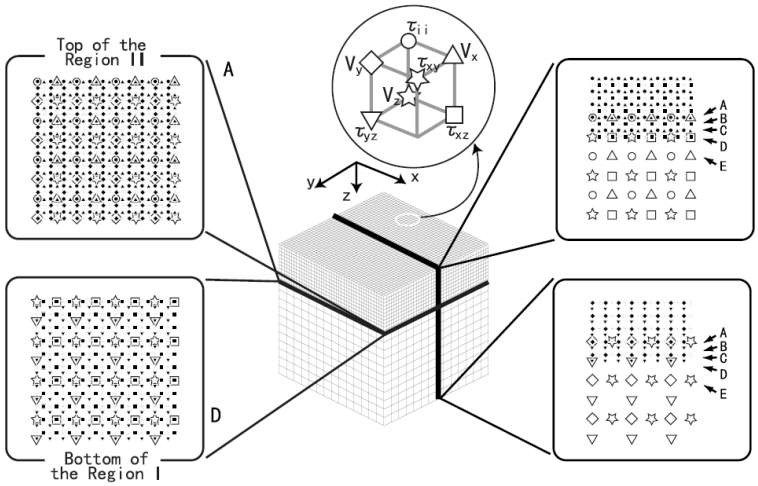

Figure 5. 7 3D discontinuous grid system. The upper region I has smaller grid size and the region II has grid size 3 times that of the region 1 [3].

The stability condition for the minimum time increment (Δt) of the calculation is given by Equation 5.2, which depends on the grid size (h) and the maximum velocity (V_p) of the layers [3].

$$\Delta t = \frac{h}{\sqrt{3}V_p} \tag{5.2}$$

To properly show the basin effect, simulation result of FDM is compared with results from the wave simulation by discrete wave number method (DWM)[32]. Discrete wave number method introduces a number of spatially distributed sources to discretize the radiated wave field (Figure 5.8) and calculate the Green's function in the frequency domain [32]. In this method, the synthetic waveform at a given distance and azimuth are synthesized by replacing the single source by an infinite array of sources that are distributed in the horizontal direction at an equal distance L. For any given wavelength corresponding to a specific frequency of excitation, the elastic energy is radiated in discrete directions only [32]. The distance L is set by satisfying Equation 5.3 [33].

$$r < \frac{L}{2} \quad and \quad \sqrt{(L-r)^2 + z^2} > \alpha t \tag{5.3}$$

where, r = *epicentre distance*
z = *hypocentre depth*
t = *calculation time length*
$\alpha = V_p$

DWN method has been used in simulation of seismic waves in stratified layers for a long time [34-36]. The synthetic waveform from DWN method can simulate the effects of different layers but the basin effect cannot be clearly understood by simple DWN method.

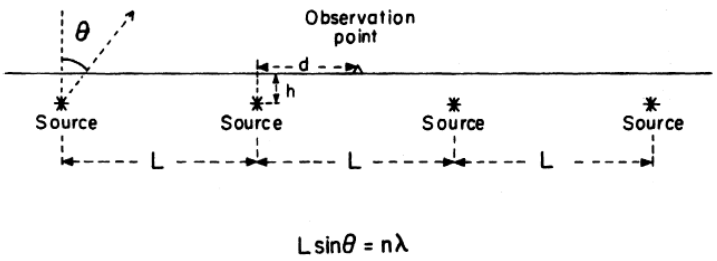

Figure 5. 8 Physical interpretation of DWN method [32].

The comparison of FDM and DWN results will show the basin effect of 3-D basin model. Here, the comparison is carried out in two different models: a planar stratified model and a small basin model. Finally, the 3-D velocity model of the Kathmandu Basin is used to simulate the largest aftershock (M_w 7.3) of the 2015 Gorkha Earthquake by FDM. The results are then compared with the observed waveforms at the eight strong-motion seismic stations to show the basin effect contribution of the 3-D velocity structure. In the simulations by FDM, 60 grids are set as the absorption boundary at the edges and bottom of the calculation area to prevent reflection from the edges and bottom.

5.3.1. Comparison of FDM and DWN methods

Planar stratified model

A three layered velocity model with physical properties of the layers and the earthquake parameters based on simulation performed in Takeo [36] (Figure 5.9) is considered to synthesize the seismic waves at 8 observation points. Four of these are 5 km apart from each other at 030° azimuth and reset four are 5km apart at 090° azimuth. Since this source has a narrow pulse width source function, the f_{max} in FDM simulation is fixed at 1.5 Hz, a grid size of 50 m is taken with five grids per wavelength.

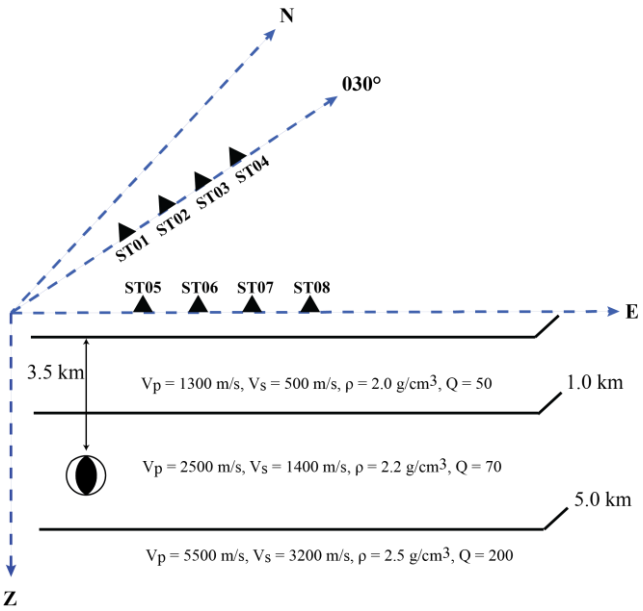

Figure 5. 9 Structure setting for ground motion simulation in planar stratified model. Modified from Takeo [36]

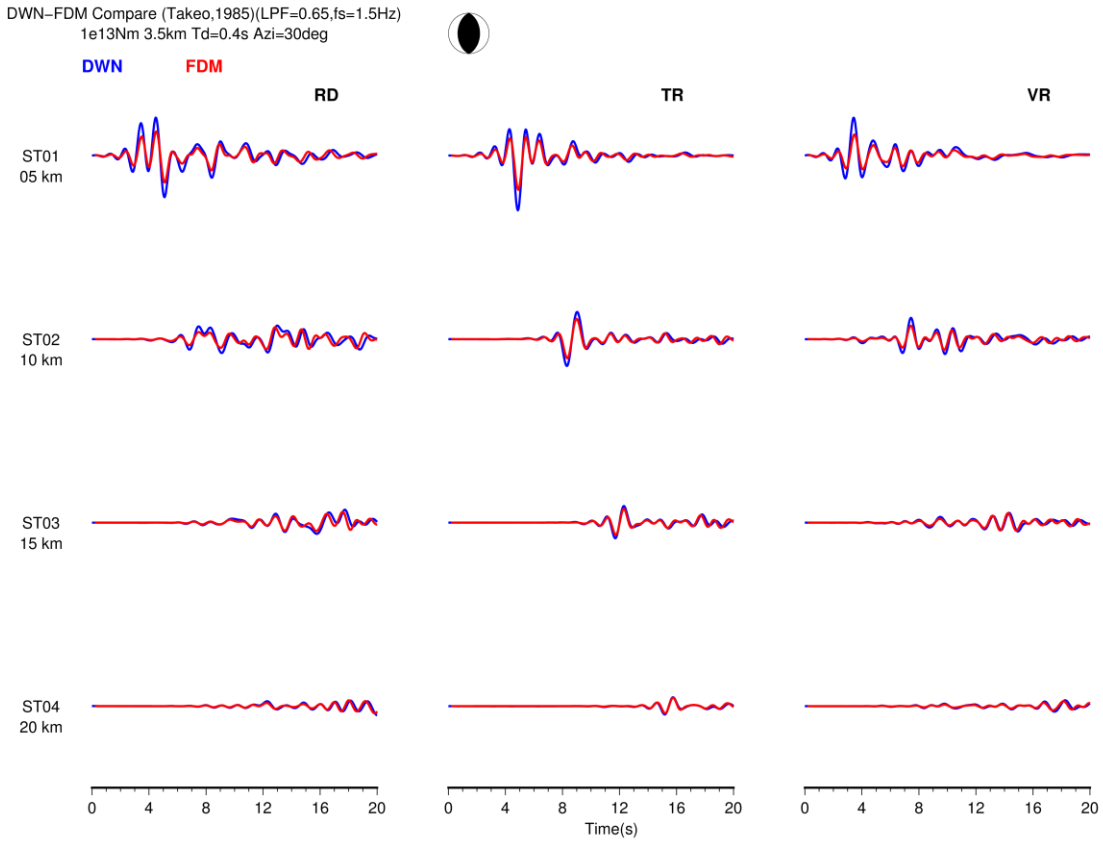

Figure 5. 10 Comparison of synthetic waveform in planar stratified model by FDM and DWN methods at observation point in 030° azimuth.

The comparison of lowpass filtered (LPF: 0.65 Hz) synthetic waveform calculated by the two methods shows good matching at both azimuths (Figure 5.10 and Figure 5.11). The waveform from DWN analysis have slightly higher amplitude than those from FDM at observation points near the source which gets smaller as the distance increases. The good matching of these synthetic waveforms with very small discrepancies indicates that in planar stratified models, both the FDM and DWN methods give very similar results.

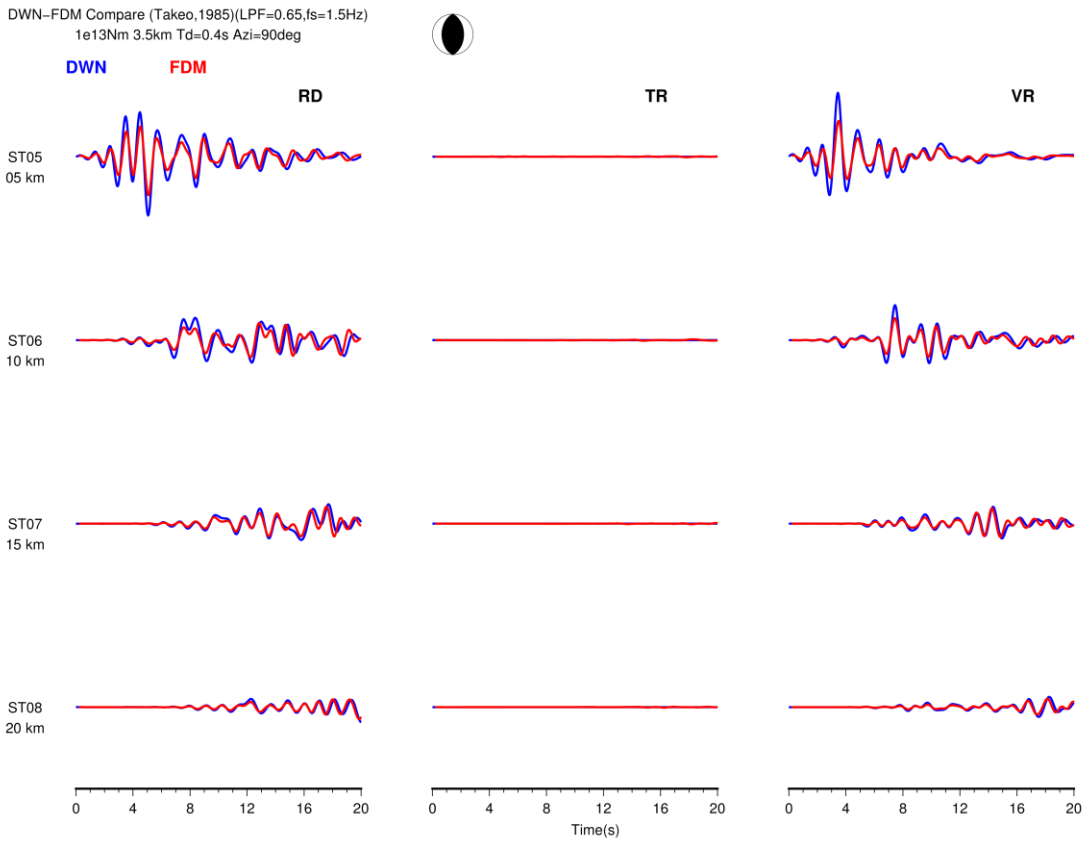

Figure 5. 11 Comparison of synthetic waveform in planar stratified model by FDM and DWN methods at observation point in 090° azimuth.

Small basin structure

It has been observed that in a planar structure, the result from any of the two methods do not vary significantly, so next, the comparison is carried out in a model which produce basin induced waves as a result of basin structure. If we take a look at area around KTP and TVU (Figure 5.4d, Figure 5.5) in the west of the basin, we can see that KTP lies on a hillock which creates smaller sub-basin structure around it. The site TVU which is near (< 2 km) from KTP on the other hand, lies over the basin sediment. The observed waveform on these two stations are quite different owing to the basin structure. A model with a similar dimension of the sub-basin where a hillock protrudes at the middle of a basin ~300 m in depth is prepared for ground motion simulation (Figure 5.12). Three layers are considered with physical properties as shown in the figure. The layer with V_s=700 m/s is the weathered rock layer and is set as ~20 m thick similar to that in the 3-D velocity structure of the Kathmandu basin.

The source is set at a depth of 30 km with focal mechanism of 30°/0°/90° right under the hillock at the centre. Five observation sites are set 4 km apart from each other at an azimuth of 030°/210°. Out of these sites, two lie outside of the basin (over half-space), two lie above the basin sediments, and one lies directly above the epicentre centre on the hill. The FDM calculation is carried out by setting a grid size of 50 m and n=10 grids/wavelength. The DWN method is also employed to calculate the synthetic waveform in these observation points considering a planar stratified models at each observation sites as DWN method cannot be used to simulate waveform in a basin structure. The waveform thus produced are then compared.

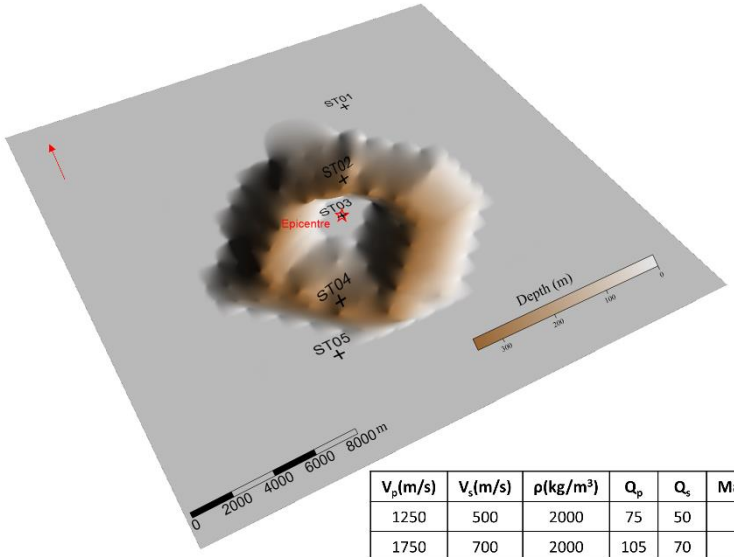

V_p(m/s)	V_s(m/s)	ρ(kg/m^3)	Q_p	Q_s	Max depth (m)
1250	500	2000	75	50	348
1750	700	2000	105	70	368
5500	3200	2400	300	200	-

Figure 5. 12 Structure of the small basin model used for ground motion simulation. The epicentre is right at the middle of the structure. Red arrow shows the North direction.

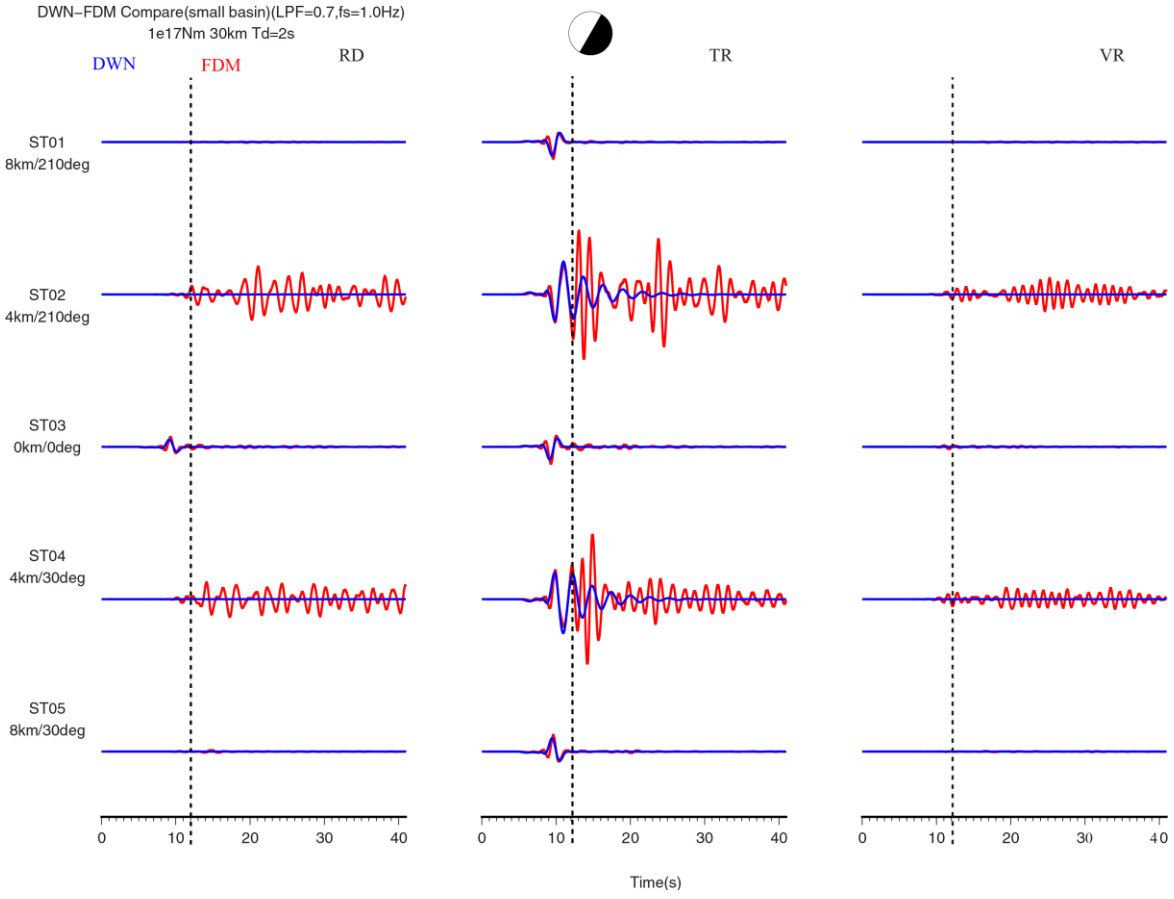

Figure 5. 13 Comparison of waveform synthesized by FDM and DWN method in the small basin structure. The black lines marks the end of direct S-wave.

The result (Figure 5.13) shows the difference in the waveform at observation sites outside and inside the basin. The focal mechanism and position of observation points ensure that there are no direct body wave on the radial and vertical component. The deep source ensures no prominent surface waves during simulation by DWN method.

Even though radial and vertical components are virtually non-existent in waveforms from DWN calculation (Figure 5.13), later phases are clear in results from FDM method. The sites ST02 and ST04 lying over the sediment show basin-induced later phases that start right after the S-wave ends (shown by black line). The surface waves and basin-induced waves are clearly visible in radial and vertical components though no direct S-waves can be observed. These surface and basin-induced waves are produced by successive reflection of the surface wave at the edge of the basin

As the epicentre is under ST03, the corresponding sites ST01-ST05 and ST02-ST04 lie in opposite directions so, we can see the reversal in polarity of the waves in these sites. The S-wave at radial component of ST03 is due to the slight offset of the site (~1cm) from the epicentre as a result of constraints in the calculation methods. We think that this similar phenomenon of smaller basin effect occurs at TVU resulting in larger later phase in the observed waveforms. So, this comparison is effective to understand the basin induced later phases in TVU records as the observed waveform in TVU are very different than the waves at nearby KTP owing to the basin effect.

5.3.2. Ground motion simulation for M_w 7.3 aftershock

The M_w 7.3 earthquake of May 12th, 2015 is the largest aftershock of the Gorkha earthquake sequence and occurred about 80 km NE of Kathmandu at the northern extremity of the main shock fault area. For the present study, this earthquake is considered for the ground motion simulation using the 3-D underground velocity model. There are different constraints about choosing the right earthquake for the FDM analysis. The M_w 7.8 main shock shows significant nonlinearity as mentioned in earlier chapters, so to model this earthquake one needs to properly address the nonlinearity of the models. Many of the smaller earthquakes occurring near the Kathmandu Basin lack information on focal mechanism and energy parameters. Smaller earthquakes also tend to have smaller signal-to-noise ratio so comparison of observed wave with synthetic wave might run into problems. In this context, the M_w 7.3 earthquake is chosen as it is large enough to have high signal-to-noise ratio and it was also recorded in all of the eight strong-motion seismic stations.

This same earthquake was used for the source modelling [37] and to determine 3-D ground shaking by employing FDM by Wei, et al. [27]. They made a simple basin structure model of Kathmandu 900 m deep and tried to reproduce the waveform. But the long period surface waves as a result of basin effect were not clearly simulated especially in the horizontal components. They pointed out the need of a detailed 3-D structure to reproduce the basin effect [27].

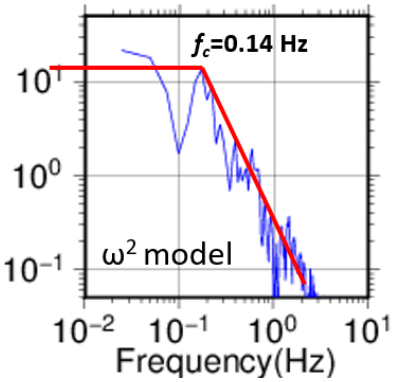

Figure 5. 14 Determining cut-off frequency from the transverse component of displacement Fourier spectra at KTP during M_w 7.3 earthquake.

Different focal mechanism and parameters for this earthquake are reported [27,38,39] but they all show a shallow low angle thrusting mechanism. The location and earthquake parameters (27.809°N 86.066°E, depth = 15.5 km, Mo=9.89E+19 Nm) including the focal mechanisms (303°/9°/110°) for current study is taken from the USGS website [38]. The simulation is carried out by using a triangular source time function. It has to be noted that the pulse width of the source time function has a large effect on the amplitude of the synthetic waveform. Other researchers [27,37] have used a pulse width of 6 s for the simulation. Nevertheless, in this work, the displacement Fourier spectra of the observed wave at the rock site KTP is used to determine the pulse width. As rock sites are devoid of site affect, it can be assumed that the shape of the velocity Fourier spectra resembles the source time function. The acceleration data recorded at the rock site KTP is integrated twice to obtain displacement. Since the Fourier spectrum of the horizontal component of the displacement at KTP follows the ω^2 model (Figure 5.14), we set the reciprocal of the cut-off frequency (f_c = 0.14 Hz) as the pulse width (7.1 s) of the source time function.

For the velocity structures (Table 5.2) of the sediments, V_p was set as a function of shear wave velocity: V_p/V_s = 2.5 [40]. The quality factor Q for the Kathmandu Basin sediments are not available. So we fix Q = 0.1 V_s (in m/s) as commonly used for long-period strong-motion simulation [41,42]. The values are consistent with the observation that Q of near surface sediments are generally around 40-60 [43]. For the deeper layers, regional 1-D velocity model of Monsalve, et al. [19] is used. The density and Q of the basement layers are set according to Grandin, et al. [37].

Table 5. 2 Physical properties of the velocity structure employed for ground motion simulation.

V_p (m/s)	V_s (m/s)	ρ (kg/m3)	Q	Depth of lower boundary(m)
500	200	1500	20	50
750	300	1600	30	330
875	350	1700	35	330
1000	400	1700	40	369
1250	500	2000	50	612
1750	700	2000	70	632
5500	3200	2400	200	3000
5700	3200	2500	200	23000
6300	3700	2700	200	>23000

Since, the epicentre is about 80 km NE of the Kathmandu Basin, the calculation area of 96 x 37.9 km is considered. The Kathmandu Basin is at the western part of this area and the epicentre near the NE corner of the area. By taking a value of n=5grid/wavelength at a spacing of 50 m grid, the maximum applicable frequency of the calculation is 0.8 Hz. The stable time increment satisfying the stability condition (Equation 5.2) is 0.004s. The first region is set at 60 grids below which the grid spacing becomes coarser to 150 m. The absorption boundary is fixed at 60 grids at the bottom and edges of the calculation area. The data obtained were lowpass filtered at 0.5 Hz (f_s = 0.7 Hz) which is well under the maximum applicable frequency. Since the records of Gorkha earthquake main shock and the largest aftershock are prominent in the long period range and the basin experienced long period shaking [27,44], the comparison is also done in the long period waveforms.

The comparison of synthetic waveform and the observed waveform show encouraging results (Figure 5.15). The 3-D model did simulate the basin effect in the sedimentary layers. The waveforms do not match cycle to cycle but the trend is a good fit. The amplitude of synthetic waveform is larger than that of the observed waveforms. The arrival time of the S-wave and the later phase matches in the synthetic and observed waves. The rock site station KTP has the least amplitude as it is devoid of basin effects. The waves show good fit even in the later phase except at TVU. The later phase of TVU couldn't be properly reproduced. This is the result of complex sub-basin structure around TVU. The presence of a local fault (lineaments) near TVU (Figure 5.2a) may also have acted as surface for wave reflection to

produce the prolonged later phase. A detailed study using microtremor array is necessary around TVU to ascertain the proper underground structure.

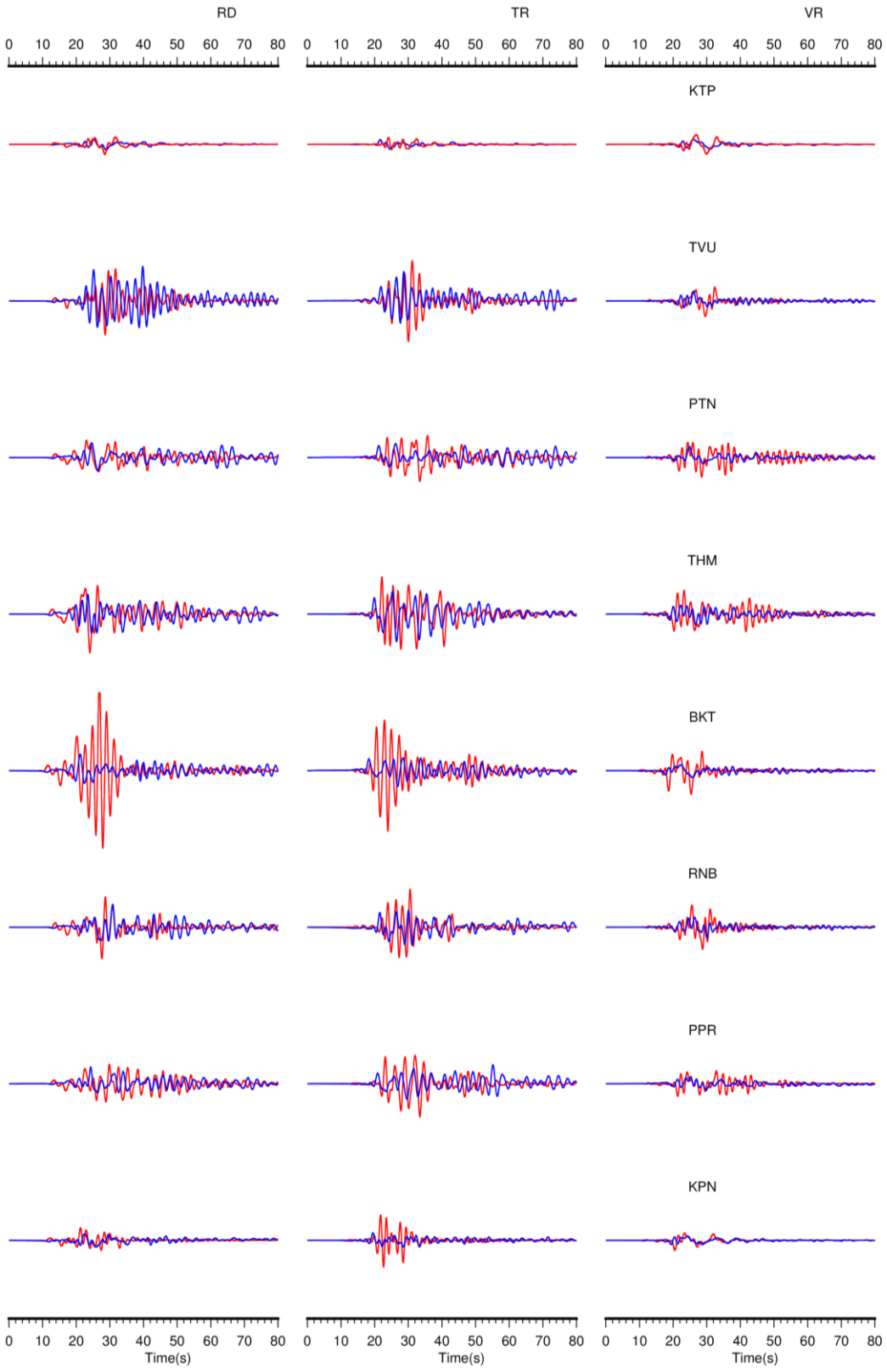

Figure 5. 15 Comparison of synthetic (red) and observed (blue) waveform of M_w 7.3 aftershock at the eight seismic stations. The waveforms are low-passed filtered with f_p = 0.5 Hz and f_s = 0.7 Hz.

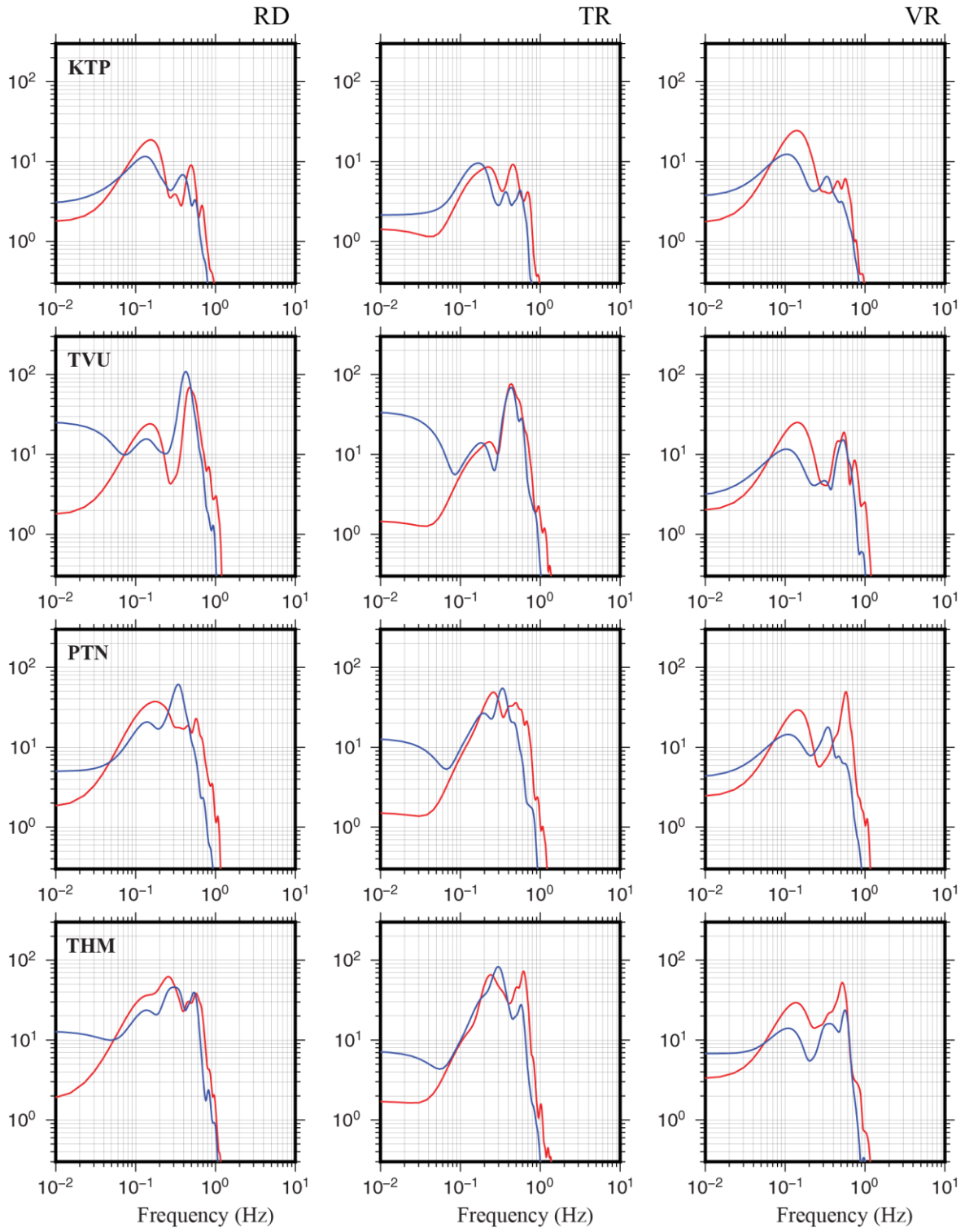

Figure 5. 16 Comparison of the Fourier spectra of observed (blue) and simulated (red) waveforms of M_w 7.3 earthquake at the permanent stations.

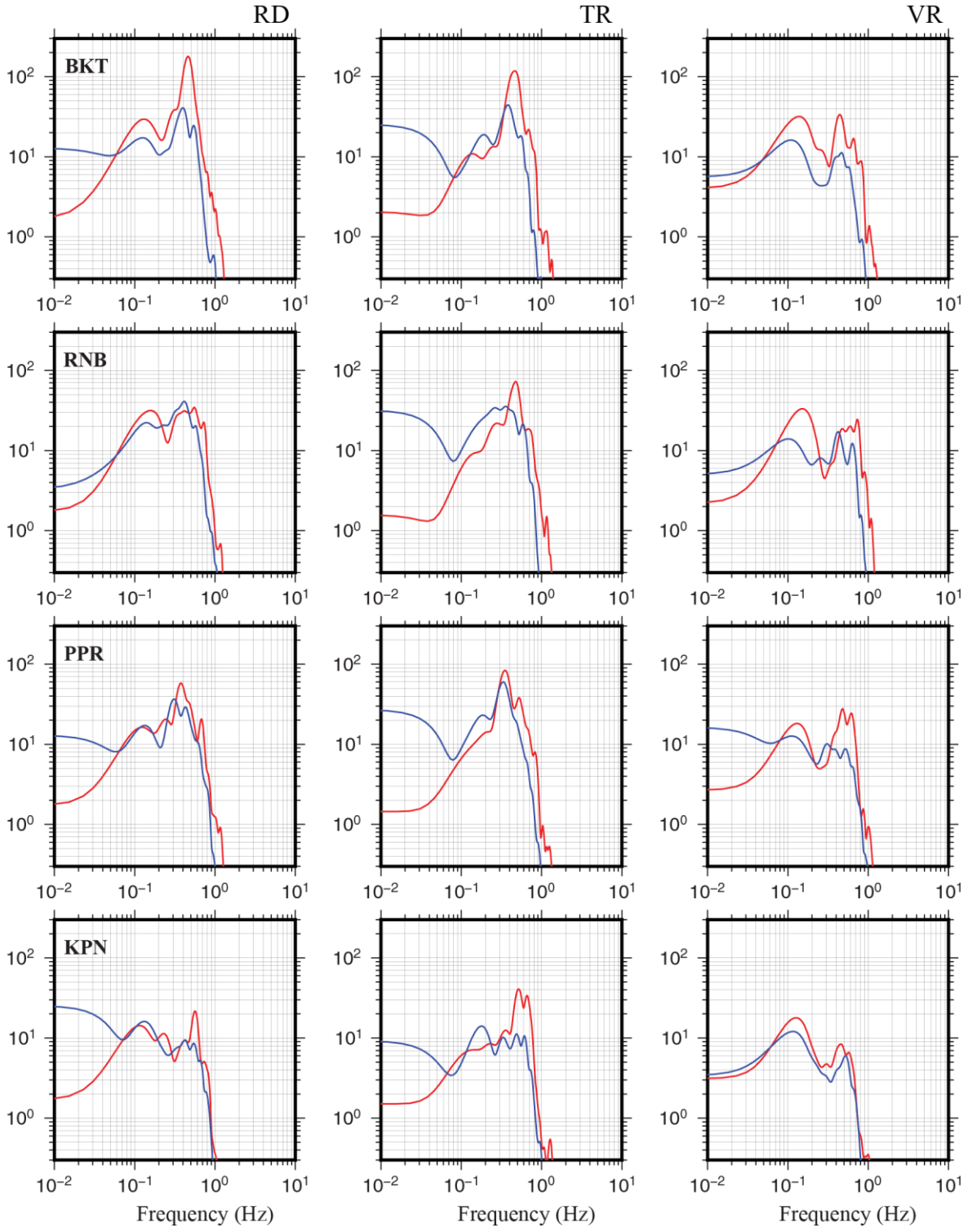

Figure 5. 17 Comparison of the Fourier spectra of observed (blue) and simulated (red) waveforms of M_w 7.3 earthquake at the temporary stations.

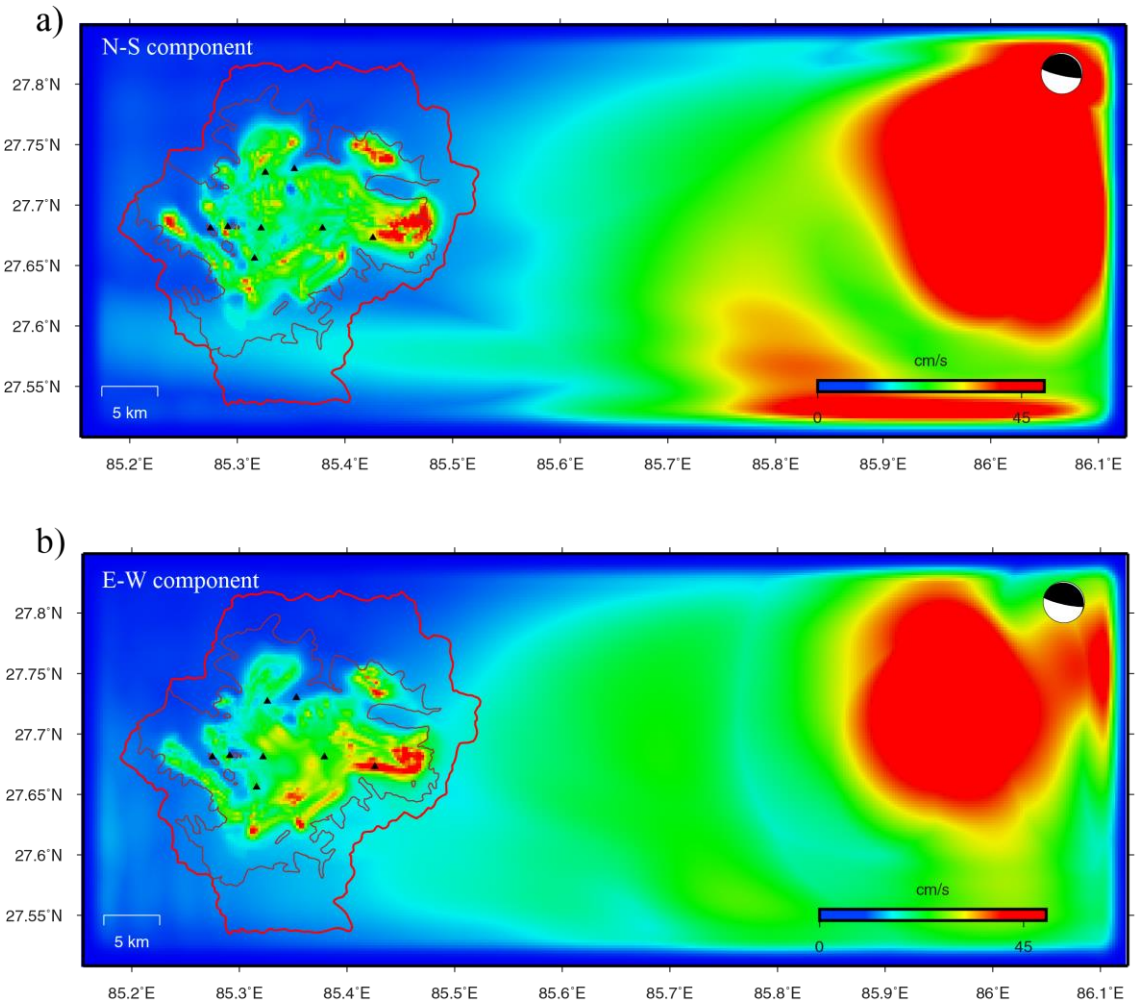

Figure 5. 18 PGV distribution of the a) N-S component and b) E-W component calculated by FDM. Red and brown boundary are repectively political and basin boundaries of Kathmandu. The eight seismic stations are shown as black triangles.

The comparison of the Fourier spectra of observed and simulated waveforms (Figure 5.16 and Figure 5.17) show good fit in frequency and amplitude. Nevertheless, the simulated waves generally show slightly higher amplitude than the observed waveforms at some sites. The overestimation of simulated waves in BKT is clearly observed in the Fourier spectra as well.

The station BKT has different waveform than the observed one. Though the frequency matches, amplitude of the synthetic S-wave is overestimated in the horizontal components. This basin effect is seen in the simulation but not clearly in the observed records. The results from 1-D propagator matrix method and H/V spectral ratio method match the observed data in BKT which is not the case in the 3-D simulation. As the station of BKT was placed on the ground floor of a newly constructed 3 story RC building, the observed wave might have been affected by the foundation interaction which acts as a spring and reduces the input motion of an earthquake. Another reason can be presence of local Since BKT station is no longer is in operation, a seismic array study locally may be able answer this question. In case of the waveforms in the vertical components, all stations have better fit than those in the horizontal components.

The peak ground velocity (PGV) (low-pass filtered 0.5 Hz) of all the grids in horizontal components show the higher values at the basin edges (Figure 5.18). The simulation shows prominent wave amplification in areas that are near to the edge rather than deep central part. Two high velocity areas are clustered around eastern and north-eastern sub-basin of Kathmandu. The southern part of the basin also

show some areas of high velocity in the E-W component. In the western edge of the basin, another high velocity area can be seen. The rock exposures inside the basin have significantly low ground velocity (blue patches inside the basin).

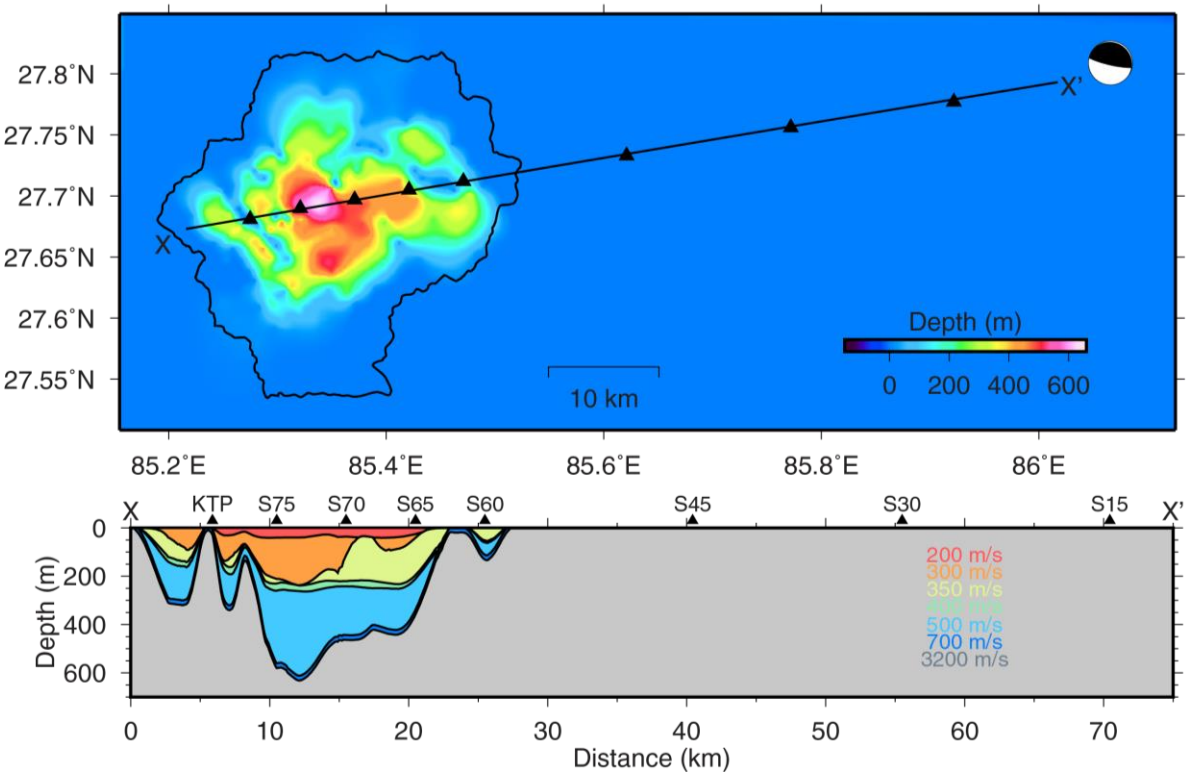

Figure 5. 19 Observation points at 260° azimuth for comparing response of rock and basin sites for ground motion simulation. The cross-section at X-X' line show the undergorund structure below the observation points.

The change in seismic waves as it is entering the basin can be understood by checking the synthetic waves at points lying at certain distance interval. For the simulation of this earthquake, seven observation points are placed between KTP and the epicentre (Figure 5.19) at an azimuth of 260°. The points are at 15 km interval outside the basin and 5 km inside the basin. The waveform in radial and transverse component (Figure 5.20) of these stations clearly show the basin effect at the sites inside the basin. This is particularly important as there are no stations outside the Kathmandu Basin to compare the difference of seismic response over basement rock and those over thick sediments.

The synthetic waves of this earthquake shows the presence of Rayleigh waves just like in the observed waves. The particle motion plot (Figure 5.21) of the radial and vertical components show the retrograde motion indicating presence of Rayleigh waves. The presence of Rayleigh waves is also seen in the observed waveform [2]. The presence of Rayleigh waves is nearly at the same time as the S-wave and it means that the S-wave part of this earthquake is contaminated by the Rayleigh waves.

The comparison of the peak ground velocity with the intensity map of 1934 Nepal-Bihar earthquake (Figure 3.3) shows interesting results (Figure 5.22). The epicentre of the 1934 earthquake is also east of Nepal though much farther than epicentre of the 2015 M_w 7.3 earthquake from the Kathmandu Basin. The areas with higher ground motion amplification by FDM simulation lie in the region of MMI X of the 1934 earthquake (M_w 8.3). The areas with maximum amplification in this study like Bhaktapur and Sankhu had suffered heavy damage during the 1934 earthquake [45]. The heavily damaged areas of Gongabu, Sitapaila, Ramkot, Panga, Sankhu, and Bhaktapur during the 2015 Gorkha Earthquake main shock (M_w 7.8) also show high ground motion in the present simulation though the epicentre of the main

shock is in the west of Kathmandu as opposed to east of M_w 7.3 earthquake. Though the results are consistent with the damage during two large previous earthquakes, simulations of 1934 and 2015 Gorkha earthquake will shed more light into this.

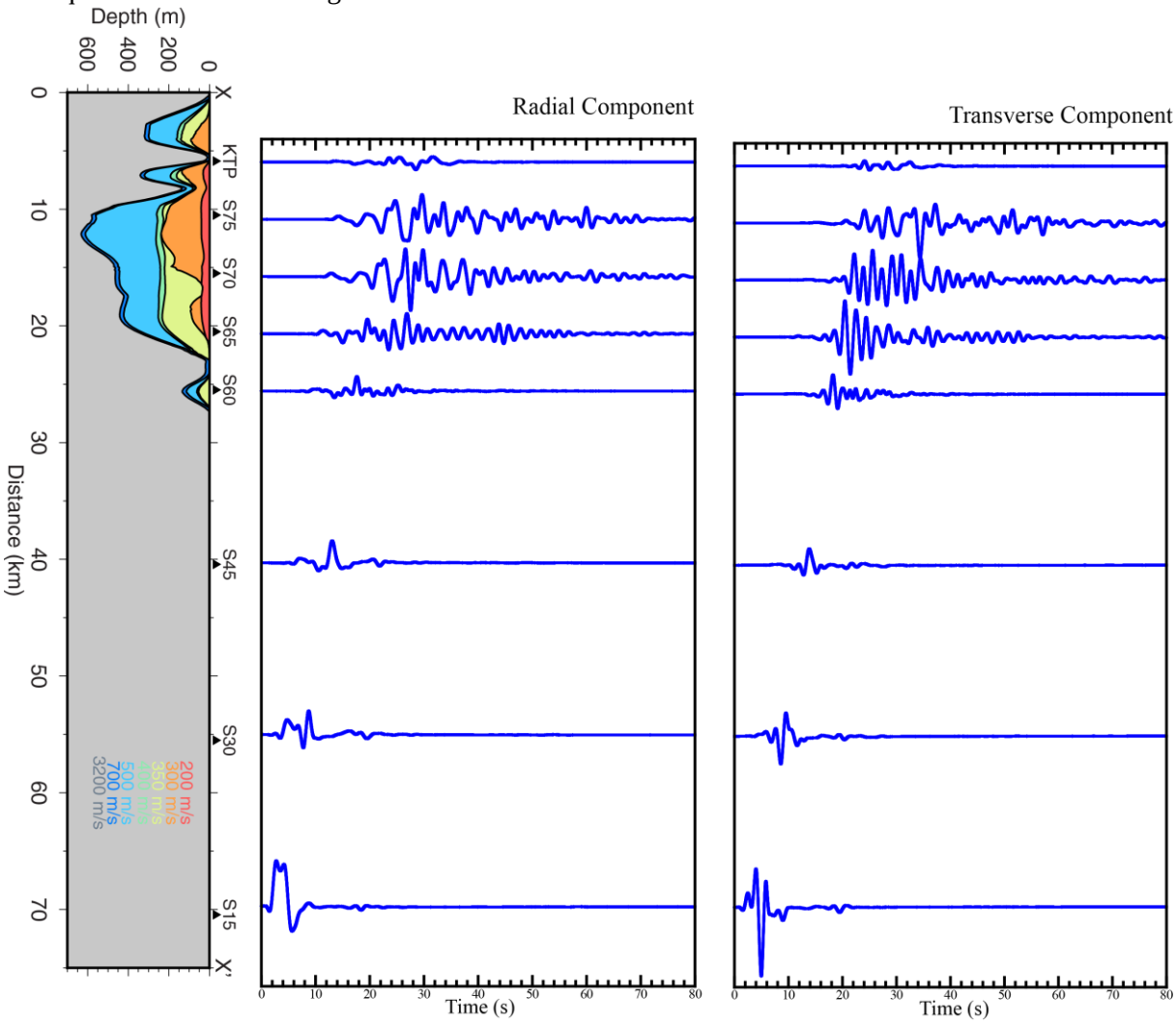

Figure 5. 20 Horizontal component response at the observation points over rock and basin sediments.

There are only few stations to compare the result inside the basin. The SATREPS project has installed 10 strong motion seismometers in different parts of the basin. The records from these stations will be used to simulate and compare future earthquakes and tune the structures at places other than the existing eight stations. The result of the gravimetric survey undergoing in the Kathmandu Basin by OYO Corporation will be a good source for tuning the model once the data is made public.

5.4 CONCLUSION

A 3D underground velocity model of the Kathmandu Basin was prepared using geological data. Though there is not enough data regarding the underground model, the present study used available borehole logs, gravity survey data, and geological cross-sections to construct the underground model of the Kathmandu Basin. The different geological units were divided into five sediment layers and a weathered rock layer. Underground structures at several points of the basin were used to create the surface map of each layer by Kriging method. The shear velocity and density of the layers were based on the average value of sediments mentioned in a study of earthquake disaster mitigation carried out in Kathmandu as well as the shear wave velocity study performed during installation of the seismic stations. The topmost layer of the velocity model is soft clay and sand with shear wave velocity of 200 m/s whereas the lowermost layer is thick pebbly, gravelly sand with shear wave velocity of 500 m/s. The sediment layers

overlie a thin (~20 m) weathered rock layer. This rock layer exposed in the rock site KTP has V_s~700 m/s and it was considered that this layer spans the whole basin at the bottom separating the sediments from the hard basement rocks (V_s = 3.2 km/s). The tectonic origin of the Kathmandu Basin means that the basement layer of Kathmandu was exposed and underwent weathering before gradually being filled with the river and lake sediments. This formed a geological unconformity at the bottom of the basin thus giving rise to the significant velocity contrast between the soft and hard layers. The 3-D model showed the undulated nature of the basin basement where there are several rock exposures jutting through the sediments thus creating a number of sub-basins. The central part of the Kathmandu Basin is the deepest with top of bedrock at the depth of more than 600 m from the surface.

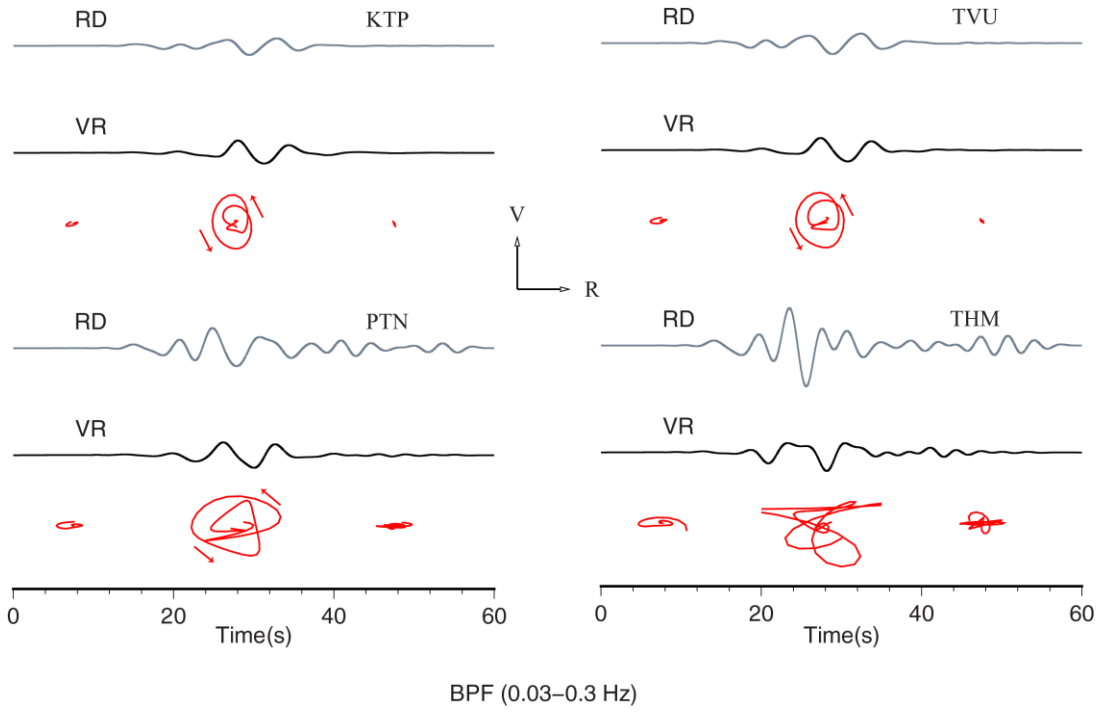

Figure 5. 21 The particle motion plot of radial (RD) and vertical (VR) component of synthetic wave shows the retrograde motion indicating presence of Rayleigh wave in 20-30 s.

To simulate the ground motion in the 3-D velocity model, staggered grid finite difference method with discontinuous grid was employed. Before that, the simulated waveform from finite difference method and discrete wave number method was compared by two different velocity models: planar stratified model and a small basin model. The small basin model had a hillock protruding at the centre of the basin: a simple representation of the area around stations KTP and TVU. The comparison showed that the result of FDM and DWN were very similar in half space and stratified structures whereas in basin sites, the FDM clearly showed the basin effects which were not seen in results of the DWN method.

Finally the 3-D velocity model was used to simulate the M_w 7.3 aftershock of the Gorkha earthquake sequence. The earthquake was chosen as the main shock showed strong nonlinear effect and smaller earthquakes had either no focal mechanism information and had low signal-to-noise ratio. This earthquake was large enough with available earthquake parameter and was recorded in all eight stations. The nonlinearity effect for the earthquake was also much smaller. The earthquake parameters were taken from the USGS website but the pulse width of the source time function for the analysis was set from the cut-off frequency of displacement Fourier spectra of the observed rock site record.

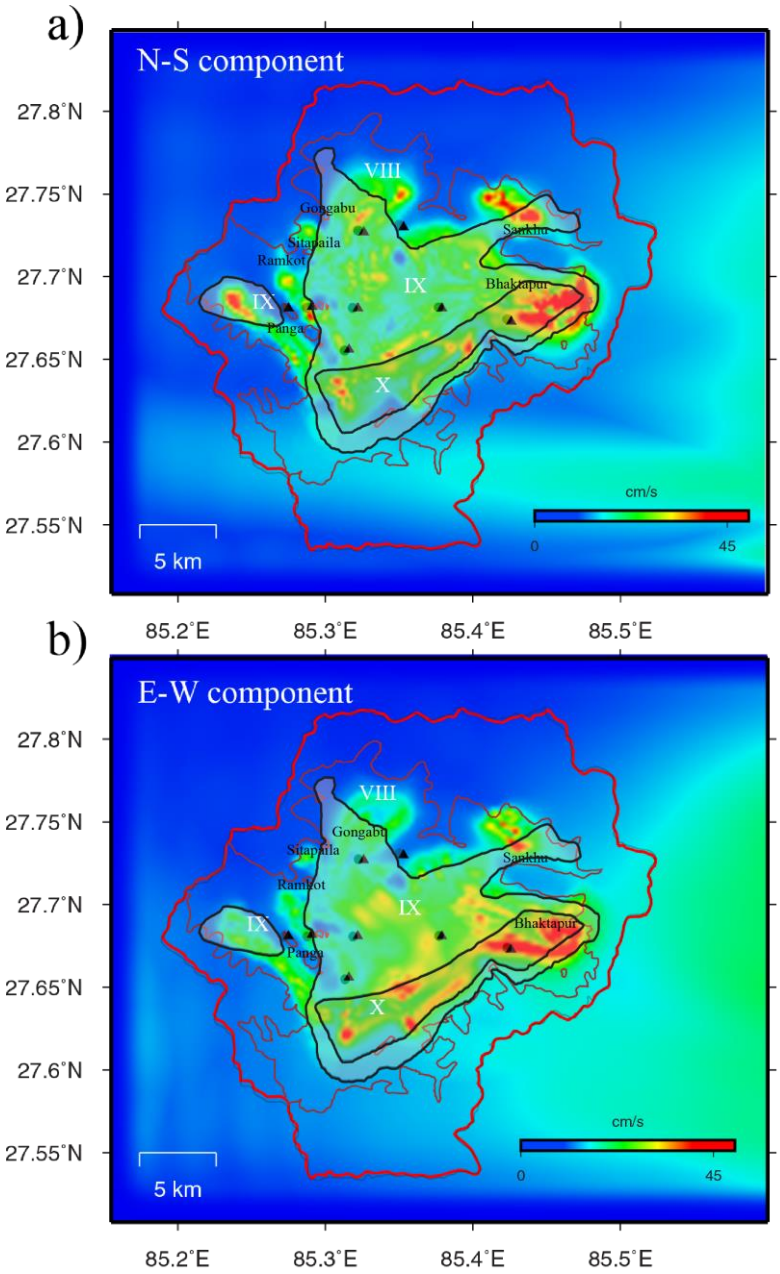

Figure 5. 22 Comparison of earthquake intensity map of 1934 earthquake [45] with PGV distribution result of M_w 7.3 simulation.

The 3-D velocity model was truncated at an altitude of 1,320 m for the FDM analysis. The area lower than 1,320 m, especially river terraces were thus filled with the topmost layer. The grid size of calculation was 50 m and maximum applicable frequency was 0.8 Hz. The comparison of the synthetic waveform with the observed waveform showed good matching in sites other than BKT. The FDM analysis was able to produce the later phases of the earthquake except at a couple of sites indicating small-scale heterogeneity around the stations. It necessitates further study around those particular stations. The synthetic waves also consist of Rayleigh waves arriving at the same time as the S-wave which was also seen in the observed wave.

As there are only eight sites to compare at the moment, comparison can be carried out with data from other stations which are now being installed in the Kathmandu Basin when they're available.

References

[1] Bilham, R. & Wallace, K. Future Mw >8 earthquakes in the Himalaya: implications form the 26th Dec 2004 Mw = 9.0 earthquake on India's eastern plate margin. *Geological Survey of India Special Publication* **85**, 1-14 (2005).

[2] Bijukchhen, S. M. *Strong Ground-Motion characteristics in the Kathmandu Basin (Strong-motion observation and damage assessment of 2015 Gorkha, Nepal Earthquake)* Masters thesis, Hokkaido University, (2015).

[3] Aoi, S. & Fujiwara, H. 3D finite-difference method using discontinous grids. *Bull Seismol Soc Am* **89**, 918-930 (1999).

[4] Dhakal, Y. P., Sasatani, T. & Takai, N. in *9 SEGJ International Symposium* (Sapporo, Japan, 2009).

[5] Moribayashi, S. & Maruo, Y. Basement topography of the Kathmandu valley, Nepal- An application of gravitational method of the survey of a tectonic basin in the Himalayas *Journal of Japan Society of Engineering Geology* **21**, 30-37 (1980).

[6] Yoshida, M. & Igarashi, Y. Neogene to Quaternary lacustrine sediments in the Kathmandu valley, Nepal. *Journal of Nepal Geological Society* **4**, 73-100 (1984).

[7] Dongol, G. M. S. Geology of the Kathmandu fluviatile lacustrine sediments in the light of new vertebrate fossil occurrences. *Journal of Nepal Geological Society* **31**, 43-57 (1985).

[8] Shrestha, O. M. *et al.* (Department of Mines and Geology, Kathmandu, 1998).

[9] Sakai, H., Fujii, R., Kuwahara, Y., Upreti, B. N. & Shrestha, S. D. Core drilling of the basin-fill sediments in the Kathmandu valley for palaeoclimatic study: preliminary results. *Journal of Nepal Geological Society* **25**, 9-18 (2001).

[10] Sakai, H. Stratigraphic division and sedimentary facies of the Kathmandu Basin Group, central Nepal. *Journal of Nepal Geological Society* **25**, 19-32 (2001).

[11] Pandey, M. R. in *12th World Conference on Earthquake Engineering* (Auckland, New Zealand, 2000).

[12] JICA. The study of earthquake disaster mitigation in the Kathmandu valley, Kingdom of Nepal. (Japan International Cooperation Agency and Ministry of Home Affairs Nepal, Kathmandu, 2002).

[13] Piya, B. K. *Generation of a geological database for the liquefaction hazard assessment in Kathmandu valley* M.Sc thesis, International Institute for Geo-Information and Earth Observation (ITC), (2004).

[14] Paudyal, Y. R., Yatabe, R., Bhandary, N. P. & Dahal, R. K. Basement topography of the Kathmandu Basin using microtremor observation. *Journal of Asian Earth Sciences* **62**, 627-637, doi:10.1016/j.jseaes.2012.11.011 (2013).

[15] Sugimura, Y. (Japan Social Fund, Kathmandu, 2012).

[16] Fujii, R. & Sakai, H. Paleoclimatic changes during the last 2.5 myr recorded in the Kathmandu Basin, Central Nepal Himalayas. *Journal of Asian Earth Sciences* **20**, 255-256 (2002).

[17] Takai, N. *et al.* Shallow underground structure of strong ground motion observation sites in the Kathmandu valley. *Journal of Nepal Geological Society* **48**, 50 (2015).

[18] Isaaks, E. H. & Srivastava, R. M. Spatial Continuity for Probabilistic and Deterministic Geostatistics *Mathmatical Geology* **20**, 313-341 (1988).

[19] Monsalve, G. *et al.* Seismicity and one-dimensional velocity structure of the Himalayan collision zone: Earthquakes in the crust and upper mantle. *Journal of Geophysical Research* **111**, doi:10.1029/2005jb004062 (2006).

[20] Bijukchhen, S. M. *et al.* Estimation of 1-D velocity models beneath strong-motion observation sites in the Kathmandu Valley using strong-motion records from moderate-sized earthquakes. *Earth, Planets and Space* **69**, 97, doi:10.1186/s40623-017-0685-4 (2017).

[21] Graves, R., Pitarka, A. & Somerville, P. Ground-motion amplification in the Santa Monica area: effects of shallow basin-edge structure. *Bull Seismol Soc Am* **88**, 1224-1242 (1998).

[22] Frankel, A., Stephenson, W. & Carver, D. Sedimentary Basin Effects in Seattle, Washington: Ground-Motion Observations and 3D Simulations. *Bulletin of the Seismological Society of America* **99**, 1579-1611, doi:10.1785/0120080203 (2009).

[23] Dhakal, Y. P. *et al.* in *JAEE International Symposium on Earthquake Engineering* (Tokyo, 2015).
[24] Rajaure, S. *et al.* Characterizing the Kathmandu Valley sediment response through strong motion recordings of the 2015 Gorkha earthquake sequence. *Tectonophysics* **714-715**, 146-157, doi:10.1016/j.tecto.2016.09.030 (2017).
[25] Graves, R. Simulating seismic wave propagation in 3D elastic media using staggered-grid finite diffrences. *Bull Seismol Soc Am* **86**, 1091-1106 (1996).
[26] Stephenson, W. J., Frankel, A. D., Odum, J. K., Williams, R. A. & Pratt, T. L. Toward resolving an earthquake ground motion mystery in west Seattle, Washington State: Shallow seismic focusing may cause anomalous chimney damage. *Geophysical Research Letters* **33**, doi:10.1029/2005gl025037 (2006).
[27] Wei, S. *et al.* The 2015 Gorkha (Nepal) earthquake sequence: I. Source modeling and deterministic 3D ground shaking. *Tectonophysics* **722**, 447-461, doi:10.1016/j.tecto.2017.11.024 (2018).
[28] Pitarka, A. & Irikura, K. Modeling 3D surface topography by finite-difference method: Kobe-JMA Station Site, Japan, Case Study. *Geophysical Research Letters* **23**, 2729-2732, doi:10.1029/96gl02493 (1996).
[29] Pitarka, A. 3D Elastic finite-difference modeling of seismic motion using staggered grids with nonuniform spacing. *Bulletin of the Seismological Society of America* **89**, 54-68 (1999).
[30] Levander, A. Fourth-order finite-difference P-SV seismograms. *Geophysics* **53**, 1425-1436 (1988).
[31] Dhakal, Y. P., Sasatani, T. & Takai, N. Validation of the Deep Velocity Structure of the Tokachi Basin Based on 3-D Simulation of Long-Period Ground Motions. *Pure and Applied Geophysics* **168**, 1599-1620, doi:10.1007/s00024-010-0237-3 (2011).
[32] Bouchon, M. A review of the discrete wavenumber method. *Pure and Applied Geophysics* **160**, 445-465 (2003).
[33] Bouchon, M. A simple method to calculate Green's functions for elastic layered media. *Bull Seismol Soc Am* **71**, 959-971 (1981).
[34] Sasatani, T. Sesimic wave propagation in a stratified half-space. *Journal of the Faculty of Science, Hokkaido University* **7**, 401-420 (1985).
[35] Koketsu, K. The extended reflectivity method for synthetic near-field seismograms. *Journal of Physical of the Earth* **33**, 121-131 (1985).
[36] Takeo, M. Near-field synthetic seismograms taking onto account the effects of anelasticity- the effects of anelastic attenuation on seismograms caused by a sedimentary layer (in Japanese). *Papers in Meterology and Geophysics* **36**, 245-257 (1985).
[37] Grandin, R. *et al.* Rupture process of the Mw=7.9 2015 Gorkha earthquake (Nepal): Insights into Himalayan megathrust segmentation. *Geophysical Research Letters* **42**, 8373-8382, doi:10.1002/ (2015).
[38] USGS. *Earthquake Hazards Program*, <http://earthquake.usgs.gov/> (2015).
[39] GCMT. *Global CMT Catalog Search*, <http://www.globalcmt.org/> (2015).
[40] Borah, K., Kanna, N., Rai, S. S. & Prakasam, K. S. Sediment thickness beneath the Indo-Gangetic Plain and Siwalik Himalaya inferred from receiver function modelling. *Journal of Asian Earth Sciences* **99**, 41-56, doi:10.1016/j.jseaes.2014.12.010 (2015).
[41] Olsen, K. B., Nigbor, R. & Konno, T. 3D viscoelastic wave propagation in the Upper Borrego Valley, California, constrained by borehole and surface data. *Bulletin of Seismological Society of America* **90**, 134-150 (2000).
[42] Satoh, T. in *13th World Conference on Earthquake Engineering* (Vancouver, Canada, 2004).
[43] Mitchell, B. J. & Romanowicz, B. *Q of the earth: global, regional, and laboratory studies*. (Birkhauser Verlg, 1999).
[44] Galetzka, J. *et al.* Slip pulse and resonance of Kathmandu basin during the 2015 Mw 7.8 Gorkha earthquake, Nepal imaged with geodesy. *Science (New York, N.Y.)*, doi:10.1126/science.aac6383 (2015).
[45] Rana, B. S. *Mahabhukampa (The Great Earthquake)*. (B.S. Rana, 1935).

CHAPTER VI
CONCLUSIONS

CHAPTER VI. CONCLUSIONS

Based on the present study focussed in the strong-motion characteristics and preparation of a 3-D velocity structure of the Kathmandu Basin following conclusions can be drawn.

Kathmandu being the cultural, political, and economic capital of the country has a number of UNESCO heritage sites that are main attraction for the tourism industry. Kathmandu though have seen a rapid population growth and unmanaged urbanization in recent years. It was hit hard by past as well as the most recent 2015 Gorkha earthquake. Given the history of it being severely hit by earthquakes time and again, a future earthquake disaster in Kathmandu not only affect a large population but it will also bring the whole country to a halt. Thus earthquake resilience and disaster mitigation study of the Kathmandu Basin is an important task.

The position of Kathmandu in a seismically active zone and amplification of seismic waves during earthquake due to thick soft sediment increase the risk of earthquake damage. The large population also increases the risk of a large number of casualties. Hence a proper understanding of basin topography and underground structure of the basin is required to properly estimate the strong-motion characteristics. An accurate 3-D structure of the basin is required to demarcate seismically vulnerable areas to draft and update the building code for earthquake disaster mitigation.

Kathmandu is a basin filled with soft fluvio-lacustrine deposit and surrounded by mountains of basement rocks. Previous studies have shown the thickness of sediment to be more than 600 m at the centre. The layers are mostly sand and silt and are unconsolidated. Due to the tectonic origin of the basin, the basement topography is not smooth so there are many rock exposures jutting out of the sediments forming smaller sub-basins with different depositional environment. This makes the geology of the Kathmandu Basin complex and varied.

As the site effect plays a major role during earthquake, the difference of sediment thickness and 3-D structure changes the response to the seismic waves. The earthquake records from eight (four permanent and four temporary) seismic stations clearly show the difference in site response. The rock site KTP and sediment site TVU are less than 2 km apart but their earthquake records vary by a large extent. The sediment sites TUV, PTN, and THM show fundamental frequency of 0.2-0.4 Hz. The main shock of the Gorkha earthquake sequence also were prominent in the long period waves. The comparison of H/V spectral ratio of weaker earthquake and strong earthquake revealed that the sediment of Kathmandu shows the nonlinearity effect, which means the high frequencies are attenuated more during large earthquake. This might be the reason for less than anticipated damage during the main shock because the higher frequencies were damped and there were not many structures in Kathmandu with longer natural periods. Nevertheless, there were damage to many buildings around the basin. A rapid visual damage assessment around the stations showed that the damage ratio was proportional to the acceleration response between 1-2 s periods. But it was clear that damage during the Gorkha earthquake was not entirely due to site affect but the low strength of structures and lack of timely maintenance were also to blame.

Since, there are not enough data regarding the underground structure of the basin, the geological cross-sections, gravity anomaly data, and few available borehole data logs were used to first model the 1-D velocity structure under the seismic stations. The boreholes were dug mostly for groundwater prospecting and they lack detailed logs. Moreover there is no information regarding the P-S logging in deeper sediment of Kathmandu. The shear wave velocity of layers were set based on the shear wave velocity study of the shallow surface and from average value of geological materials. The 1-D structures thus prepared were then tuned by forward modelling of seismic waves by Propagator Matrix method by S-wave H/V spectral ratio method. The comparison between simulated waveform and observed waveform were good fit. The 1-D simulation cannot explain the later phases as those phases were effect of basin structure. A 3-D modelling was necessary to reproduce the later phases and surface waves produced due to basin effect.

The 3-D velocity structure was constructed based on the cross-sections, 1-D models, borehole logs, and gravity anomaly survey data. The different geological formations were grouped into 5 layers of sediments according to their lithology. For preparation of the surface of each layer, kriging of several points with underground structure in Surfer software. The 3-D velocity model shows the deepest part of the basin in the centre reaching a depth of 612 m. The significant property of the basin model is the presence of small sub-basins as a result of uneven basin topography. The model also showed a high velocity contrast between the weathered rock layer at the bottom of the basin and the basement rock beneath it.

The finite difference method (FDM) was employed to simulate the ground motion in the 3-D model. The parameters of the largest aftershock (M_w 7.3) of Gorkha earthquake was used in the 3-D velocity structure. The synthetic waveform and the observed waveform were then compared which gave encouraging results. The synthetic waveform replicated the later phases like in the observed wave. Later phases at site TVU couldn't be properly simulated indicating a need of seismic array study locally around the station. The waveform at BKT had the least fitting with overestimation in the simulation. This might be an effect of foundation interaction in the station resulting in the reduced observed motion as the station was housed inside a newly constructed 3 story building. The areas with larger ground motion from the simulation matched with damage map of the 1934 earthquake as well as the 2015 Gorkha earthquake to some extent.

Since there are few borehole data, most of them shallow, they cannot clearly show the extent of distribution of the layers. The presence of sub-basins inside Kathmandu gives rise to varied deposition environment which results in formation of interfingering and lenses of sediment. For the FDM, the top should be planar so the 3-D model is truncated at 1320 m altitude and the areas lower in altitude, mostly low lying river areas, are filled with the topmost layer. At the moment, there are only eight observation points in the basin to compare the results. The ongoing SATREPS project have installed 10 more strong-motion seismometers. Once the data is available, the records from these stations can be used for comparison.

The 3-D velocity structure in a place like the Kathmandu Basin where the data is very limited will further be tuned with availability of additional data. The 3-D velocity structure constructed by present study nevertheless, can be an important tool in the disaster management study of the Kathmandu Basin. It can be used for simulation of a probable scenario earthquake in the 'seismic gap' of western Nepal and demarking the seismically vulnerable areas of Kathmandu for engineering purpose.

RESEARCH ACTIVITIES

The works presented in this dissertation have been published and presented in the following papers and proceedings.

1. Peer-reviewed papers (first author)

   - Bijukchhen, S., Takai, N., Shigefuji, M., Ichiyanagi, M. & Sasatani, T. Strong-motion characteristics and visual damage assessment around seismic stations in Kathmandu after the 2015 Gorkha, Nepal, Earthquake. *Earthquake Spectra* **33**, S219-S242, doi:10.1193/042916eqs074m (2017).

   - Bijukchhen, S. M., Takai, N., Shigefuji, M., Ichiyanagi, M., Sasatani, T. & Sugimura, Y. Estimation of 1-D velocity models beneath strong-motion observation sites in the Kathmandu Valley using strong-motion records from moderate-sized earthquakes. *Earth, Planets and Space* **69**, 97, doi:10.1186/s40623-017-0685-4 (2017).

2. Peer-reviewed papers (co-author)

   - Takai, N., Shigefuji, M., Rajaure, S., Bijukchhen, S. M., Ichiyanagi, M., Dhital, M. R. & Sasatani, T. Strong Ground Motion in the Kathmandu Valley during the 2015 Gorkha, Nepal, Earthquake. *Earth, Planets and Space* **68**, doi:10.1186/s40623-016-0383-7 (2016).

   - Ichiyanagi, M., Takai, N., Shigefuji, M., Bijukchhen, S., Sasatani, T., Rajaure, S., Dhital, M. R. & Takahashi, H. Aftershock activity of the 2015 Gorkha, Nepal, earthquake determined using the Kathmandu strong motion seismographic array. *Earth, Planets and Space* **68**, doi:10.1186/s40623-016-0402-8 (2016).

3. Conference Proceedings (first author)

   - Bijukchhen, S., Takai, N., Shigefuji, M., Ichiyanagi, M., Sasatani, T., Rajaure, S. & Dhital, M. R. A comparative study of strong ground motion records from 30 August 2013 south Tibet earthquake on the rock and soil sites of Kathmandu Valley. *Journal of Nepal Geological Society* **48**, 48 (2015).

   - Bijukchhen, S., Takai, N., Shigefuji, M., Ichiyanagi, M. & Sasatani, T. Trial construction of 1-D velocity structures of the Kathmandu Valley using the medium and large earthquake records, in *5th IASPEI/IAEE International Symposium: Effects of Surface Geology on Seismic Motion*. (Taipei, Taiwan, 2016).

   - Bijukchhen, S., Takai, N., Shigefuji, M., Ichiyanagi, M. & Sasatani, T. Strong-motion observation and damage assessment in Kathmandu, Nepal after April 25, 2015 Gorkha Earthquake, in *16th World Conference on Earthquake Engineering*. (Santiago, Chile, 2017).

   - Bijukchhen, S., Takai, N., Shigefuji, M., Ichiyanagi, M. & Sasatani, T. Preparation of 1D velocity structure using records from moderate sized earthquakes, in *IAG-IASPEI Joint Scientific Assembly*. (Kobe, Japan, 2017).

   - Bijukchhen, S., Takai, N., Shigefuji, M., Ichiyanagi, M. & Sasatani, T. Identification of Nonlinear soil response in the Kathmandu Valley during the 2015 Gorkha, Nepal Earthquake (Mw7.8), in *Seismological Society of Japan Fall Meeting*. (Kagoshima, Japan, 2017).

ACKNOWLEDGMENTS

I would like to express my sincere gratitude to Associate Professor Nobuo TAKAI for his invaluable guidance, consistent support, and supervision throughout five years of my time as his student. I'm much indebted to Professor Tsutomu SASATANI for guiding and providing valuable suggestions, encouragement, and support throughout all the study. Similar gratitude goes to Assistant Professor Michiko SHIGEFUJI and Masayoshi ICHIYANAGI for worthy suggestions, help, and support. Without all these encouragement, support, and guidance, this work would not have come in the present form.

I'm obliged to Professor Masanori IIBA and Professor Taichiro OKAZAKI of the Examination Committee for valuable inputs and suggestions. I'm thankful to Ministry of Education of Japan for providing me MEXT scholarship to make this study possible.

I express my sincere thanks to all the members of Urban Disaster Protection Planning Laboratory for their constant co-operation. I thank my friends back home who helped me gather valuable information and materials necessary for this work. I am obliged to Professor Megh Raj DHITAL for his constant encouragement.

My deep gratitude to my parents, Narayan Man BIJUKCHHEN and Shova PRADHAN, and my brother Suban who supported and inspired me in every step of my life. Last but not the least, I am thankful to my wife Archana who believed in me and constantly encouraged me.